Characterization of the potential drug target serine acetyltransferase (CysE) from *Acinetobacter baumannii*: A Pacific lens on biochemical research

A thesis
submitted in partial fulfilment
of the requirements for the degree
of
Master of Science (Research) in Molecular and Cellular Biology
at
The University of Waikato
by
Jessicca Eva Usu

THE UNIVERSITY OF
WAIKATO
Te Whare Wānanga o Waikato

2024

Abstract

Antimicrobial resistance (AMR) presents a critical global health threat, with *Acinetobacter baumannii* being a key pathogen due to its multidrug resistance. With no new antibiotic classes discovered since the 1980s, novel therapeutic targets are urgently needed. This thesis explores the potential of targeting the cysteine biosynthesis pathway, specifically the enzyme serine acetyltransferase (CysE), as a means to develop innovative antimicrobial strategies. Cysteine plays a pivotal role in bacterial survival and defense, particularly in oxidative stress resistance. Targeting its biosynthesis may impair bacterial virulence and enhance susceptibility to immune responses.

This research focuses on the characterization of CysE from *A. baumannii*, which uniquely expresses a short and full-length of this enzyme. While we were unable to optimize expression of the short form in this thesis, the long form was successfully expressed, purified, and biochemically and structurally characterized for the first time. Using X-ray crystallography, we present the three-dimensional structure of CysE from *A. baumannii* to a resolution of 2.14 Å. CysE adopts a homohexameric conformation, forming a dimer of trimers, and features an alpha-helical extension. SAXS analysis validated that the long form exists as a homohexamer in solution. Furthermore, using enzymatic assays we show CysE has serine acetyltransferase activity and is sensitive to feedback inhibition by pathway product L-cysteine, highlighting the regulatory mechanisms of this crucial enzyme. This work improves our understanding of cysteine biosynthesis in *A. baumannii* and provides a model for structure-based virtual inhibitor screening to identify potential new antimicrobials.

In addition to its scientific objectives, this research is framed within the Fa'afaletui framework, an Indigenous Samoan methodology that ensures cultural perspectives are integrated into the scientific process. This approach ensures that Pacific values inform the direction of AMR research, fostering solutions that are not only scientifically rigorous but are also culturally relevant and accessible. The research serves to address the health inequities faced by Pacific peoples, particularly in relation to infectious diseases and AMR, and provides a foundation for future antimicrobial drug development efforts.

Acknowledgments

"E sui faiga ae tumau fa'avae"—Our practices may change, but the values and foundations of the cultural traditions remain.

I begin by acknowledging the rich cultural heritage that has shaped my journey, grounding me in values of service, resilience, and the pursuit of knowledge.

I owe a profound debt of gratitude to my supervisor, Dr. Joanna Hicks, whose guidance and support have been beyond measure. Her openness in allowing me to weave my cultural heritage into this research, and her belief in my vision, is something I can hardly express in words. Her encouragement to bring the Pacific lens into a field where it is rarely seen has empowered me in ways I will carry forward into every aspect of my future work.

A special thanks to Dr. Erica Prentice for her invaluable assistance in the analysis of the kinetic data and for showing me how to efficiently use Excel to do the hard work for me. I also extend my heartfelt thanks to Dr. Keely Oldham for her never-ending support, invaluable tips and tricks of the lab, and thoughtful welfare checks. Thank you both for proofreading this thesis and providing invaluable feedback.

My heartfelt thanks go to Judith for being an amazing lab mum, always keeping the lab running smoothly. A huge thank you to my lab family for making what was at times a really hard journey both bearable and memorable. From the amazing Christmas parties and morning teas to my unforgettable first conference at Hanmer Springs and my first trip to the South Island, you all made coming into the lab a joy.

I am deeply grateful to the Maurice Wilkins Centre and the Ministry for Pacific Peoples for their generous funding and support throughout my research. Their contributions made this work possible and allowed me to pursue my passion for science and community.

Lastly, I want to express my deepest gratitude to my family. To my parents, thank you for looking after my youngest and giving me the peace of mind to focus on my research. To my children, thank you for your patience and understanding. And to my husband, a massive thank you for believing in my dreams and always being in my corner, cheering me on. Your unwavering support has been my greatest strength.

Fa'afetai, Fa'afetai tele lava.

Table of Contents

List of Figures

List of Tables

List of Equations

Glossary

Acetyl-CoA	acetyl-coenzyme A
ACB	*Acinetobacter calcoacerticus-baumannii*
AHLs	acyl-homoserine lactones
ABC	ATP-binding cassette
Abs	Absorbance
AMR	Antimicrobial resistance
ANZ	Aotearoa New Zealand
Arg	arginine, amino acid
Asp	aspartate, amino acid
APS	adenosine 5'-phosphosulfate
ASU	asymmetric unit
bp	base pair
Bap	Biofilm-associated protein
CoA	co-enzyme A
CDC	center for disease control prevention
CSC	cysteine synthase complex
CysE	serine acetyltransferase
CRE	carbapenem-resistant enterobacteriaceae
CRAb	carbapenem-resistant *Acinetobater baumannii*
DTNB	5,5′-Dithiobis(2-nitrobenzoic acid) / Ellman's reagent
EDTA	ethylenediaminetetraacetic acid
ESR	Environmental Science and Research
ESGC(s)	evolutionarily stable gene cluster(s)
FPLC	fast protein liquid chromatography
Glu	glutamate, amino acid
Gly	glycine
GSH	glutathione
Hexahis-tag	hexa-histidine tag
His	histidine, amino acid
IC_{50}	inhibitor concentration where activity is reduced by 50%
IMAC	immobilized metal affinity chromatography
IPTG	isopropylthio-β-galactosidase
K_{av}	gel phase distribution co-efficient

k_{cat}	enzyme rate constant
k_{cat}/K_M	catalytic efficiency constant
K_d	dissociation constant
kDa	kilo Dalton
K_i	inhibitor constant
K_M	Michaelis constant
KO	knockout
LB	Luria Bertani
L-cys	L-cysteine
L-ser	L-serine
LβH	Left-handed parallel β-helix
MD	molecular dynamics
MM-GBSA	molecular mechanics-generalized Born surface area
MMK	Michaelis Menten kinetics
MBLs	metallo-β-lactamases
MDR	multidrug-resistant |
MR	molecular replacement
MWCO	molecular weight cut off
OAS	*O*-acetylserine
OmpA	Outer membrane protein A
OXA	oxacillinases
PAGE	polyacrylamide gel electrophoresis
PAPS	3'-phosphoadenosine-5'-phosphosulphate
PCR	polymerase chain reaction
PDB	protein data bank
PEG	polyethylene glycol
pI	isoelectric point
pLDDT	predicted local distance difference test
PLP	pyridoxal 5'-phosphate
PMN	polymorphonuclear neutrophil
Pro	proline, amino acid
Rg	radius of gyration
ROS	reactive oxygen species
RT	room temperature
s	second(s)
SAT	serine *O*-acetyltransferase
SATase	serine *O*-acetyltransferase

SDS	sodium dodecyl sulphate
SEM	standard error of mean
Ser	serine, amino acid
SSN	sequence similarity network
SAX	small-angle X-ray scattering
tNCS	translational non-crystallographic symmetry
TEMED	tetramethylethylenediamine
Tris	tris(hydroxymethyl)aminomethane
Val	valine, amino acid
V_{max}	maximum reaction rate
WHO	world health organization
XDR	Extensively drug-resistant
XDS	X-ray detector software

Chapter One

Introduction

1.1 Introduction

Drug-resistant infections are rapidly increasing and discovering new druggable targets within pathogenic bacteria is not just a scientific pursuit today; it is a race against time to safeguard the future. Antimicrobial resistance (AMR), where microorganisms become resistant to the drugs designed to treat them and continue to grow and survive, is not only a threat to human health but also to modern agriculture and the stability of food production. The escalation of AMR further jeopardizes the safety of routine medical procedures, potentially turning even common surgeries into life-threatening events, and placing considerable strain on our healthcare systems (Fischbach & Walsh, 2009; Gandra *et al*., 2014; Tiseo *et al*., 2020; Yoneyama & Katsumata, 2006). The ubiquitous use of antimicrobials has accelerated the emergence of AMR by intensifying the selective pressure for genes responsible for mechanisms that reduce the efficacy of antibiotics (Yam *et al*., 2019). This has led to the steady rise in extensively drug-resistant (XDR) and multidrug-resistant (MDR) strains of pathogenic bacteria such as carbapenem *Acinetobacter baumannii*, XDR *Pseudomonas aeruginosa*, carbapenem-resistant *Enterobacteriaceae* (CRE) and XDR and MDR *Mycobacterium tuberculosis*. These pathogens are included on the World Health Organization (WHO)'s 2017 Priority One list as critical, commonly referred to as the "dirty dozen", highlighting their significant threat to human health (World Health Organization, 2017).

Compounding the issue, no new classes of antibiotics have been discovered since the late 1980s, highlighting a desperate need for novel therapeutic targets to combat AMR. While derivatives of existing antibiotic classes continue to be developed (Cho *et al*., 2014; Ezelarab *et al*., 2018; Papp-Wallace *et al*., 2023), they often target the same bacterial mechanisms as current antibiotics and inadequately address rapidly evolving resistance mechanisms (Frávega *et al*., 2016; Jia & Zhao, 2021; Sproston *et al*., 2018). Globally, in 2019, AMR was directly responsible for 1.27 million deaths and a further 4.95 million deaths were associated with bacterial antibiotic resistance (Murray *et al*., 2022; World Health Organization, 2023). This significantly exceeds the earlier 2014 estimate of 700,000 deaths per year (O'neill, 2014). The Institute of Environmental Science and

Research (ESR) tasked with managing AMR surveillance in Aotearoa New Zealand (ANZ), reports that the country experiences significantly lower AMR rates than the global average, however, these rates are on the rise. In 2019, AMR directly caused 330 deaths in ANZ and an additional 1,500 deaths where AMR was a contributing factor (Institute for Health Metrics and Evaluation, 2024). These statistics emphasize the deadly impact of AMR, and in the absence of new interventions it is projected that annual healthcare costs will reach $100 trillion USD by 2050, highlighting the economic burden AMR poses (Wellcome Trust & UK Government, 2016).

Within ANZ, there are different impacts at the community level which are important to address, especially the vulnerability of Māori and Pacific people. Hospital admission rates for infectious diseases among Pacific peoples and Māori are approximately double compared to European and other groups, underscoring significant ethnic inequities (Baker *et al*., 2012). These inequities are driven by multiple factors, including social determinants such as socioeconomic status and access to healthcare, both of which are closely linked to higher rates of infectious disease (Metcalfe *et al*., 2019). Additionally, within Pacific communities there are notable health inequities, particularly in rural areas where healthcare access is more limited. This situation is exacerbated by the global spread of carbapenem-resistant *A. baumannii* strains, as highlighted by a recent study showing their movement between India, Fiji, Samoa, Australia, and New Zealand (Baleivanualala *et al*., 2023). This spread emphasizes the broader threat of AMR to Pacific peoples and highlights the critical need for understanding misconceptions around antibiotics and AMR within these communities. Addressing this is crucial for developing culturally informed healthcare initiatives. There is a need for future studies to bridge the gap in understanding and improve health outcomes for Pacific peoples, leveraging culturally sensitive methodologies to address these disparities comprehensively.

With a steady rise in AMR, compounded by significant health inequities and decades without new antibiotic developments, the urgency for novel therapeutic strategies is clearer than ever. These strategies must differ from those currently targeted by existing antimicrobials to effectively overcome antibiotic resistance (Hicks *et al*., 2022). Targeting amino acid biosynthesis presents a promising avenue for antimicrobial development, given their essential role in survival, reproduction and virulence of pathogens (Martho *et al*., 2019; Seo & Kwon, 2023; Toh-e *et al*., 2018). The amino acid

cysteine plays a critical role in protein synthesis and function (Campanini *et al*., 2015; Hicks *et al*., 2022; Kredich & Tomkins, 1966). Furthermore, it plays a pivotal role in bacterial defense mechanisms as it is a precursor to glutathione. This tripeptide is a strong intracellular antioxidant, vital for protecting bacterial cells against oxidative damage from the host immune system during infection. Inhibiting the synthesis of cysteine diminishes the bacterium's ability to counteract oxidative stress, impairing their defense mechanism and increasing their susceptibility to immune system attacks (Verma & Gupta, 2021). For example, the inactivation of the cysteine biosynthetic pathway in *M. tuberculosis* significantly impacts the bacterium's resistance to oxidative stress and antibiotics such as clofazimine (Burns-Huang & Mundhra, 2019). Additionally, deletion of cysteine synthase in *Salmonella* Typhimurium caused a 500-fold increase in sensitivity to the antibiotic ciprofloxacin (Turnbull & Surette, 2010). Furthermore, the importance of the cysteine biosynthetic enzyme, serine acetyltransferase (SAT) also known as CysE, in bacteria has been highlighted, and its inhibition has shown to significantly impact bacterial growth and survival (Agarwal et al., 2008; C. Chen et al., 2019; Magalhães et al., 2020). These examples highlight the potential of targeting cysteine biosynthesis to develop novel antimicrobial strategies.

With the essential role that cysteine plays in both protein functionality and bacterial defense mechanisms, potential targets within the cysteine biosynthesis pathway can be identified. CysE is a key enzyme in the pathway, making it a prime candidate for antimicrobial targeting. Additionally, mammals obtain cysteine from dietary methionine and therefore lack cysteine biosynthetic enzymes (Griffith, 1987). This research set out to examine CysE enzymes across four pathogenic bacteria; *Enterobacter* cloacae, *A. baumannii*, *P. aeruginosa,* and *M. tuberculosis*. Interestingly *A. baumannii* possesses two isoforms of CysE - a truncated and a full-length isoform. Notably, there are no experimentally determined three-dimensional (3D) structures of CysE available for any of these organisms. Given the unique presence of both a truncated and a full-length form of CysE in *A. baumannii*, both isoforms were ordered along with the other codon-optimized synthetic constructs of CysE from Twist Bioscience. As part of a summer research project, we previously optimized expression for CysE from *Escherichia coli*, which was adapted for optimizing expression conditions for CysE homologs (Usu, 2023, Summer research project). We screened protein expression conditions to optimize protein yield, which resulted in *E. cloacae* and *A. baumannii* being successfully optimized

producing sufficient yield for downstream biochemical characterization. However, due to the intriguing fundamental questions posed by the dual isoforms of CysE in *A. baumannii*, we chose to focus our investigations on this organism. Some of these questions include: Why does *A. baumannii* have two isoforms of CysE? Does the biochemical activity differ between these two isoforms? Are both isoforms sensitive to feedback inhibition by L-cysteine, and at what level of sensitivity? Furthermore, if inhibited, will the inhibitor work on both isoforms?

1.2 Pathogenesis of *Acinetobacter baumannii*

A. baumannii is a gram-negative aerobic bacillus, that is pleomorphic and non-motile. It has emerged as a challenging nosocomial pathogen, mainly due to it possessing an array of virulence factors and remarkable adaptability to hospital environments (Bergogne-Bérézin & Joly-Guillou, 1991; Wendt *et al.*, 1997). Historically, the genus *Acinetobacter* was proposed in 1954 by Brisou and Prévot (Brisou & Prévot, 1954), and the recognition of *A. baumannii* as a significant pathogen became more prominent in the late 1970s and early 1980s (Bergogne-Bérézin & Towner, 1996). Early descriptions under different names, such as "*Micrococcus calcoaceticus*" evolved into the current understanding of *A. baumannii* as a notable cause of hospital-acquired infections. This pathogen is associated with a variety of nosocomial infections, including bloodstream infection (bacteremia) (Russo *et al*., 2019), urinary tract infections (Jiménez-Guerra *et al*., 2018), and secondary meningitis (Siegman-Igra *et al*., 1993). However, it is predominantly known for causing nosocomial ventilator-associated pneumonia (VAP) in intensive care units (ICUs) (Luna & Aruj, 2007). It has a high incidence rate among immunocompromised individuals, especially among those who have long hospital stays greater than 90 days (Vázquez-López *et al*., 2020). The bacterium's ability to survive on dry surfaces for extended periods has further contributed to its global transmission in healthcare settings, facilitating outbreaks of MDR and XDR strains (Wong *et al*., 2017). The persistence of these strains in hospitals poses significant challenges for infection control and treatment protocols, as outbreaks are often associated with high morbidity, mortality, prolonged hospital stays, and increased healthcare costs. The limited therapeutic options available for treating these infections often force clinicians to resort to more toxic, second-line antibiotics like colistin, which, while effective in some cases, can lead to severe side effects and are not always successful in eradicating infections

(Falagas *et al*., 2009). Furthermore, the organism's capacity for biofilm formation is particularly concerning as it facilitates both chronic persistence on hospital surfaces and resistance to standard disinfection methods, greatly enhancing its transmissibility and complicating infection control efforts (Perez *et al*., 2007). Additionally, biofilms also protect bacteria from the host immune response and antibiotic treatments, contributing to the high rates of treatment failures (Coyne *et al*., 2011).

A range of genetic and functional adaptations that underpin the pathogenicity of *A. baumannii* have been identified. A study that looked at over 3,000 *Acinetobacter* genomes identified evolutionarily stable gene clusters (ESGCs) were conserved within the pathogenic clades of *A. calcoaceticus-baumanii* (ACB) complex (Djahanschiri *et al*., 2022). These gene clusters reveal critical aspects of metabolic pathways, regulatory networks, and functional modules that contribute to the pathogenicity of *A. baumannii*. Among these, the LuxR/LuxI quorum sensing system plays a critical role. Quorum sensing, which includes a signaling molecule synthase (LuxI) and a receptor protein (LuxR), allows the bacteria to regulate gene expression collectively and is critical to biofilm formation. This system is further enhanced in *A. baumannii* by the production of acyl-homoserine lactones (AHLs), which act as intermediate messengers, strengthening its capacity to form biofilms, a critical factor in chronic infections and antibiotic resistance (Niu et al., 2008). This adaptation enhances *A. baumannii's* persistence in hospital environments and its resistance to treatments.

The ability to acquire essential micronutrients like iron and zinc is vital for the survival and virulence of *A. baumannii* in the nutrient-limited environment of the human body. The bacterium expresses high-affinity siderophore systems to sequester iron from the host, supporting bacterial growth and promoting the expression of other virulence factors (Wong *et al*., 2017). Additionally, *A. baumannii* has evolved to utilize a wide range of carbon sources provided by the human host, highlighting its metabolic flexibility. The ability to metabolize kynurenine, a substance produced by humans to modulate the immune response, is unique to the ACB clade and suggests a mechanism by which *A. baumannii* can interfere with host immunity (Djahanschiri *et al*., 2022).

The outer membrane proteins of *A. baumannii*, including the well-characterized Outer membrane protein A (OmpA), are crucial for its virulence. These specific porins and

efflux pump proteins not only facilitate the uptake of nutrients but also contribute to AMR by actively expelling a broad spectrum of antibiotics, reducing therapeutic efficacy (Marchand *et al*., 2004). Moreover, the presence of a polysaccharide capsules enhances the bacterium's ability to evade host immune surveillance mechanisms such as phagocytosis and complement-mediated killing, providing a further advantage in surviving hostile host environments (Russo et al., 2019). Enzymatic factors such as phospholipases and proteases further augment the pathogenic potential of *A. baumannii* by disrupting host cell membranes and modulating immune responses, facilitating deeper tissue invasion and spread (Coyne *et al*., 2011). These multifactorial virulence strategies underscore the complexity of infections caused by *A. baumannii* and highlight the critical need for innovative approaches to effectively manage and prevent these challenging healthcare-associated infections.

1.3 Antimicrobial-Resistance in *Acinetobacter baumannii*

The rise of *A. baumannii* as a major nosocomial pathogen is a global issue, largely due to its established capacity to develop resistance to multiple classes of antibiotics. This resistance presents significant challenges to healthcare systems around the world, making infections difficult to treat and control. *A. baumannii* is particularly known for its ability to acquire diverse resistance mechanisms, resulting in MDR and XDR that are resistant to nearly all commercially available antibiotics (Hamidian & Nigro, 2019). Since the 1980s, the incidence of resistant *A. baumannii* infections has surged globally, particularly in hospital settings. In 2009, surveillance data from over 100 centers worldwide indicated widespread resistance to ceftazidime, with 61% and 67% were resistant to ciprofloxacin. Additionally, resistance to carbapenems and tobramycin is on the rise (Rhomberg & Jones, 2009). A more recent global study, which analyzed 4,320 *A. baumannii* isolates collected between 2016 and 2018, found significant regional differences in resistance rates, with overall global resistance to meropenem was 67%, with the highest rate (83%) in the Africa/Middle East region (Seifert *et al*., 2022). Similar variations were noted for levofloxacin and amikacin, with global resistance rates of 71% and 57%, respectively. North America had the lowest resistance rates for meropenem (36%), levofloxacin (45%), and amikacin (22%). Colistin resistance remained low across all regions, ranging from 1.2% to 7.3%. These findings emphasize the urgent need for ongoing surveillance and the

development of new treatment options due to the high resistance rates, particularly in the Africa/Middle East and Latin America regions.

The ability of *A. baumannii* to develop resistance through various mechanisms, including β-lactamase production, efflux pump utilization, and alterations in membrane permeability, underpins its persistence and prevalence in healthcare facilities (Kyriakidis *et al*., 2021). Among the β-lactamases, enzymes such as AmpC cephalosporinases, oxacillinases (OXA), and metallo-β-lactamases (MBLs) play particularly crucial roles in conferring resistance to a broad range of β-lactam antibiotics (Bonomo & Szabo, 2006; Mugnier *et al*., 2008). These enzymes hydrolyze β-lactam antibiotics, including penicillin's, cephalosporins, and carbapenems, rendering them ineffective (Higgins *et al*., 2010; Peleg *et al*., 2008). Additionally, *A. baumannii* utilizes multiple efflux pump systems, such as the AdeABC, AdeIJK, and AdeFGH pumps, which actively expel antibiotics from the bacterial cell, reducing intracellular drug concentrations (Coyne *et al*., 2011). Mutations in genes encoding antibiotic target sites, such as DNA gyrase and topoisomerase IV, further contribute to resistance by decreasing the binding affinity of antibiotics like fluoroquinolones (Vila *et al*., 1997).

In New Zealand, the epidemiology of carbapenem-resistant *A. baumannii* (CRAb) reveals a troubling trend. From 2010 to 2018, 73% of carbapenem-resistant isolates were detected from 2015 onwards, with a significant proportion linked to prior overseas hospitalizations, particularly in Fiji and Samoa (Blakiston *et al*., 2022). The ST2 clonal lineage, a major driver of antimicrobial resistance globally, further complicates treatment efforts due to its rapid acquisition and dissemination of resistance genes. *A. baumannii's* persistence in healthcare settings, aided by its ability to form biofilms and survive on surfaces, results in severe clinical outcomes, including prolonged hospital stays and increased healthcare costs (Lin & Lan, 2014). These factors underscore the critical need for novel therapeutic approaches, such as targeting the bacterium's oxidative stress response mechanisms, to effectively combat this resistant pathogen.

1.4 Cellular Oxidative Stress and L-Cysteine

L-cysteine is a pivotal amino acid in bacterial physiology, serving as a cornerstone for various essential cellular processes. It is integral to the synthesis of vital thiol/sulfur-

containing biomolecules such as iron-sulfur cluster proteins, lipoic acid, L-methionine, thiamine, biotin, and coenzyme A, all of which are crucial for metabolic functions and cellular integrity (Aguilar-Barajas *et al*., 2011; Kessler, 2006; Kredich, 2008). Moreover, L-cysteine is vital for transforming sulfur from external sources into cellularly accessible forms, underscoring its importance in bacterial survival and adaptation. L-cysteine is also a precursor for the synthesis of glutathione (GSH), a major cellular thiol antioxidant (Walsh *et al*., 2020). Upon host infection *A. baumannii* is exposed to environments with high levels of reactive oxygen species (ROS) such as hydrogen peroxide (H_2O_2) (Y. Zhao et al., 2023), superoxide anions (O_2^-), and hydroxyl radicals (·OH). These ROS can cause significant damage to cellular components including DNA, proteins, and lipids. The production of ROS is a key defense mechanism employed by the host immune system, particularly through the rapid oxidative burst generated by polymorphonuclear neutrophils (PMNs) and macrophages to eliminate invading pathogens (Juttukonda *et al*., 2018).

To survive and proliferate in such a hostile environment, *A. baumannii* has evolved robust oxidative stress response mechanisms (Gebhardt *et al*., 2020). Central to *A. baumannii*'s defense against oxidative stress is its ability to utilize L- cysteine effectively. L-cysteine is crucial not only for synthesizing GSH but also for producing other reducing agents like thioredoxin, which are essential for mitigating intracellular oxidants (Carmel-Harel & Storz, 2000; Kredich, 2008). GSH, synthesized from L-cysteine by glutathione reductase, plays a critical role in scavenging free radicals and preventing unwanted oxidation of cellular components (Meister & Anderson, 1983). By maintaining robust glutathione levels, *A. baumannii* can neutralize ROS, thus preventing damage to its DNA, proteins, and lipids. Another way *A. baumannii* withstands oxidative stress is by physical adaptations and virulence factors. For instance, the bacterium employs various adhesion molecules such as fimbriae and outer membrane proteins to attach to host tissues and surfaces. Fimbriae facilitate binding to biotic surfaces like bronchial epithelial cells, aiding in the colonization of the respiratory tract (Seifert *et al*., 1993). This initial adhesion is crucial for the pathogen's ability to resist shear forces in the host environment and establish a stable niche. Moreover, *A. baumannii* forms biofilms, which are complex communities of bacteria that adhere to surfaces and are encased in a self-produced extracellular matrix. Biofilm formation is critical for colonization and survival under harsh conditions. Biofilm-associated protein (Bap) is essential for biofilm maintenance

and maturation, facilitating adherence to cells and enhancing the bacterium's ability to resist desiccation (Richards *et al*., 2015). OmpA also plays a significant role in biofilm integrity and adherence to epithelial cells. OmpA induces apoptosis in host cells by entering the cell and stimulating the release of cytochrome c and apoptosis-inducing factor, while also helping to evade the host immune response by binding FactorH, an inhibitor of the alternative complement pathway (Richards *et al*., 2015). The alternative complement pathway is part of the immune system that helps clear pathogens by promoting inflammation and phagocytosis. By binding FactorH, *A. baumannii* inhibits this pathway, thereby reducing its chances of being attacked by the host immune system.

Approximately one-third of *A. baumannii* strains produce a polysaccharide capsule known as the K1 capsule. This capsule works in conjunction with cell wall lipopolysaccharides to prevent complement activation and delay phagocytosis by immune cells, providing both physical protection and immune evasion capabilities (Kaplan *et al*., 1985). Additionally, this bacterium possesses an efficient siderophore-mediated iron acquisition system that allows it to survive in iron-deficient conditions. The bacterium produces acinetobactin, a catechol siderophore, which sequesters iron from the host, ensuring its availability for bacterial growth and metabolism (Eijkelkamp *et al*., 2011). The biosynthesis of acinetobactin and other siderophores involves several cysteine-dependent enzymes, highlighting the importance of L-cysteine in these processes.

1.5 Sulfate and Thiosulfate Transport in *Acinetobacter baumannii*

The *de novo* biosynthesis of L-cysteine is a well-conserved pathway across bacteria and higher plants (Jeelani *et al*., 2017; Yi *et al*., 2013), playing a crucial role in making inorganic sulfur available to organisms. In *A. baumannii*, sulfur assimilation and cysteine synthesis are integral for survival and pathogenicity. The bacterium assimilates inorganic sulfur sources like sulfate and thiosulfate from its environment, which are transported into the cell via specific transporters (Gebhardt *et al*., 2020; Guédon & Martin-Verstraete, 2006). Sulfate is the preferred sulfur source for many organisms and is the second most abundant soluble oxyanion in bacterial cells after phosphate (Silver & Walderhaug, 1992). *A. baumannii* utilizes two main classes of sulfate transporter proteins: the ATP-binding cassette (ABC) superfamily and the major facilitator superfamily (MFS). The CysPUWA family, part of the ABC superfamily, is a high-affinity transporter system comprising

CysP, the periplasmic sulfate-binding protein; CysU and CysW, the membrane-bound components forming the channel for sulfate transport; and CysA, the ATPase that provides energy through ATP hydrolysis (Figure 1.1) (Aguilar-Barajas *et al*., 2011; Hicks *et al*., 2022). This system ensures efficient uptake of sulfate even in low concentrations, making it crucial for the bacterium's adaptability in various environments. Additionally, MFS transporters facilitate sulfate ion movement across the cell membrane using ion gradients. These secondary transporters provide an alternative route for sulfate uptake, complementing the high-affinity ABC transporters. Genomic analyses of *A. baumannii* have identified genes associated with both ABC and MFS transporter families, underscoring their importance in sulfate assimilation (Gebhardt *et al*., 2020; Pokhrel *et al*., 2023).

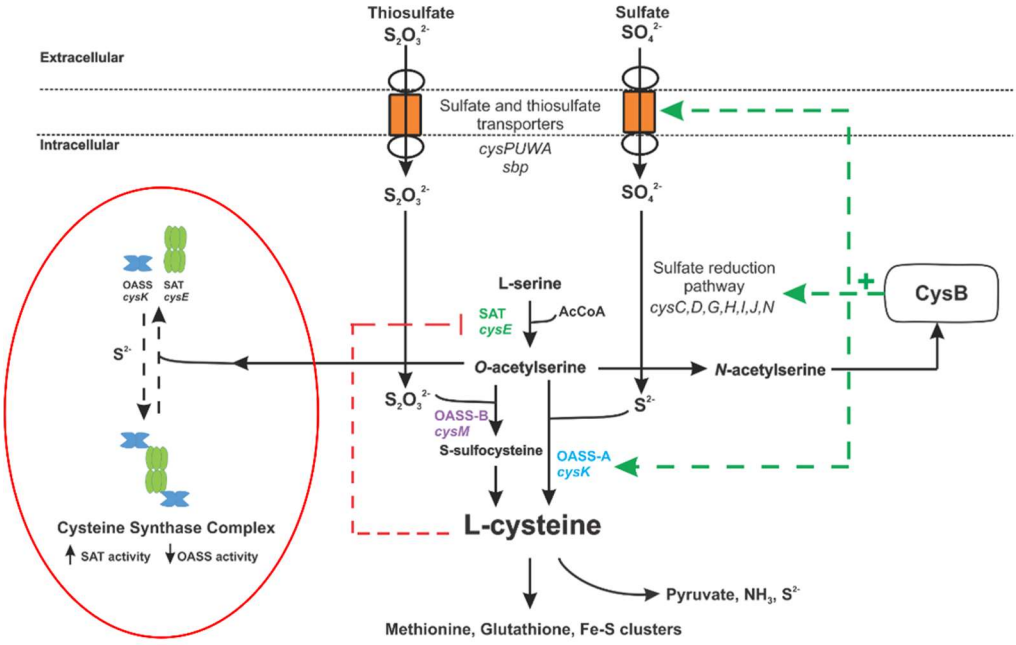

Figure 1.1: Overview of sulfur acquisition and assimilation pathways in bacteria.

Inorganic sulfur uptake and assimilation pathways converge to be separately condensed with *O*-acetylserine to form cysteine. Highlighted in red is the formation of the cysteine synthase complex in the cysteine biosynthesis pathway. Figure adapted from (Hicks *et al*., 2022).

Once inside the cell, sulfate is reduced to sulfide through a series of enzymatic reactions, which is then incorporated into L-cysteine (section 1.5.1). This pathway is essential for synthesizing vital biomolecules and maintaining cellular redox balance, particularly under oxidative stress conditions (Gebhardt *et al*., 2020; Guédon & Martin-Verstraete, 2006).

1.5.1 Reduction of Sulfate to Sulfide

In many bacteria, including *E. coli* and *S. typhimurium*, sulfate assimilation involves a series of enzymatic steps that convert sulfate (SO_4^{2-}) to sulfide (H_2S). Typically, this pathway includes the conversion of sulfate to adenosine 5'-phosphosulfate (APS) by ATP sulfurylase (CysDN), followed by the reduction of APS to sulfite (SO_3^{2-}) by APS reductase (CysH), and then the reduction of sulfite to sulfide by sulfite reductase (CysIJ) (Kredich, 2008). In most Gram-negative bacteria, APS is further phosphorylated to phosphoadenosine 5'-phosphosulfate (PAPS) by APS kinase (CysC), which serves as an intermediate in the pathway before being reduced to sulfite. However, *A. baumannii* and many non-enteric bacteria lack the APS kinase (*cysC*) gene, which means PAPS is not an intermediate in this pathway. Instead, it uses APS reductase (CysH) directly to reduce APS to sulfite (Bick *et al*., 2000). Additionally, *A. baumannii* lacks a CysJ homolog, so the reduction of sulfite to sulfide is carried out solely by the NADPH-sulfite reductase subunit CysI (Pokhrel *et al*., 2023).

1.5.2 Cysteine Biosynthesis Pathway

Cysteine is synthesized by two enzymes: serine acetyltransferase (CysE/SAT, EC 2.3.1.30) and *O*-acetylserine sulfhydrylase (CysK/OASS, EC 2.5.1.47). The first step of the pathway L-serine is acetylated by CysE through an acetyl-CoA dependent reaction producing the intermediate *O*-acetylserine (OAS). The second step OAS is condensed by CysK that displaces the acetoxy group with bisulfide to produce L-cysteine. The pathway is feedback regulated by its product cysteine (Figure 1.2) (Kredich et al., 1969).

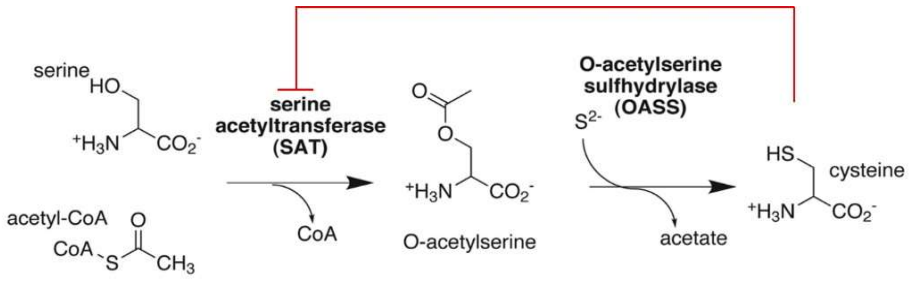

Figure 1.2: Overview of cysteine biosynthesis.

Two step bienzymatic pathway of cysteine biosynthesis. First step is catalyzed by CysE (SAT) producing the intermediate *O*-acetylserine and the second step catalyzed by CysK (OASS). The red line indicates the feedback inhibition of CysE by cysteine. Figure adapted from (Yi *et al*., 2013).

The critical role of CysE in cysteine biosynthesis is well-established. In bacterial species such as *E. coli* and *Haemophilus influenzae*, deletion of the *cysE* gene results in cysteine auxotrophy, meaning the bacteria are unable to synthesize cysteine without supplementation in the growth medium (Akerley et al., 2002; Warr et al., 2019). This consistency across multiple bacterial species underscores the essential function of CysE in *de novo* cysteine biosynthesis. Although *A. baumannii* contains two isoforms of CysE, their specific roles and biological significance remain unclear, highlighting the need for further investigation into their contributions to cysteine biosynthesis.

1.6 Regulation of Cysteine Biosynthesis

The regulation of cysteine biosynthesis in *A. baumannii* involves multiple layers of control to ensure sulfur assimilation and cysteine production align with the cell's metabolic needs and environmental availability. Central to this regulation are the genes encoding the enzymes serine acetyltransferase (*cysE*) and *O*-acetylserine sulfhydrylase (*cysK*), which catalyze the two-step synthesis of cysteine from serine and sulfide. One of the two ways this pathway is regulated is at the protein level by feedback inhibition via L-cysteine. High intracellular levels of L-cysteine inhibit the activity of CysE (Benoni, *et al*., 2017; Johnson *et al*., 2004). This prevents the surplus production of cysteine, which can be detrimental to bacteria. This mechanism is well conserved across bacteria and plants (Benoni, Beck, *et al*., 2017; Chronis & Krishnan, 2004; Johnson *et al*., 2004; Kredich & Tomkins, 1966). In addition to feedback inhibition, the regulation of cysteine biosynthesis involves the formation of the cysteine synthase complex (CSC), composed of CysE and CysK (Kredich *et al*., 1969; Kredich & Tomkins, 1966). The interaction between these enzymes is essential for modulating their activity and stability, fine-tuning the cysteine biosynthesis pathway.

1.6.1 The Cysteine Synthase Complex

The CysE and CysK enzymes bind to form the bienzymatic CSC, that is closely connected to the control of sulfur metabolism in the cell (Hicks & Mullholland, 2018). The complex exhibits a high degree of conservation amongst bacterial species and distinguishes itself from other macromolecular structures by not directing substrates towards other enzymes. When in the complex CysK activity is inhibited, due to the C-terminal tail of CysE binding to and occluding the CysK active site (Campanini *et al*., 2005; Huang *et al*., 2005;

Mino *et al*., 2000). Conversely, CysE is catalytically active in the CSC, although is sensitive to feedback inhibition from L-cysteine. Moreover, in complex formation CysE is protected from cold inactivation and proteolysis, thus stabilizing the protein (Kumaran *et al*., 2009). The intermediate OAS in millimolar amounts dissociates the complex (Kredich *et al*., 1969; Wang & Leyh, 2012). The CSC is thought to assemble in one of two ways with either one active site or both active sites of each CysK dimer occupied by the C-terminus of CysE. In the first model (Figure 1.3A), the C-terminus of CysE binds to one active site of each CysK dimer, potentially allowing for partial enzymatic activity of CysK. In the second model (Figure 1.3B), both active sites of the CysK dimer are occupied by the C-terminus of CysE, leading to a complete inhibition of CysK activity.

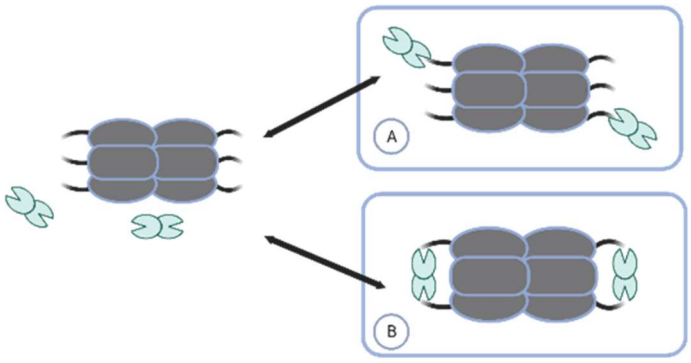

Figure 1.3: CSC possible binding models.

Two possible binding models for the CSC, (A) one active site of each CysK (green) dimer is occupied by the C-terminus (black) of CysE (gray), (B) both active sites are occupied. Figure made using Biorender.

Recent studies have further revealed the structural organization of the CSC using a combination of small-angle X-ray scattering (SAXS) and protein painting techniques (Rosa *et al*., 2019). This approach has demonstrated significant insights into the quaternary structure of the CSC in solution, providing a more comprehensive understanding of its assembly and function. SAXS data have shown that only one active site of the CysK dimer is involved in direct interaction with CysE, supporting a model (Figure 1.3A) where one CysK active site is occupied by the C-terminus of CysE, while the other site remains accessible but is allosterically inhibited. This partial inhibition model is consistent with previous functional data indicating that CysK retains about 10% of its activity in the presence of a molar excess of CysE (Benoni, *et al*., 2017). Moreover, protein painting has identified specific interaction hotspots on CysK involved in complex formation. These include residues lysine K226, K87, and K102, which become buried

upon complex formation, suggesting a conformational change in CysK that stabilizes the dimer interface and supports allosteric communication between the two CysK subunits. Additionally, on CysE, residue arginine R242, part of the conserved PARIV sequence, plays a crucial role in binding to CysK, indicating its involvement in the critical binding interface (Rosa *et al*., 2019).

CSC binding has been confirmed in *E. coli* (Benoni, *et al*., 2017; Mino *et al*., 1999), *H. influenzae* (Salsi *et al*., 2010) and also in plants (Yi *et al*., 2013). In *E. coli* size exclusion chromatography was used to monitor CSC formation and found that CysE elutes at a molecular mass corresponding to its hexameric form, while CysK forms a homodimer (Figure 1.4). The stoichiometry of the CSC was determined to be one CysE hexamer binding to two CysK dimers, a 3:2 protomer ratio. This specific stoichiometric configuration is consistent with previously determined models from other bacterial species (Kredich *et al*., 1969; Kumaran *et al*., 2009). The study also found that CysE within the CSC exhibited an apparent activation at high L-serine concentrations, relieving substrate inhibition and feedback inhibition by L-cysteine. The dissociation constant for the CSC was determined to be in the nanomolar range, indicating a high-affinity interaction (Benoni, *et al*., 2017).

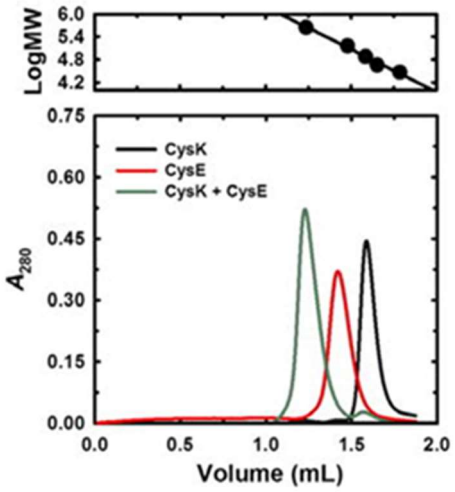

Figure 1.4: Analytical gel filtration of the CSC from *E. coli*

Gel filtration chromatograph of CSC (CysE + CysK). The panel above illustrates molecular mass calibration using carbonic anhydrase (29 kDa), ovalbumin (45 kDa), conalbumin (75 kDa), glyceraldehyde-3-phosphate dehydrogenase (144 kDa), and ferritin (440 kDa). Figure adapted from (Benoni, *et al*., 2017)

This was additionally confirmed in our lab through a co-lysis process followed by gel filtration chromatography. The gel filtration purification of CSC (Figure 1.5) showed that the large peak at 64.8 ml corresponds to a high yield and purity of CSC, as indicated by the doublet bands visible in the SDS-PAGE gel. The broadness of the peak could be due to variations in the complex's stoichiometry.

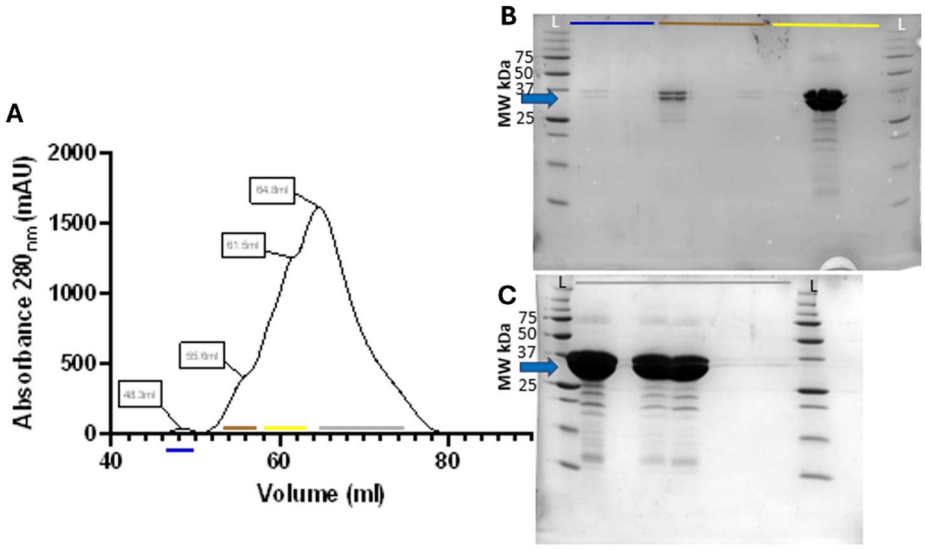

Figure 1.5: Gel filtration purification of CSC using co-lysis method

A) S200 16/60 Superdex gel filtration chromatogram shows elution of a large peak at 64.8 ml. B & C) 12% SDS-PAGE gel shows high yield and purity of CSC (brown bar, yellow bar, and grey bar). CSC proteins (CysK top band, 34.5 kDa, CysE bottom band 29.5 kDa) are labeled with a blue arrow, Plus Protein Standards (L) in kDa are labeled. Purification was carried out at room temperature.

1.6.2 Genetic Regulation of Sulfate Transport and Cysteine Biosynthesis

Genomic analysis of *A. baumannii* revealed that the *cysE* and *cysK* genes are often located in close proximity, suggesting coordinated regulation. Regulatory elements, such as promoters and operons, control the expression of these genes in response to sulfur availability and cellular demand (Gebhardt *et al*., 2020; Pokhrel *et al*., 2023). In *E. coli,* the regulation of sulfate transport and cysteine biosynthesis involves a sophisticated network of transcriptional regulators such as CysB and Cbl (CysB-like) proteins (Aguilar-Barajas *et al*., 2011; Kredich, 2008). CysB, a LysR-type transcriptional regulator, activates the transcription of genes involved in sulfate assimilation and cysteine biosynthesis in response to low intracellular cysteine levels, in the presence of its inducer, OAS (Henikoff *et al*., 1988). It also serves a dual role, as negative regulator of its own expression. However, in *A. baumannii*, an obvious CysB homolog is absent (Pokhrel et

al., 2023). Instead, the genome encodes a Cbl homolog, which shares 50% identity with the *E. coli* Cbl proteins. Cbl acts as a global regulator, controlling the expression of genes involved in the acquisition and reduction of various sulfur sources (Pokhrel *et al*., 2023). This includes the cysPTWA operon and the *cysD* and *cysN* genes, which are essential for sulfate uptake and reduction. Another key regulator in *A. baumannii* is GigC, also part of the LysR family transcription regulator that shares only 23% identity with *E. coli* CysB. GigC acts as both an activator and a repressor. It activates the expression of the *cysI* and *cysDN* genes, which are involved in the reduction of sulfate to sulfide and represses the expression of the *cysH* gene (Gebhardt *et al*., 2020). Despite these insights, it is not yet clear what regulates the expression of the genes encoding CysE and CysK in *A. baumannii* (Pokhrel *et al*., 2023). This indicates gaps in our understanding of the full regulatory network governing sulfur metabolism in this pathogen.

1.7 CysE

1.7.1 Structural Characteristics of CysE

Serine acetyltransferase (SAT), also known as CysE, is part of the *O*-acetyltransferase family (EC 2.3.1.30) found in both plants and bacteria. Despite significant sequence variation, there is strong structural conservation between bacterial and plant SAT enzymes (Olsen *et al*., 2004; Yi *et al*., 2013). This family is characterized by a hexapeptide repeat [LIV]-[GAED]-X_2-[STAV]-X, which forms the unique left-handed β-helix (LβH) typical of this family (Figure 1.6, black box) (Johnson *et al*., 2005; Raetz & Roderick, 1995). CysE enzymes contain two structural domains: an N-terminal α-helical domain and a C-terminal LβH domain. The LβH domain is shaped like a triangular prism and assembles with two other monomers to form a trimer (Johnson *et al*., 2005). These trimers further dimerize through hydrophobic interactions at their N-terminal faces, resulting in a hexameric structure (Pye *et al*., 2004). Notably, CysE enzymes are the only members of the hexapeptide acyltransferase family that form a hexameric configuration, as opposed to the more common trimeric form (Johnson *et al*., 2005). This hexameric arrangement is crucial for the formation of the bi-enzyme CSC and regulation of sulfur metabolism (Benoni, *et al*., 2017; Mino *et al*., 1999; Wirtz & Hell, 2006).

Using Clustal Omega (Madeira *et al*., 2024) a sequence alignment was generated with the six bacterial CysE homologs and analyzed with ESPript 3.0 (Figure 1.6) (Robert & Gouet,

2014). The long form of CysE from *A. baumannii* shows low sequence similarity when compared to CysE homologs *Yersinia pestis* (24.1%), *E. coli* (23.1%), and *E. cloacae* (22.2%), but moderate sequence similarity with *M. tuberculosis* (32.1%) and the short form of CysE from *A. baumannii* (28.6%). Interestingly, despite the sequence variation, critical functional regions such as the hexapeptide repeat (Figure 1.6, highlighted in black box) and highly conserved active site residues (Figure 1.6, highlighted in blue boxes) are maintained across these homologs, suggesting that these regions are essential for the enzyme's catalytic activity and structural integrity. These conserved motifs underline the evolutionary pressure to retain key functional features necessary for the enzyme's role in cysteine biosynthesis, despite divergence in overall sequence similarity.

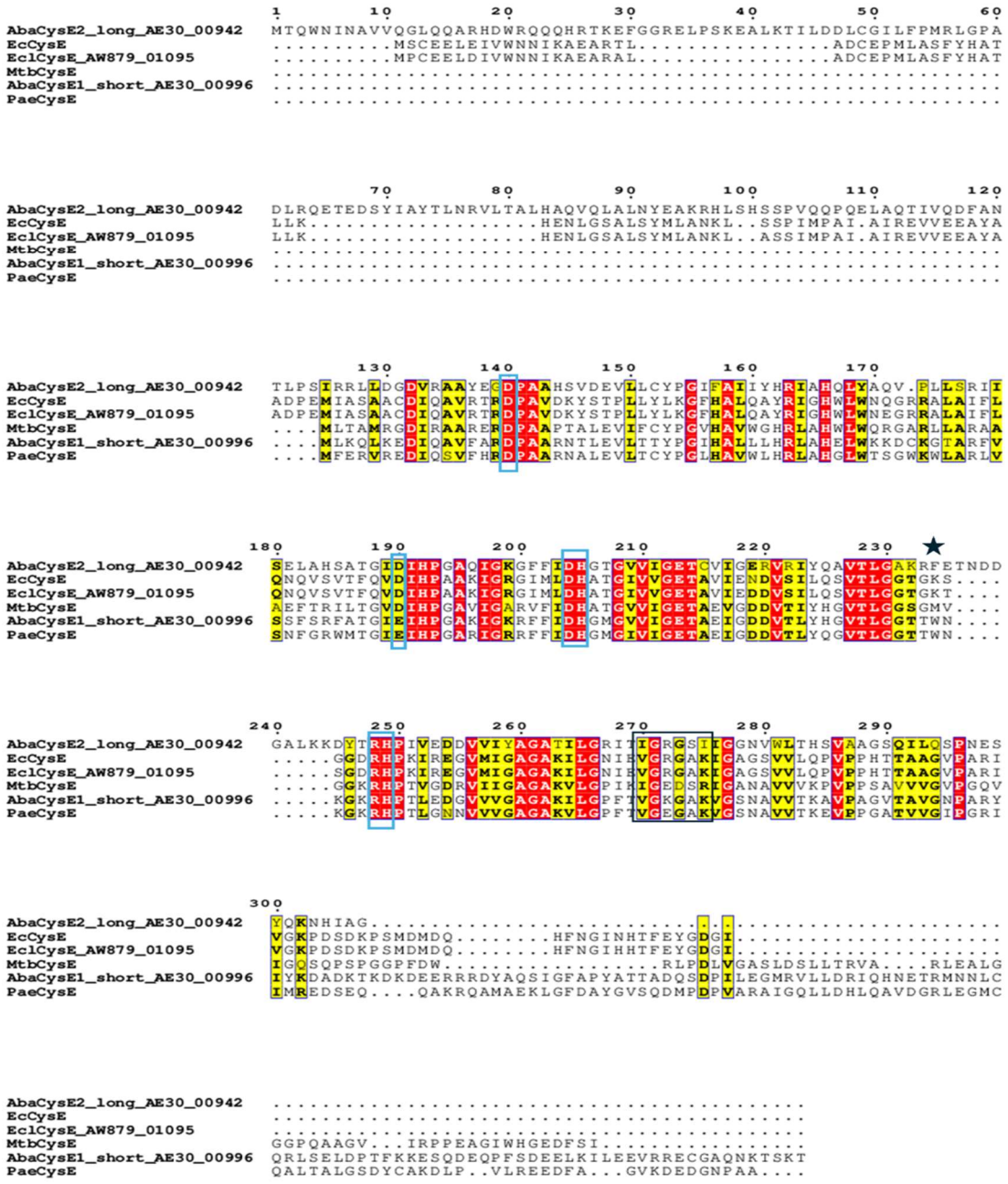

Figure 1.6: CysE peptide sequence alignment.

A. baumanii AE30_00942 long form peptide sequence was aligned to the following CysE homologs: *Y. pestis* (24.1% sequence similarity); *E. coli* (23.1% sequence similarity); *E. cloacae* (22.2% sequence similarity); *M. tuberculosis* (32.1 %sequence similarity); *A. baumannii* AE30_00996 short form (28.6% sequence similarity); *P. aeruginosa* (27% sequence similarity). Highly conserved residues are highlighted in red, and less conserved highlighted in yellow. Active site residues are in blue boxes, example of hexapeptide repeat in black box and black star above the sequence is the extended β-loop for AbaCysE2_long. Sequence alignment created using Clustal Omega. Figure created using ESPript 3 (Robert & Gouet, 2014).

A notable feature of the CysE structure is the flexibility of the C-terminal tail, which can adopt different conformations depending on the substrate bound. This flexibility is depicted in Figure 1.7, which illustrates the conformational changes in the C-terminal tail of CysE under different substrate-bound conditions. In the presence of L-serine, as seen in the CysE structure from *Glycine max* soybean (PDB: 4n69) (Figure 1.7A), the C-terminal tail is undefined, allowing substrate binding. Similarly, with CoA bound (PDB: 4n6b) (Figure 1.7B), the tail remains flexible. However, when L-cysteine is bound, as in the *E. coli* CysE structure (PDB: 1t3d), the C-terminal tail folds into a conformation that directly competes with the binding site of acetyl-CoA/CoA, thereby inhibiting the enzyme's activity (Figure 1.7C). This structural adaptation highlights the enzyme's regulation mechanism through feedback inhibition by L-cysteine, by preventing accidental acetylation of cysteine and maintaining sulfur metabolism balance.

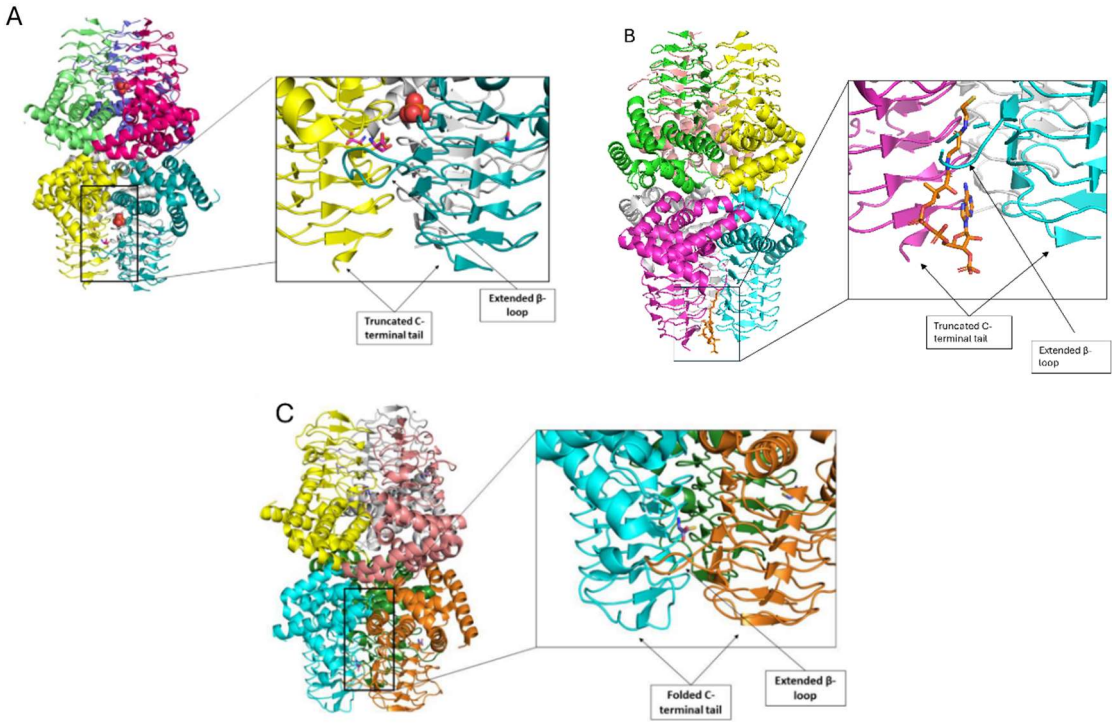

Figure 1.7: Conformation of C-terminal tail with different substrates bound of CysE

A) CysE from *Glycine max* soybean (PDB: 4n69) with L-serine bound (represented as pink sticks) and phosphate represented as spheres. B) CysE from soybean *G. max* (PDB: 4n6b) with CoA bound (represented as orange sticks). CysE from *E. coli* (PDB: 1t3d) with L-cysteine bound (represented as purple sticks). Image made in PyMOL.

The LβH family, such as CysE, possess a conserved histidine residue alongside a conserved aspartate, which is crucial for facilitating the acetyl-transfer reaction via acid-

base catalysis (Johnson *et al*., 2005). In *E. coli* CysE with L-cysteine bound the aspartate residue (Asp143) is position at 2.8 Å to the conserved histidine (His158), which is thought to convert the histidine into a strong base (Figure 1.8) (Pye *et al*., 2004). These conserved residues are crucial for the stabilization of L-cysteine within the active site.

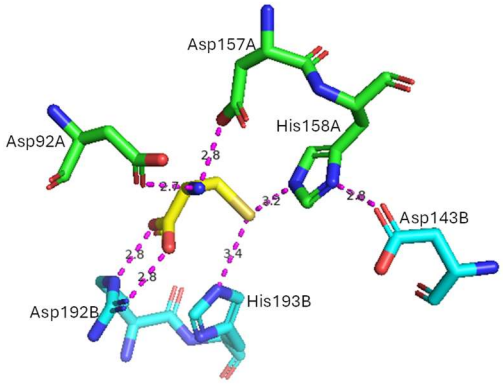

Figure 1.8: *E. coli* CysE active site residues with L-cysteine (PDB: 1t3d).

L-cysteine bound in active site denoted as yellow sticks. The active site residues are also displayed as sticks and are color-coded based on their respective chains: chain A residues are green, and chain B residues are cyan. The ionic interactions within the active site are depicted as magenta dashed lines, with the distances in angstroms. Figure created in PyMOL.

His158 facilitates the activation of the β-hydroxyl group of L-serine, enabling it to carry out a nucleophilic attack on the acetyl thioester of acetyl-CoA by functioning as a base and accepting a hydrogen from the hydroxyl group (Figure 1.9,highlighted in yellow and blue, respectively). This nucleophilic attack on acetyl CoA results in the formation of a ternary complex involving the enzyme, L-serine, and acetyl-CoA (E:L-serine:acetylCoA). Subsequently, histidine acts as a general acid, donating a hydrogen to the sulfur atom of acetyl-CoA, which causes the complex to break down and the products to be released. The critical role of these active site residues in catalysis has been confirmed through site-directed mutagenesis studies (Guan *et al*., 2008). Additionally, findings from solvent deuterium isotope effect experiments indicate that the formation of the E:L-serine:acetylCoA complex is the rate-limiting step in this reaction (Quinn & Sutton, 2011).

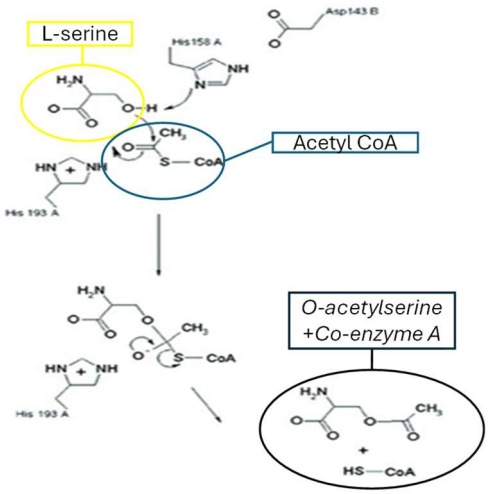

Figure 1.9: Mechanistic action of CysE in *E. coli*

Substrates L-serine and Acetyl-CoA are shown in yellow and blue, respectively. The reaction products, *O*-acetylserine and coenzyme A are circled in black. Figure adapted from (Pye *et al*., 2004).

1.7.2 CysE Kinetic Mechanisms

CysE catalyzes the first step in the biosynthesis of cysteine by transferring an acetyl group from acetyl-CoA to L-serine to form *O*-acetylserine. There have been considerable studies on whether this reaction follows a sequential mechanism or a ping-pong (double-displacement) mechanism. In a ping-pong mechanism, the enzyme releases one of the products before all substrates have fully bound, creating an enzyme intermediate during the process. On the other hand, a sequential mechanism requires both substrates to bind to the enzyme before any products are released. This can occur in either a random sequence, where the order of substrate binding and product release is flexible, or in an ordered sequence, where substrates must bind, and products are released in a specific order. Both mechanisms ultimately result in the formation of a ternary complex (enzyme:substrateA:substrateB) (Fersht, 2017). Earlier work suggested CysE follows a ping-pong mechanism, where an acetyl-enzyme intermediate is formed before the final product is released. This model implied that the enzyme processes each substrate sequentially in two distinct steps, without the simultaneous binding of both substrates (Leu & Cook, 1994). However, this theory was later challenged (Hindson & Shaw, 2003), who provided substantial evidence that CysE from *E. coli* operates through a random-order sequential mechanism. Their kinetic analyses and inhibition studies demonstrated that both substrates must bind to the enzyme, forming a ternary complex, without the involvement of a covalent intermediate, effectively ruling out the ping-pong mechanism.

Furthermore, CysE studies from *H. influenzae* reported that it uses an ordered sequential mechanism, where acetyl-CoA must bind first before L-serine (Johnson *et al.*, 2004) (Figure 1.10). This variation indicates that while the overall process is sequential, the order of substrate binding can differ between species. These differing views underscore the complexity of CysE's catalytic process, suggesting that kinetic behavior may vary depending on the experimental conditions or the specific organism. Understanding these mechanisms is critical for the development of antimicrobial strategies targeting CysE, particularly in combating pathogens like *A. baumannii*.

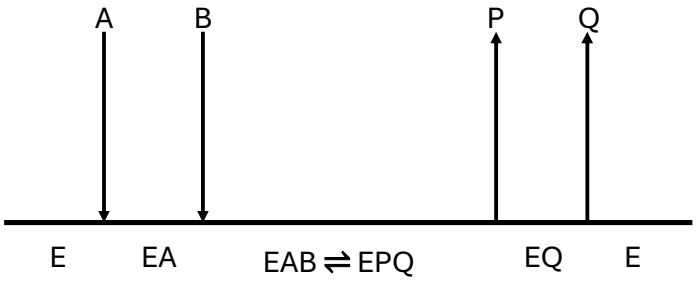

Figure 1.10: Ordered sequential mechanism for CysE from *H. influenzae*

The scheme here depicts that the substrate acetyl-CoA binds first (A), and substrate L-serine binds second (B), and the product co-enzyme A leaves first (P) followed by the product *O*-acetylserine (Q). A = acetyl-CoA, B = L-serine, EAB = enzyme and substrates complex, EPQ = enzyme and products complex, P = co-enzyme A, Q = *O*-acetylserine. Figure adapted from (Johnson *et al*., 2004)

1.8 Antimicrobial Targeting of CysE

The growing threat of antimicrobial resistance has spurred significant research into novel therapeutic targets, particularly within essential metabolic pathways unique to bacteria. One such promising target is the enzyme serine acetyltransferase (CysE), which catalyzes the rate limiting step in the *de novo* cysteine biosynthesis pathway. The antimicrobial targeting of CysE has garnered attention due to its critical role in bacterial survival, especially under conditions of oxidative stress, and its absence in mammals, making it an attractive target for selective antibiotic development.

Recent studies have explored the inhibition of CysE in various pathogenic bacteria, with encouraging results. In the context of methicillin-resistant *Staphylococcus aureus* (MRSA), researchers identified six potential CysE inhibitors, showing inhibitory effects on MRSA growth (Chen *et al.*, 2019). These compounds exhibited half-maximal

inhibitory concentrations (IC_{50}) ranging from 29.83 to 203.13 μM, with two compounds demonstrating strong antibacterial activity, comparable to the established antibiotic clindamycin. Notably, these inhibitors also hindered MRSA biofilm formation, underscoring their potential as novel anti-MRSA agents. CysE has also been studied as a potential drug target in *E. coli*, with computational screening methods leading to the identification of several inhibitors. Among these, the most promising candidate demonstrated moderate inhibitory activity, with an inhibition constant (K_i) of 72 μM, as confirmed through subsequent assays (Turnbull & Surette, 2010). More recently, work on CysE from *Neisseria gonorrhoeae* has yielded promising results, with the identification of a potent inhibitor exhibiting an IC_{50} value of 13 μM (Hicks et al., 2022). The progress in identifying and characterizing CysE inhibitors across various pathogenic bacteria highlights the enzyme's viability as a drug target. These findings strongly support the research focus on characterizing CysE from *A. baumannii*, particularly given the current gaps in our understanding of how this enzyme is regulated, the absence of experimental CysE 3D structures from this organism, and the intriguing presence of two distinct isoforms. Further exploration of these aspects could reveal critical insights into the enzyme's function and its potential as a drug target in combating AMR.

1.9 Fa'afaletui Research Framework

As a Samoan researcher, this study is intricately woven with rigorous scientific enquiry and deeply rooted in the principles of the Fa'afaletui framework. This is an Indigenous methodology, which emphasizes the importance of collective engagement and the integration of diverse perspectives to forge comprehensive knowledge (Goodyear-Smith & 'Ofanoa, 2022). Using the Fa'afaletui framework may provide a valuable lens for this research, offering a holistic and culturally grounded methodology that complements and enhances traditional scientific inquiry. This approach is especially relevant in addressing global challenges such as AMR, where understanding and solutions must transcend individual and cultural boundaries. By incorporating Fa'afaletui, this research process is not only scientifically thorough but also culturally resonant and ethically robust. Furthermore, it ensures that the research journey honors the Samoan principle of weaving together insights from various fale (houses), enriching the research landscape and enhancing the applicability of the findings. This framework will shape and guide the research, demonstrating the integration of scientific inquiry with cultural insights. This

culturally informed approach may provide a valuable lens for this research, offering a holistic and culturally grounded methodology that complements and enhances traditional scientific enquiry.

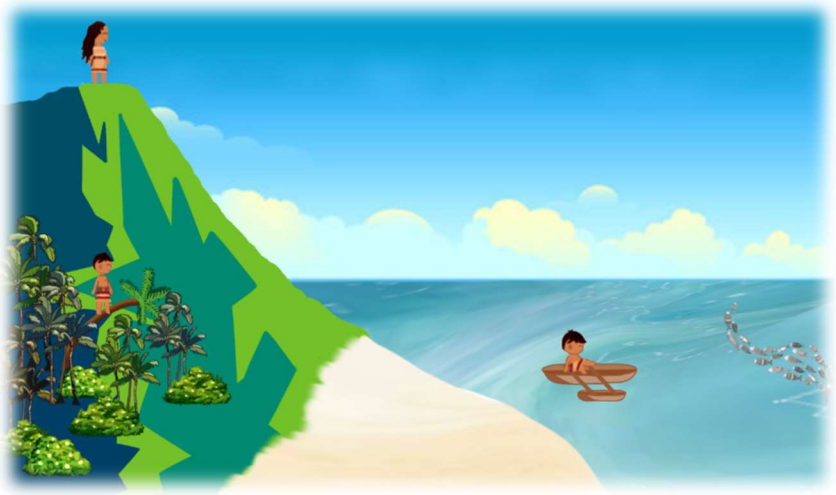

Figure 1.11: Fa'afaletui research framework

A Samoan research framework which translates to mean ‘ways of weaving together’ discussions from different fale (houses). This process integrates various knowledge levels within collective representation, enriching the Samoan worldview. Derived from the Pacific philosophy of connectedness, Fa’afaletui promotes culturally appropriate insight and intel gathering through a holistic approach. The framework includes three perspective: Mountain top view: this provides a comprehensive line of sight; Treetop view: This offers the management and operational perspective; Canoe view: This view is closest to the school of fish, representing those directly involved or affected by the environment (Tamasese *et al*., 2005). This depiction was created by Julia Seutatia -Tulua Usu, 2024.

1.10 Research Objectives

Mountain Top View: This research provides a comprehensive line of sight by characterizing a key enzyme in the *A. baumannii* cysteine biosynthetic pathway, CysE (EC 2.3.1.30). Understanding the biochemical and biophysical properties of CysE from *A. baumannii* will guide future research for the development of new antimicrobials and enhance our understanding of the pathogenicity of *A. baumannii*. The following objectives were set to achieve this:

Treetop View: This offers the management and operational perspective, ensuring the systematic achievement of the research goals through detailed planning and execution of experiments.

Canoe View: This view is closest to the school of fish, representing those directly involved or affected by the environment, emphasizing the hands-on experimental work and optimization processes necessary for the research.

Objective 1: Optimize Expression of *A. baumannii* Long and Short Form CysE
Optimize the expression of the long and short forms of CysE from *A. baumannii* to obtain sufficient yield for subsequent experiments and analyses.

Objective 2: Biochemical Characterization of CysE from *A. baumannii*
Investigate the serine acetyltransferase activity and L-cysteine inhibition of CysE from *A. baumannii*. This will involve adapting established kinetic assays to measure CysE activity and subsequent characterization of Michaelis-Menten kinetics, reaction mechanisms, and L-cysteine inhibition.

Objective 3: Structural characterization of CysE from *A. baumannii*
Determine the three-dimensional structure of CysE using protein crystallization and X-ray diffraction. This includes collecting an apoenzyme structure, as well as structures complexed with either substrate (L-serine), and the product feedback inhibitor L-cysteine. Perform small angle X-ray scattering (SAXS) analysis to provide additional insights into the structural properties of CysE in solution.

Chapter Two

Materials and Methods

2.1 Introduction

The biochemical characterization of the CysE enzyme from *Acinetobacter baumannii* is crucial for understanding its role in the cysteine biosynthetic pathway and its potential as a target for new antimicrobial strategies. This chapter details the materials and methods employed in this study, encompassing the optimization of enzyme expression, kinetic assays, structural analysis, and inhibition studies. Incorporating the Fa'afaletui framework into the research methodology was essential for ensuring that the study was both scientifically sound and culturally relevant. This Indigenous methodology emphasizes the importance of collective engagement and the integration of diverse perspectives, providing a holistic approach that complements traditional scientific inquiry. Through extensive review of research methodology literature by Indigenous researchers worldwide (Ryder *et al*., 2020; Wilson, 2008), and Pacific research methodologies, a significant gap was identified in the application of such methodologies within the field of molecular and cellular biology. This gap underscores the importance and innovation of integrating the Fa'afaletui framework in this study. The methodological choices were informed by both scientific rigor and the cultural insights gained through the Fa'afaletui framework, ensuring a comprehensive and culturally relevant approach. However, by using this methodology over other Pacific mythologies does not undermine or diminish their value but rather this integration aims to enhance the reliability and relevance of the findings, providing a solid foundation for future work.

2.2 Fa'afaletui Framework Methodology

The Fa'afaletui framework will be applied in this research through a structured approach that integrates collective engagement and diverse perspectives, aligned with the three core views: Mountain Top, Treetop, and Canoe.

Mountain Top View: Guidance from Pacific academics and Samoan elders will be sought to shape the research direction, ensuring it addresses antimicrobial resistance (AMR) with both scientific and cultural relevance. This approach provides a

comprehensive perspective on the significance of the CysE enzyme in *A. baumannii*.

Treetop View: Operational aspects will be managed to align experimental design with cultural principles. Collaboration with other researchers, especially those from Pacific communities, will ensure that the methodologies are both scientifically rigorous and culturally sensitive.

Canoe View: The hands-on experimental work will involve close collaboration with researchers to optimize conditions and interpret results. This phase emphasizes the importance of culturally appropriate communication and ensures that the research resonates with the values and needs of the community. Throughout the process, open dialogue with all stakeholders will be maintained, embodying the Fa'afaletui framework's principle of interconnectedness and ensuring that the research journey honors both scientific inquiry and cultural heritage.

2.3 Cloning of CysE for Expression in *Escherichia coli*

The *cysE* gene for the long form of *A. baumannii* (AE30_00942), the short form of *A. baumannii* (AE30_00996), *E. cloacae* (AW879_01095), *M. tuberculosis* (Rv2335), and *P. aeruginosa* (PA3816) were codon-optimized for *E. coli* and synthesized by Twist Bioscience (Appendix A). It was cloned into the pET28a plasmid using NdeI and XhoI restriction sites for expression with an N-terminal His-tag. Plasmids were transformed into chemically competent *E. coli* BL21 (DE3) cells. Positive transformants were selected by overnight incubation at 37 °C on Luria-Bertani (LB) agar (Appendix A.2) supplemented with 50 $\mu g.ml^{-1}$ kanamycin.

2.4 Long-term Storage of *E. coli* BL21 CysE Expression Strains

Seeder cultures were initiated by inoculating a single colony from a transformation plate into 10 ml LB broth containing 50 $\mu g.ml^{-1}$ kanamycin and were incubated overnight at 37 °C with shaking at 180 rpm. Glycerol stocks were then prepared by mixing 0.5 ml of the seeder culture with an equal volume of sterile 50% glycerol (w/v), and were stored at -80 °C.

2.5 Optimization of Protein Expression in *E. coli* BL21

Preliminary small-scale expression studies were initially carried out based on previous work done on *E. coli* CysE (Jessicca Usu, University of Waikato). These studies involved

inoculating from a single colony (16h growth LB plate + 50 μg.ml^{-1} kanamycin, 37 °C) into 10 ml LB broth supplemented with 50 μg.ml^{-1} kanamycin and incubating at 37 °C, 160 rpm for 3 hours. Once cultures reached mid-log phase (optical density at A_{600} = 0.5-0.7), expression was then induced with the addition of 1 mM isopropylthio-β-D-galactosidase (IPTG) and the cultures were incubated overnight at 22 °C, 160 rpm shaking. For constructs that did not yield high levels of protein, further optimization was pursued by varying glucose concentrations (0%, 1%, and 2% w/v final concentration) and incubation temperatures (22 °C, 30 °C, and 37 °C). Subsequent small-scale expression cultures were prepared by inoculating 100 μl of seeder cultures into 10 ml LB broth supplemented with 50 μg.ml^{-1} kanamycin, shaking at 160 rpm for 3 hours, followed by induction with 1 mM IPTG and overnight incubation at temperatures of 22 °C, 30 °C, and 37 °C, shaking at 160 rpm. Expression cultures were centrifuged at 9,000 rpm for 20 minutes at 4 °C, and the supernatant was discarded.

2.5.1 Nickel Pulldown for Small-Scale Expression Analysis

Nickel pull downs were conducted to verify the presence of the target protein from small-scale expression trials. The pellet was resuspended in 1 ml of lysis buffer (50 mM Tris pH 8.0, 200 mM NaCl, 20 mM imidazole), half a cOmplete™ Mini, EDTA-free Protease Inhibitor tablet (Roche, Switzerland) and transferred to a sterile 1.5 ml Eppendorf tube. The samples were sonicated using a QSonica Q700 (Newtown, USA) with a 2 mm microtip. Sonication settings included 1.0-second bursts alternating with 1.0-second rests for a total of 1.0 minute at an amplitude of 4. Following sonication, the samples were centrifuged at 13,000 rpm at 4 °C for 20 minutes. For analysis of each expression trial, 3 μl of the insoluble pellet and soluble supernatant were mixed with 12 μl of lysis buffer and 5 μl of 4x SDS loading dye (Appendix B.2).

Nickel resin (Sephacryl® High Performance by Sigma-Aldrich) was pre-equilibrated by aliquoting 50 μl into 1.5 ml tubes (one aliquot per expression trial) and washed with 1 ml of lysis buffer. The resin was then centrifuged at 1,000 rpm for 30 seconds at room temperature to pellet, and the supernatant was discarded. The soluble cell lysate was then added to the pre-equilibrated resin, mixed thoroughly in a thermomixer for 10 minutes at 850 rpm at room temperature, and subsequently centrifuged at 1,000 rpm for 30 seconds. The supernatant was carefully removed, and the resin underwent three wash steps with

1 ml of lysis buffer each, followed by centrifugation at 1,000 rpm for 30 seconds at room temperature. After the final wash, the supernatant was discarded, and 50 µl of 4x SDS loading dye was added to the resin and mixed well.

2.6 Large-Scale CysE Expression Cultures

Large-scale expression cultures were initiated by inoculating 10 ml of seeder culture (prepared as per section 2.4) into 500 ml of LB broth with 50 $\mu g.ml^{-1}$ kanamycin. Cultures were incubated at 37 °C, 160 rpm until mid-log phase (optical density at A_{600} = 0.5-0.7). Protein expression was induced by adding IPTG (to final concentration of 1 mM), then cultures were incubated overnight at 22 °C, 160 rpm. Following this, the cultures were centrifuged at 4,000 rpm for 20 minutes at 4 °C, and the supernatant was discarded. The remaining cell pellet was resuspended in 20 ml of lysis buffer (50 mM Tris pH 8.0, 200 mM NaCl, 20 mM imidazole) and transferred to a 50 ml tube. This resuspension was then centrifuged for an additional 20 minutes at 9,000 rpm at 4 °C. Following centrifugation, the supernatant was discarded, and the pellet stored at -80 °C.

2.7 Purification of CysE

CysE was purified using established methods for *Neisseria gonorrhoeae* CysE (Keely Oldham, University of Waikato) utilizing immobilized metal affinity (IMAC) and gel filtration chromatography. Solubility was evaluated with SDS and native-PAGE, and the oligomeric state was determined by gel filtration and native-PAGE.

2.7.1 Immobilized Metal Affinity Chromatography

Frozen CysE cell pellets (from section 2.6) were thawed at room temperature and resuspended in 20 ml of lysis buffer (50 mM Tris pH 8.0, 200 mM NaCl, 20 mM imidazole) with one cOmplete™ Mini, EDTA-free Protease Inhibitor tablet (Roche, Switzerland) added. Cells were lysed using a QSonica Q700 (Newtown, USA) with a 6 mm microtip probe. Sonication was performed on ice at an amplitude of 12, alternating 1.0-second bursts with 1.0-second rests, totaling 1.5 minutes of sonication. The lysate was then centrifuged at 13,000 rpm for 20 minutes at 4 °C, and the supernatant was sequentially filtered through 1.2, 0.45, and 0.2 µm filters (Minisart® Sartorius, New York, USA).

IMAC purification was conducted at room temperature using an NGC FPLC system (Bio-Rad, New Zealand). The filtered supernatant was manually loaded onto a HisTrap™ HP 5 ml column (GE Life Sciences, New Zealand) that was pre-equilibrated in lysis buffer. The column was washed with 20 ml lysis buffer at 2 $ml.min^{-1}$ to remove unbound proteins. A gradient of elution buffer (50 mM Tris pH 8.0, 200 mM NaCl, 1 M imidazole) was gradually increased to 50%, over 25 ml, to elute the Hexahis-tagged CysE.

2.7.2 Gel Filtration Chromatography

At room temperature (22 °C), IMAC peak fractions containing CysE were concentrated to 1 ml using a 10,000 Da MWCO spin concentrator (Amicon®, Germany) at 4,000 rpm for 20 minutes. The concentrate was loaded onto an Enrich 650 analytical gel filtration column (Bio-Rad Laboratories, USA), pre-equilibrated in gel filtration buffer (50 mM Tris pH 8.0, 100 mM NaCl) at a flow rate of 1 $ml.min^{-1}$. After loading 1 ml of protein via a sterile 0.2 µm syringe filter (Acrodisc® Pall Life Science, USA), 28 ml of buffer was run through the column to elute the protein. Fractions of eluted protein were collected, analyzed via nanodrop (section 2.7.5), and stored at room temperature.

2.7.3 SDS and Native-PAGE Gel Electrophoresis

Native-PAGE gels were used for both native and SDS-PAGE electrophoresis by adding SDS to the sample loading buffer and running buffer. Gels, consisting of 12% resolving and 5% stacking layers, were prepared in-house using a multi-gel caster (Hoefer). The 'Resolving Layer' components, listed in Table 2.1, were mixed and poured into the caster with a 3 cm gap at the top, which was filled with 3 ml of isopropanol to allow polymerization for 30 minutes. After polymerization, the isopropanol was removed, and the 'Stacking Layer' (Table 2.1) was added to the top edge of the gel caster. Well combs were then inserted, and the gels were left to set at room temperature for 30 minutes and stored at 4 °C for up to four weeks.

For electrophoresis, 15 µl of protein sample mixed with 5 µl of 4x SDS loading dye was loaded per well, alongside 10 µl of Precision Plus Protein™ ladder (Bio-Rad Laboratories, USA) for each gel. The electrophoresis was initially run at 100 V in 1x Tris-Glycine SDS

running buffer (Appendix B.2.) until the dye reached the end of the stacking gel, then the voltage was increased to 150 V until the dye migrated to the end of the gel.

Proteins were stained with Coomassie Fairbanks stain (Appendix B.2.); gels were microwaved for 30 seconds and then agitated at room temperature for five minutes at om an orbital shaker. After staining, gels were rinsed with milli-Q water and soaked in a 10% acetic acid-destaining solution overnight. Protein bands were visualized using an Invitrogen™ iBright™ imager (ThermoFisher, New Zealand).

Table 2.1: Components for five resolving layer native-PAGE gels.

Ammonium persulfate (APS) stock solution was prepared fresh weekly.

Components	**12% Resolving layer (ml)**	**5% stacking layer (ml)**
Resolving buffer (1.5 M Tris, pH 8.8)	7.5	-
Stacking buffer (1.0 M Tris, pH 6.8)	-	1.6
30% Polyacrylamide/Bis (375:1) (v/v)	12.0	2.125
10 % APS (w/v)	0.15	0.063
10% TEMED	0.015	0.0063
MQ.H_2O	10.35	8.625

2.7.4 Measuring the Oligomeric State of CysE

The Enrich650 gel filtration column (Bio-Rad Laboratories, USA) was calibrated with Gel Filtration Standards (Bio-Rad Laboratories, USA) in buffer (50 mM Tris pH 8.0, 200 mM NaCl). The resulting calibration curve is detailed in (Appendix B.2.). The molecular weight of CysE was determined by calculating the gel phase distribution coefficient (K_{av}) from the peak elution volume (V_e) using Equation 2.1, where V_o is the column void volume and V_c is the total column volume. This K_{av} value was then used to estimate CysE's molecular weight from the calibration standard curve.

Equation 2.1: Formula for calculating gel phase distribution coefficient (K_{av})

$$K_{av} = \frac{V_e - V_o}{V_c - V_o}$$

2.7.5 Measuring Protein Concentration via Nanodrop™

Protein concentration was measured using a Nanodrop™ 2000 (Thermofisher, USA) by detecting absorbance at 280 nm, which corresponds to the absorbance of tryptophan residues. Concentration calculations were based on the Beer-Lambert law (Equation 2.2). The absorbance readings were adjusted using the Nanodrop™ calibration (1 Abs = 1 mg.ml^{-1}) and the molar absorption coefficient of the AbaCysE2_long protein (Ɛ = 0.912L mol^{-1}.cm^{-1}), as determined by ProtParam (Gasteiger *et al*., 2005).

Equation 2.2: Beer-Lambert equation.

A= absorbance, ε = molar absorption co-efficient (L mol^{-1}.cm^{-1}), l =pathlength (cm) and c =concentration (molL^{-1}).

$$A = \varepsilon c l$$

2.8 Kinetic Assay Parameters

Protein was purified using IMAC and gel filtration chromatography (sections 2.7.1 and 2.7.2). Concentration was determined by measuring absorbance at 280 nm with a Nanodrop™ (section 2.7.5). All protein used in assays was freshly purified and used on the same day. Assays were conducted in gel filtration buffer (50 mM Tris pH 8.0, 100 mM NaCl). Master stocks of L-serine and acetyl-CoA substrates were prepared in the same buffer and kept on ice for the duration of the assays. An enzyme working stock of 0.2 mg.ml^{-1} (0.04 µM, CysE monomer 36.2 kDa) was prepared fresh at the start of the assay and maintained at room temperature (22 °C) throughout the experiments.

2.8.1 Assay protocols

Assays were performed in a 500 µl quartz cuvette with a total assay volume of 400 µl. The components of the assay detailed below (Table 2.2).

Table 2.2: Kinetic assay protocol.

Substrate concentrations were varied by adjusting the volume of the substrate master stock added, except when the required volume was less than 4 µl or greater than 40 µl. In those cases, a more diluted or concentrated stock was used to maintain the assay's overall temperature, as substrate stocks were kept on ice during the assays. The enzyme amount used for each reaction remained constant at 0.04 µM.

Component	**Volume (µl)**
Buffer	298-377
L-serine	0.4-80
Acetyl-CoA	0.4-40
Enzyme	3.2
Total	400

All substrate stocks were prepared in assay gel filtration buffer (50 mM Tris, pH 8.0, 100 mM NaCl). Acetyl-CoA stock aliquots were stored at -80 °C according to the manufacturer's instructions to prevent unwanted hydrolysis to coenzyme A. These stocks were thawed at room temperature and kept on ice for short-term use during assays. Acetyl-CoA, purchased as a powdered tri-lithium salt from Roche (MW = 827.5 g/mol), was stored at 4 °C as a powder. L-serine stocks were also prepared and stored at -80 °C.

The serine acetyltransferase activity of CysE was monitored by measuring the depletion of the substrate acetyl-CoA at 232 nm ($\Delta\varepsilon_{232}$ = 4500 M^{-1} cm^{-1}, absorbance of the thioester bond), using a method adapted from (Chronis & Krishnan, 2004) and further optimized by Keely Oldham (Oldham *et al*., 2022). Absorbance at 232 nm was recorded every second for a total of 30 seconds using a Spectrophotometer Hitachi F7000 (Auckland, New Zealand). Initial velocity data (ΔAbsorbance/second) was obtained from linear regression analysis of the first ten seconds of the reaction unless otherwise specified. The catalytic rate (ΔAbsorbance/second) of CysE was calculated directly from the depletion of acetyl-CoA, with the rate divided by -1, as one mol of acetyl-CoA is used to produce one mol of *O*-acetylserine. All data points were collected in duplicate unless otherwise noted. All assays were conducted at room temperature (22 °C).

2.8.2 Michaelis-Menten Analysis

The Michaelis constant (K_M) represents the substrate concentration at which an enzyme reaches half of its maximum theoretical rate (V_{max}) (Fersht, 2017). K_M indicates the enzymes affinity for its substrate; a lower K_M value implies higher affinity, requiring less substrate to achieve enzyme saturation, while a higher K_M suggests lower affinity, necessitating more substrate for saturation. V_{max} is the theoretical maximum rate of the enzyme when substrate concentration is saturating. This theoretical value provides insight into the enzyme's catalytic potential under optimal conditions, although it is rarely achieved in practical experiments.

K_M and V_{max} were calculated by varying the concentration of each substrate while keeping the other at saturating levels ($\geqslant$ 2 x K_M). Michaelis-Menten curves for L-serine (0.1-100 mM) and acetyl-CoA (0.1-1 mM) were obtained under these conditions. Non-linear regression analysis of the Michaelis-Menten equation (Equation 2.3) in GraphPad Prism (version 9.4.1, GraphPad Software) was used to determine K_M and V_{max}.

Equation 2.3: Michaelis-Menten equation.

S =substrate, K_M =Michalis constant, v =rate, v_{max} =theoretical maximum rate.

$$v = \frac{v_{max}[S]}{K_M + [S]}$$

Enzyme catalytic efficiency was assessed by calculating the catalytic constant (k_{cat}) and the specificity constant (k_{cat}/K_M). The catalytic constant, k_{cat}, represents the turnover number and is calculated as follows:

Equation 2.4: Catalytic constant equation.

Where v_{max}= maximum reaction rate (s^{-1}) and $[E]$= molar concentration of the enzyme.

$$k_{cat} = \frac{v_{max}}{[E_0]}$$

The specificity constant (k_{cat}/K_M) indicates catalytic efficiency and is calculated by dividing k_{cat} by K_M, where K_M is the Michaelis constant. Catalytic efficiency values were calculated for each substrate to evaluate enzyme performance.

2.8.3 CysE Inhibition Assays

Assays were conducted using a modified version of the method from section 2.8.1. Modifications involved adding L-cysteine (0.01-50 µM final concentration) to the assay mixture prior to initiating the reaction with the enzyme. Fresh L-cysteine stocks (0.1 and 1.0 mM) were prepared in gel filtration buffer (50 mM Tris, pH 8.0, 100 mM NaCl) and kept on ice during preparation and assays to prevent oxidation to L-cystine.

2.8.3.1 Substrate Inhibition

Substrate inhibition was assessed using non-linear regression to fit the substrate inhibition model Equation 2.5 in GraphPad Prism (version 9.4.1, Windows, GraphPad Software, La Jolla California, USA).

Equation 2.5: Substrate inhibition equation.

S = substrate, K_i = inhibition constant, K_M = Michaelis constant, v = rate, v_{max} = theoretical maximum rate

$$v = \frac{v_{max}[S]}{K_M[S]\left(\frac{1+[S]}{K_i}\right)}$$

2.8.3.2 Calculating cysteine inhibition values.

The IC_{50} values, representing the concentration of inhibitor that reduces the enzyme activity by 50%, were determined by fitting the "log [inhibitor] vs. normalized response" model Equation 2.6 to the rate data (s^{-1}) using GraphPad Prism (version 8.2.0, Windows, GraphPad Software, La Jolla, California, USA). The software calculated IC_{50} by plotting the enzyme rate against the logarithms of increasing L-cysteine concentrations.

Equation 2.6: Equation to calculate L-cysteine IC_{50}

I = inhibitor concentration, v = rate, v_0 = rate without inhibition present, v/v_0 = normalized rate.

$$\frac{v}{v_0} = \frac{100}{(1 + 10^{([1]-log\ \ _{50})})}$$

2.9 Structural Characterization of CysE

The structural characterization of enzymes is pivotal in understanding their function and potential as drug targets. Despite the characterization of CysE structures from various bacteria, the structure of CysE from *A. baumannii* remains unexplored. This gap in knowledge is significant because determining the structure of CysE from *A. baumannii* is essential for evaluating its validity as a drug target. Such validation is crucial for developing new antimicrobial compounds to combat nosocomial infections caused by this pathogen. High-resolution structures of CysE, both in its apo form and with substrates bound, are necessary for computational inhibitor screening. This screening can lead to the identification of lead compounds for further development (Reichau *et al*., 2011). This thesis aims to address this gap by purifying, crystallizing, and determining the structure of CysE from *A. baumannii* using X-ray crystallography. Furthermore, small angle X-ray scattering (SAXS) analysis will be performed to provide additional insights into the biophysical properties of CysE in solution.

2.9.1 Small Angle X-ray Scattering Analysis

Small-angle X-ray scattering (SAXS) data were collected on the BioSAXS beamline at the Australian Synchrotron (Melbourne, Victoria) using a Pilatus3X 2M detector. The beamline is equipped with a superconducting undulator source, providing a flux of approximately 10^{14} photons/s at 12.0 keV photon energy, which was used for these measurements. The samples were run in size exclusion chromatography (SEC-SAXS) mode to separate components in solution. The chromatography setup included a Cytiva Superdex 200 Increase 5/150 GL 5 mL column (Massachusetts, USA), and the sample was loaded using a coflow system to reduce radiation damage. For the coflow setup, the sample was injected into the capillary, surrounded by a sheath of buffer to minimize interaction with the X-ray beam. The buffer used for all measurements was 50 mM Tris, pH 8.0, 100 mM NaCl, and the enzyme concentration was 5.5 $mg.ml^{-1}$. The raw scattering data were processed and analyzed using the standard pipeline provided by the BioSAXS beamline, which includes automated data reduction and primary analysis to produce scattering curves. All experiments were conducted under temperature-controlled conditions to ensure sample stability during data collection.

2.9.2 Crystallization of CysE

2.9.2.1 Protein purification

CysE protein was expressed and purified as described in sections 2.6 and 2.7, respectively. Protein concentration was then determined via Nanodrop™ as per section 2.7.5.

2.9.2.2 High throughput crystallization screens

High throughput crystallization screens were used to identify conditions favorable to producing crystals suitable for X-ray diffraction. The screens used included Index™-HR2-144, PEGRx HT™-HR2-086, CrystalHT™-HR2-130, SaltRxHT™–HR2-136 and Additive Screen HT™-HR2-138 (Hampton Research, U.S.A). Setup was performed in low profile 96 well INTELLI-PLATES using a Mosquito crystallization robot (TTP LabTech Ltd., USA). Each condition utilized 200 µl of reservoir solution and 200 nl of sitting drops, comprising a 1:1 mixture of reservoir solution and concentrated protein. Crystal growth was monitored weekly under a dissection microscope.

2.9.2.3 Hanging drop fine screens

Favorable crystallization conditions identified from high throughput screens were refined by scaling up to hanging drop fine screens using 24-well VDX trays. Reservoirs were filled with 500 µl of mother liquor (well reservoir). Hanging drops were created on siliconized cover slips by mixing equal volumes (1:1 µl or 2:2 µl) of mother liquor and concentrated protein, then inverting them over wells sealed with silicone grease. Crystallization parameters such as pH, drop size, protein concentration and precipitant were optimized. Drops were examined daily for the first week and weekly thereafter under a dissection microscope for crystal growth.

2.9.2.4 Ligand co-crystallization

High-throughput screens were prepared according to the protocol described in section 2.9.2.2, with the modification of incorporating L-serine or L-cysteine into the concentrated protein stocks, reaching final concentrations of 5 mM and 8 mM, respectively. Promising conditions were subsequently refined by conducting fine drop screens, as outlined in section 2.9.2.3 with the addition of the ligand to the protein drop.

2.9.2.5 Ligand soaking

Ligand soaking was used as an alternative approach to determine the structure of CysE complexed with either substrates or inhibitors. This technique was applied to both L-serine and L-cysteine. For the soaks, L-cysteine (8 mM) or L-serine (5 mM) was added to the mother liquor solution. The crystals were then grown and prepared for data collection following the procedure outlined in section 2.9.2.3, with an additional soaking step (30 minutes) incorporated before transferring the crystals to the cryo-protectant solution (2.9.2.7).

2.9.2.6 Final structure crystallization condition

Purified protein was concentrated to 4.7 $mg.ml^{-1}$ and stored at room temperature away from direct sunlight for short periods, CysE precipitates if kept for longer than two days. The fine screen was based around a crystallization condition from the high throughput screen HR2-136 SaltRxHT™ consisting of 2.0 M sodium formate and 0.1 M sodium acetate trihydrate at pH 4.6 (Hampton Research, USA). This mixture served as both precipitant and buffer for CysE crystallization. Trays were prepared following the protocol in section 2.9.2.3, with crystals for X-ray diffraction grown using hanging drops of 1:1 µl (mother liquor to protein concentrate) at 18 °C.

2.9.2.7 Crystal preparation for X-ray diffraction

Crystals were transferred using a cryo-loop to a cryo-protectant solution, which included the modified mother liquor with an added 15% glycerol (v/v). They were then flash cooled in liquid nitrogen and stored briefly for one day before data collection.

2.9.3 Data Collection

X-ray diffraction data were collected at the Australian Synchrotron (Melbourne, Victoria) on the MX2 beamline (McPhillips *et al*., 2002), utilizing an EIGER X 16M detector (Dectris, Switzerland). The AreaVision interface was used for high-resolution alignment of crystals to the X-ray beam, allowing snapshots of crystals in .jpg format. Sample mounting was supported by a Leica M205C stereo microscope for precise positioning. The beamline offered user-changeable energy and automated beam-steering for optimal data collection. This session was conducted entirely remotely, following the Australian Synchrotron's established protocols. Access to the beamline and diffraction data was

managed through the Guacamole interface, with users controlling ADXV windows directly to visualize diffraction patterns.

The dataset was collected from a single crystal at 100K. Detector distance was 300 mm and data was collected in 0.5 degree wedges over 36s producing 3600 frames.

2.9.4 Data Processing

2.9.4.1 Indexing, integration and scaling

The dataset diffraction images were indexed, integrated, and scaled using XDS (Kabsch, 2010). Reflections were merged with AIMLESS (Evans & Murshudov, 2013) from the CCP4 suite (Winn *et al*., 2011). Data quality was assessed via AIMLESS and by manually inspecting diffraction images in ALBULA (Dectris, Switzerland).

2.9.4.2 Detection of twinning and non-crystallographic symmetry

Data was analyzed for evidence of twinning and translational non-crystallographic symmetry (tNCS) in AIMLESS from the CCP4 suite (Evans & Murshudov, 2013; Winn *et al*., 2011) and *phenix.xtriage* from the PHENIX suite.

2.9.5 Structural Analysis

2.9.5.1 Matthew's coefficient

The total number of monomers in the asymmetric unit was determined by calculating the solvent content using the Matthew's coefficient (Matthews, 1968) program, as a part of the CCP4 program suite (Winn *et al*., 2011).

2.9.5.2 Molecular replacement

The sequence of CysE from *A. baumannii* was input into the AlphaFold 3 server, producing an in-silico model. A single monomer was extracted from this file, in PyMOL and low-confidence regions of the model were removed to improve accuracy (The PyMOL Molecular Graphics System, Version 2.3.2 Schrödinger, LLC). Molecular replacement was carried out using *phenix.phaser* (McCoy *et al*., 2007) from the PHENIX suite (Adams *et al*., 2010).

2.9.5.3 Model building and refinement

The initial model was constructed and refined using the program phenix.autobuild (Terwilliger *et al*., 2008) from the PHENIX suite. Subsequent manual building was performed using COOT (Emsley & Cowtan, 2004). During the manual refinement in COOT, the 2Fo-Fc and Fo-Fc electron density maps were contoured at 1σ and 3σ, respectively. After each round of structural adjustments, *phenix.refine* was employed to carry out real-space refinement (Afonine *et al.*, 2012).

2.9.5.4 Structural analysis

Ramachandran outliers were evaluated using MolProbity (Chen *et al.*, 2010) from the PHENIX suite (Adams *et al.*, 2010). Visual representations of the model and electron density maps were created using PyMOL (The PyMOL Molecular Graphics System, Version 2.3.2 Schrödinger, LLC) and COOT (Emsley & Cowtan, 2004). Hydrogen bonds were categorized as moderate with distances between 2.5-3.2 Å and weak within the 3.3-4.0 Å range, based on (Jeffrey, 1997). Bond distances were measured using PyMOL. Structural comparisons were performed by calculating root mean square distances (r.m.s.d) using the alignment tool in PyMOL. Surface area and buried residue analyses at the trimer/hexamer interfaces were conducted with PDBePISA (Krissinel & Henrick, 2007). Secondary structural features were identified using ENDscript 3.0 (Robert & Gouet, 2014) and visually confirmed in PyMOL.

Chapter Three

Results and Discussion

3.1 Results and Discussion

3.1.1 Optimized Expression and Purification of CysE

3.1.1.1 Transformation of CysE

Successful characterization of CysE from different organisms required the purification of soluble and active protein. The genes encoding CysE were codon-optimized for *E. coli* by Twist Bioscience and directly transformed into BL21 (DE3) cells. This process was performed for five constructs: *E. cloacae* CysE (EclCysE), *A. baumannii* short form CysE (AbaCysE1_short), *A. baumannii* long form CysE (AbaCysE2_long), *P. aeruginosa* CysE (PaeCysE), and *M. tuberculosis* CysE (MtbCysE). To confirm the presence of the transformed plasmids, colony polymerase chain reaction (cPCR) was performed on the transformant colonies. T7 forward and reverse primers were used for amplification. The positive control (+) for the cPCR was the resuspended plasmid in TE buffer provided by Twist Bioscience, which also served to verify the accuracy of the sequence received. The negative control (-) consisted of a reaction without any plasmid and showed no bands on the gel, indicating that there was no contaminating DNA. The results of the cPCR were visualized on 1% agarose gel electrophoresis and showed the successful transformation of the constructs into *E. coli* BL21 (DE3) (Figure 3.1). This was evident by the presence strong bands consistent with the predicted size for the PCR product (~1000bp) for the two colonies picked from each organism.

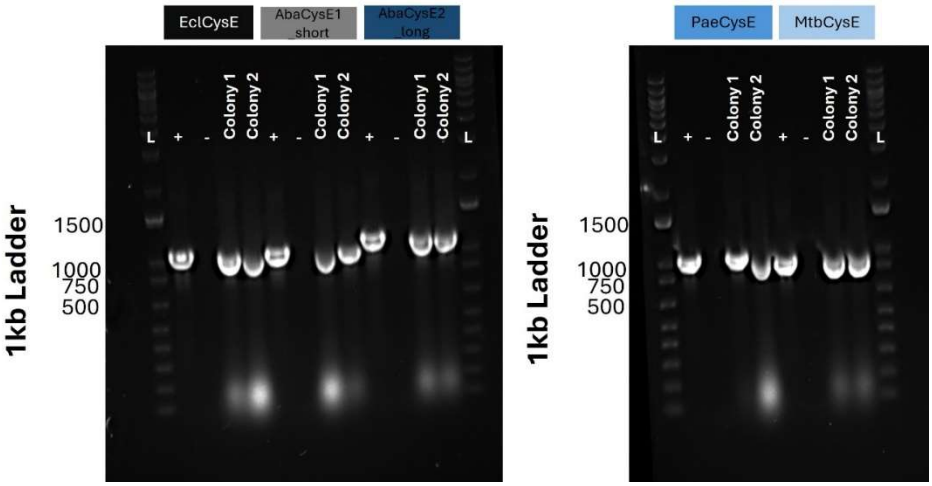

Figure 3.1: Agarose gels (1%) cPCR of transformants

Colonies were picked from Kanamycin LB plates. Positive control (+), negative control (-), colony 1 and colony 2 from each organism are labeled. Sizes of the 1 kb plus ladder (L) used are labeled.

3.1.1.2 Expression trial

From previously optimized expression trials carried out for *E. coli* CysE (EcCysE), a small-scale preliminary expression of all five constructs was performed as per section 2.5. The small-scale preliminary expression indicated high protein yield for the long form of *A. baumannii* (AbaCysE2_long) and *E. cloacae* (EclCysE) (Figure 3.2A, highlighted in red). Since this was the first time these proteins were expressed in our lab, a His-tag stain (InVision His-Tag In-gel stain, thermoFisher scientific) following the manufacturer's instructions to confirm the protein contained a His-tag and the approximate sizes of the proteins. For the His-tag stain, a positive control of a known protein with a Histidine tag was used, in this case, EcCysE, showing that the His-tag stain was optimized (Figure 3.2B and D lane 1 (+)). The expected molecular weights of EclCysE is 29.33 kDa, AbaCysE1_short is 29.90 kDa and AbaCysE2_long is 33.92 kDa (Figure 3.2).

The constructs from *P. aeruginosa* CysE (PaeCysE), and *M. tuberculosis* CysE (MtbCysE) did not appear to have adequate expression, as there were no over expressed bands at the predicted molecular weight in the insoluble pellet, the supernatant or in the Ni beads present in either the Coomassie or His-tag stained gels (Figure 3.2C and D). The expression of AbaCysE1_short was very low, with the presence of faint, small bands and consistent with the predicted molecular weight (Figure 3.2A, highlighted in blue). From the His-tag stain there is protein in the insoluble pellet and the Ni beads (Figure 3.2B,

highlighted in blue). It is interesting to note that PaeCysE, MtbCysE and AbaCysE1_short are the short forms of the CysE enzyme, and all have either low or no expression.

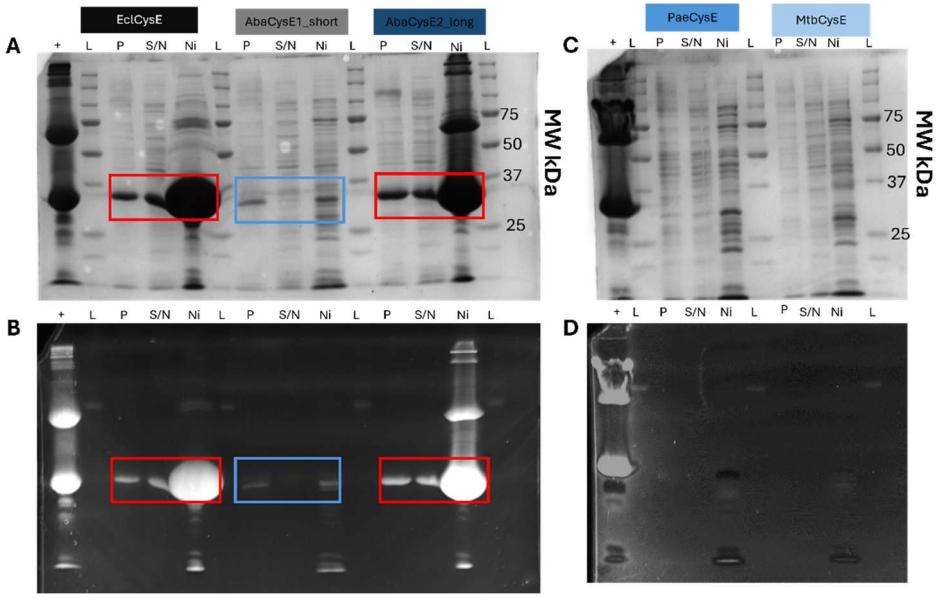

Figure 3.2: 12% SDS-PAGE gels of preliminary small-scale nickel pull down.

A) & C) Coomassie blue stain of the five constructs. A) EclCysE (black bar) predicted molecular weight (MW) 29.33 kDa, AbacysE1_short (grey bar) protein predicted MW 29.88 kDa, AbaCysE2_long (navy blue bar) predicted MW 33.92 kDa. C) PaeCysE (cerulean blue bar) predicted MW 27.90 kDa and MtbCysE (sky blue bar) predicted MW 23.77 kDa. B) & D) his-tag stain of 12% SDS-PAGE gel lane 1 in both positive control of EcCysE predicted MW 36.2 kDa. Molecular weights of Precision Plus Protein Standards (L) in kDa are labeled, the insoluble pellet (P), soluble supernatant (S/N), nickel resin (Ni) and the positive control (+).

Efforts were made to optimize the expression of AbaCysE1_short and PaeCysE. Given the limited availability of 3D structures and characterization information on the short form of CysE from any bacterial organism (Qiu *et al*., 2013; Rahisuddin *et al*., 2024), it was essential to focus on these constructs. We decided not to investigate MtbCysE further due to the time constraints and the potential requirement to transform MtbCysE into *Mycobacterium smegmatis* to obtain adequate yields of soluble protein. Additionally, the presence of two isoforms of CysE in *A. baumannii* presented intriguing questions about the role of the short form in cysteine biosynthesis warranted further investigation.

The expression trial for the short form CysE (AbaCysE1_short) was conducted as per section 2.5. The conditions tested are listed in Table 2.3 and Table 2.4, comparing expression with and without the addition of glucose added at three different temperatures.

The addition of low concentrations of glucose is intended to suppress the T7 promoter from expressing the protein in the absence of an inducer (IPTG). Increased expression with the addition of glucose could indicate that glucose is suppressing the basal expression in the absence of IPTG, but it may also suppress expression when IPTG is present, leading to decreased protein production. However, we observed increased expression with AbaCysE1_short under conditions with glucose (conditions 2, 3, 5, and 7) compared to those without glucose (conditions 1, 4, and 6), with optimal expression at condition 5 (30°C, 2% glucose). Conversely, for PaeCysE, no significant difference was observed between trials with or without glucose, with condition 11 (37°C, 0% glucose) showing the most optimal expression. This behavior aligns with known mechanisms where glucose can repress the basal level expression of T7 RNA polymerase by reducing cAMP levels, thus lowering the activation of the lac promoter controlling the T7 RNA polymerase gene (Samuelson, 2011; Zhang & Studier, 1997).

Table 3.1: AbaCysE1_short expression culture test conditions

Condition number	Test conditions
1	22ºC, 0% glucose
2	22ºC, 1% glucose
3	22ºC, 2% glucose
4	30ºC, 0% glucose
5	30ºC, 2% glucose
6	37ºC, 0% glucose
7	37ºC, 1% glucose

Table 3.2: PaeCysE expression culture test conditions

Condition number	Test conditions
8	22ºC, 2% glucose
9	30ºC, 0% glucose
10	30ºC, 2% glucose
11	37ºC, 0% glucose
12	37ºC, 1% glucose

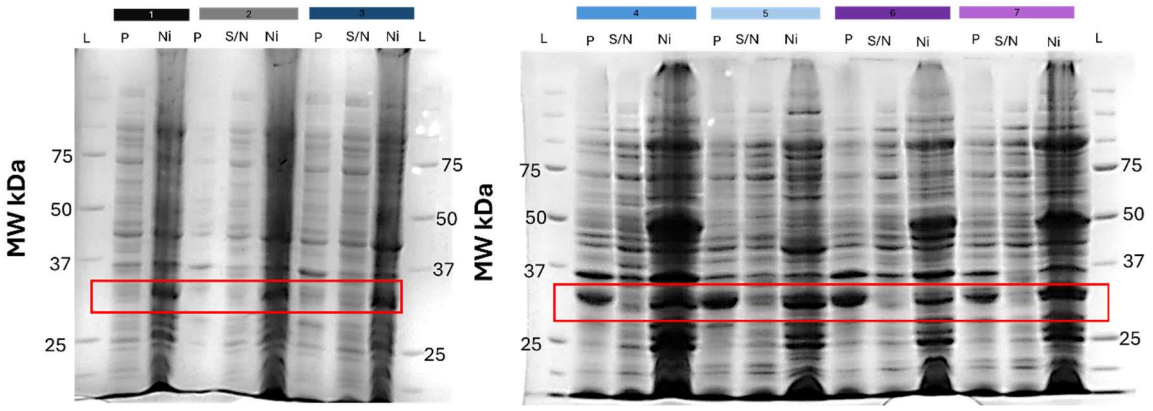

Figure 3.3: 12% SDS-PAGE gel of AbaCysE1_short expression trial nickel pulldown.

Highlighted in red is the short form *A. baumannii* CysE protein (predicted MW 29.8 kDa), see Table 3.1 for details of conditions 1 – 7 AbaCysE1_short was subjected to. Molecular weights of Precision Plus Protein Standards (L) in kDa are labeled, (the insoluble pellet (P), soluble supernatant (S/N) and nickel resin (Ni).

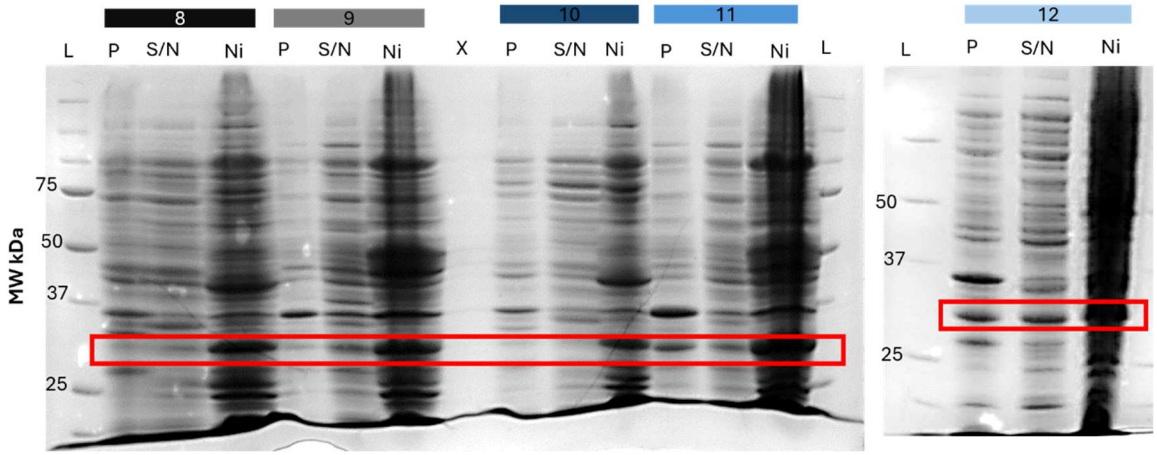

Figure 3.4: 12% SDS-PAGE gel of PaeCysE expression trial nickel pulldown.

Highlighted in red is the *P. aeruginosa* CysE protein (predicted MW 27.9kDa), see Table 3.2 for details of conditions 8 – 9 PaeCysE was subjected to. Molecular weights of Precision Plus Protein Standards (L) in kDa are labeled, (the insoluble pellet (P), soluble supernatant (S/N), empty well (X) and nickel resin (Ni).

To improve solubility of PaeCysE optimization of lysis buffer pH was also conducted (7.5, 7.7 and 7.9). However, this did not improve the yield of soluble protein. Given the poor expression of PaeCysE and due to time constraints, we decided to take only the short form of CysE from *A. baumannii* through for further optimization. Using the optimized condition 5 (30°C, 2% glucose), we moved to large-scale expression. Despite initial expression observed for AbaCysE1_short in the small-scale trials, there was no expression observed in large-scale expression cultures (as per section 2.6). Due to time constraints, we prioritized obtaining the objectives for AbaCysE2_long.

3.1.1.3 Expression and purification of AbaCysE2_long

AbaCysE2_long was successfully purified by IMAC and gel filtration chromatography as per section 2.7. The IMAC purification chromatogram showed that AbaCysE2_long elutes at ~25% elution buffer (250 mM of imidazole) (Figure 3.5A). There is a later peak at 100% imidazole, this is due to the elution of non-specific proteins at increased imidazole concentrations (Bornhorst & Falke, 2000). The corresponding SDS-PAGE gel of the IMAC fractions, demonstrates a laddering effect of bands, this may be due to other higher oligomeric forms of AbaCysE2_long on the gel as higher molecular weight bands, e.g., the dimer, trimer, and or hexamer of AbaCysE2_long or this could be due to insufficient protein denaturation (Figure 3.5B). The gel indicates that most of the *E. coli* proteins present in the supernatant are effectively removed during the IMAC purification process (Figure 3.5B). While there are bands present at approximately 70 kDa, the majority of the protein eluted at the predicted molecular weight of 36 kDa (Figure 3.5B, blue arrow). Fractions that corresponded with the peak observed at ~50ml on the chromatogram trace during IMAC purification (Figure 3.5, highlighted with asterisk) was used for gel filtration purification as per section 2.7.2.

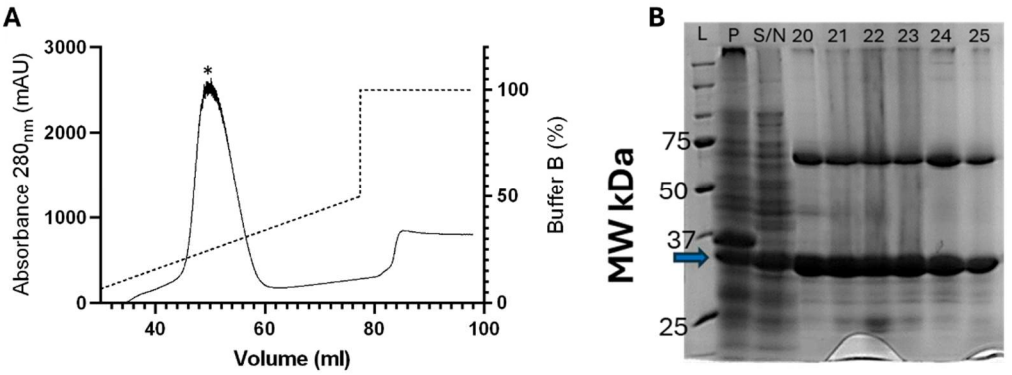

Figure 3.5: IMAC purification of AbaCysE2_long at room temperature

A) IMAC chromatogram showing absorbance at A280nm (left Y-axis) against elution volume in milliliters (X-axis) and concentration of elution buffer in percent (right Y-axis). Data from 0-30ml has been excluded for scaling purposes. B) 12% SDS-PAGE gel of AbaCysE2_long IMAC purification. Protein is labeled with a blue arrow and is present in all samples (the insoluble pellet (P), soluble supernatant (S/N), and IMAC fractions (20-25)). Molecular weights of Precision Plus Protein Standards (L) in kDa are labeled.

IMAC purified protein fraction underwent a final purification step via gel filtration chromatography (section 2.7.2). AbaCysE2_long eluted as a single peak from the Enrich 650 analytical gel filtration column with an elution volume of 13.18ml (Figure 3.6A, blue

bar, asterisk indicating peak). A calibration curve was constructed (Appendix B.2.), which allowed for the estimation of the molecular weight based on the elution volume. The estimated molecular weight of AbaCysE2-long was determined to be 209.9 kDa, which suggests that AbaCysE2_long elutes as a hexamer (6 x 36.2 = 217.2kDa). Previous optimizations found that when concentrating between the IMAC and gel filtration concentrations the protein would disassociate into trimers, for this purpose we have avoided concentrating at low temperatures due to CysE being highly unstable and is subject to cold inactivation (Mino *et al*., 2001; Yi *et al*., 2013). No protein was detected in the void volume of the column (5.96 ml), indicating that AbaCysE2_long did not aggregate and remained soluble throughout the purification process. The corresponding SDS-PAGE analysis of the gel filtration fractions shows a pure protein band of approximately 36kDa (Figure 3.6B, blue arrow).

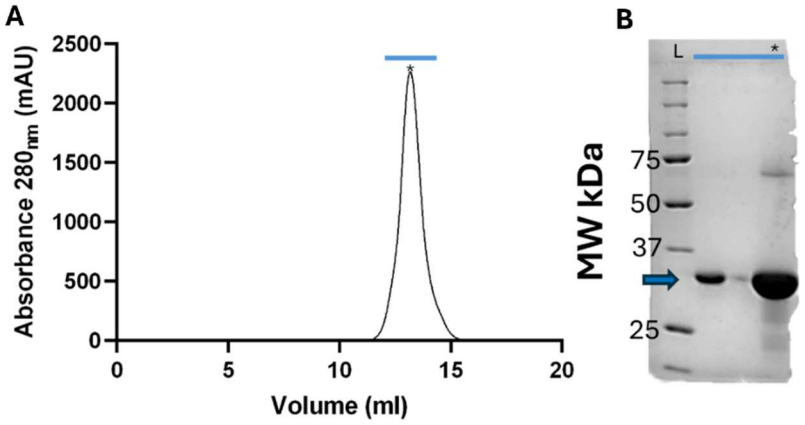

Figure 3.6: Gel filtration purification of AbaCysE2_long

A) Enrich 650 gel filtration chromatogram showed the elution of a single large peak at 13.18ml. B) 12% SDS-PAGE analysis of gel filtration fractions showed high yield and purity of AbaCysE2_long (blue bar). AbaCysE2_long protein band labeled with a blue arrow and an asterisk at the top of the lane to indicate the peak fraction. Molecular weights of Precision Plus Protein Standards (L) in kDa are labeled. Purification was conducted at room temperature.

3.1.2 Analysis of CysE long form from A. baumannii

3.1.2.1 Kinetic Assay

Assays were set up as described in section 2.8, with all raw data available via the link provided in Appendix B.3. Preliminary assays were conducted to determine the optimal

enzyme concentration for Michaelis-Menten kinetic analysis. It was found that 30 seconds was optimal to observe a clear and linear initial velocity. This optimization ensures the accuracy and reliability of the collected enzyme kinetics data under the experimental conditions. The assay utilized concentrations of 0.45 mM and 10 mM acetyl-CoA and L-serine respectively, based on saturating substrate concentrations for *Neisseria gonorrhoeae* CysE reported by (Oldham *et al*., 2022). All assays were conducted in assay buffer composed of 50 mM Tris pH 8.0, 100 mM NaCl at 22 °C. This buffer was chosen as it matches the conditions used during enzyme purification (section 2.7), and the temperature was selected to prevent loss of activity due to cold inactivation, a well-documented phenomenon for CysE (Mino *et al*., 2001; Yi *et al*., 2013).

Enzyme concentrations ranging from 0.028 µM to 0.14 µM were tested to find an optimal concentration where sufficient linear velocity was observable within the 30-second assay period. This range is consistent with the optimized assays parameters previously conducted (Oldham *et al*., 2022). *A. baumannii* CysE demonstrated a positive linear dependence of initial velocity (V_0) on protein concentration (Figure 3.7), consistent with findings of other CysE enzymes from *E. coli* (Benoni, De Bei, *et al*., 2017). Therefore, an enzyme concentration of 0.044µM was selected as it provided a clear and measurable initial velocity within the linear range of the enzyme activity. Additionally, using this concentration ensures reproducibility and reliability of results across multiple experiments, minimizes enzyme consumption and limits substrate depletion. It also aligns with concentrations used in comparable studies, facilitating validation and comparison of results while providing optimal sensitivity for detecting changes in substrate concentration.

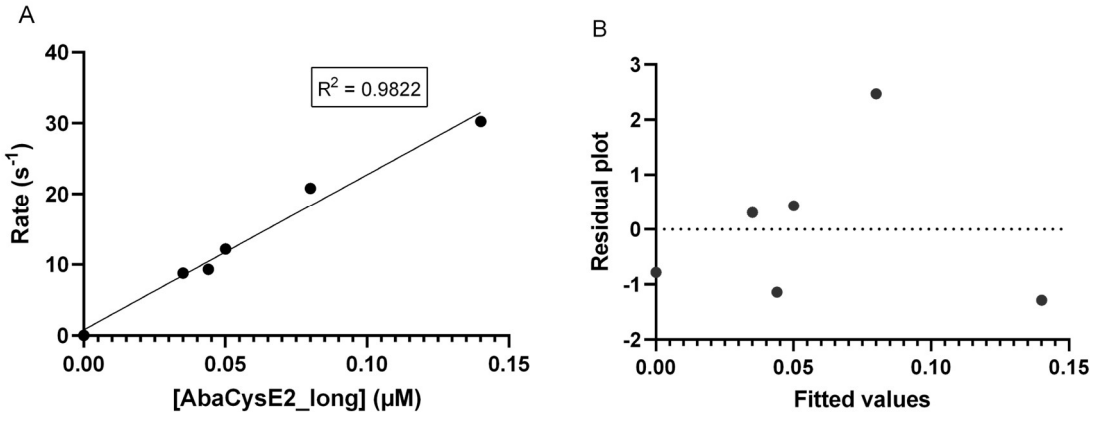

Figure 3.7: Dependence of V_0 on AbaCysE2_long concentration.

A) AbaCysE2_long activity at 232 nm with varying enzymatic concentrations ranging from 0.028 µM to 0.14 µM. The initial velocity (V_0) was measured over a 30-second assay period. Data is fitted with a linear regression (GraphPad Prism version 9.2.4). B) Residuals vs fitted values assumptions of linearity test found model meets assumptions.

3.1.2.2 Michaelis-Menten Kinetics of AbaCysE2_long

For the Michaelis-Menten kinetic analysis for AbaCysE2_long the concentration of one substrate (A) is kept constant at the saturating level, while the concentration of the second substrate (B) is varied. This approach simplifies the analysis by allowing the enzyme to behave as if it were a single-substrate enzyme, thereby generating apparent K_M and V_{max} constants for substrate B (Fersht, 2017). This ensures that the constant substrate remains at a level high enough to avoid becoming the rate-limiting factor, thereby allowing the analysis to accurately reflect the kinetics of the variable substrate. The K_M and V_{max} parameters offer valuable insights into the enzyme's affinity for its substrates and critical for determining catalytic efficiency measurements such as k_{cat} and k_{cat}/K_M. These parameters are also essential for conducting inhibition assays.

The L-serine Michaelis-Menten plot was created by plotting initial velocities (s^{-1}) against increasing concentrations of L-serine (0.1 – 100 mM) at saturating concentrations of acetyl-CoA of 0.45 mM as per section 2.8 (Figure 3.8). The curve observed ($R^2 = 0.9770$) indicates a good fit to the Michaelis-Menten model, displaying a classical rate curve where the reaction rate increased with substrate concentration and eventually plateaued at higher concentrations, indicating substrate saturation. The K_M and k_{cat} values calculated were 5.77 ± 1.56 mM and 1.24 x 10^2 ± 9.20 s^{-1}, respectively.

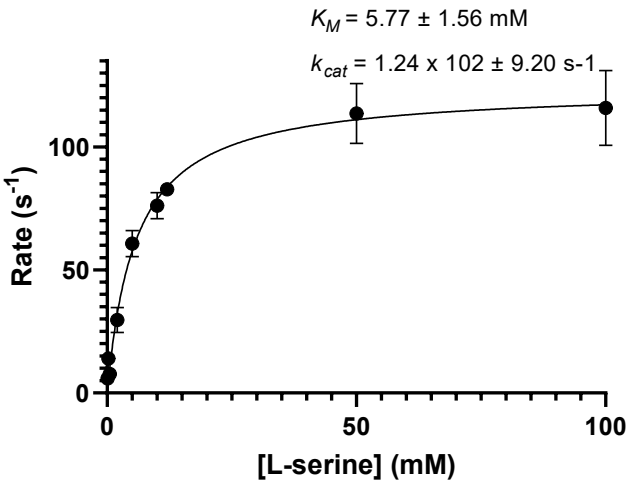

Figure 3.8: Michaelis-Menten fitted curve for L-serine.

Acetyl-CoA was maintained at saturating concentration of 0.45 mM. Each point represented the mean of duplicate measurements, with error bars showing the SD. Data was collected at 22 ºC.

Michaelis-Menten plot for acetyl-CoA was generated by plotting the initial reaction velocities (s^{-1}) against varying concentrations of acetyl-CoA (0.01-1 mM) while maintaining a constant, saturating concentration of L-serine (10 mM). The curve observed (R^2 = *0.9681*) fit well with the Michaelis-Menten model and allowed the determination of K_M and k_{cat} of 0.27 ± 8.78 x 10^{-2} mM and 9.95 x 10^1 ± 1.22 x 10^1 s^{-1} respectively (Figure 3.9). The K_M values for the substrates L-serine and acetyl-CoA (5.77 mM and 0.27 mM respectively) indicates that *A. baumannii* CysE has a significantly higher affinity for acetyl-CoA compared to L-serine. To explore the potential for substrate inhibition, the same data was analyzed using a substrate inhibition model. This model suggested a marginally better fit (R^2 = 0.9693) compared to the Michaelis-Menten model (R^2 = *0.9681*), providing best-fit values of k_{cat} = 1.21 x 10^2 s^{-1}, K_M = 0.37 mM, and K_i = 4.67 mM, where K_i represents the inhibition constant for substrate inhibition. The superimposed plots (Figure 3.9, substrate inhibition model red dashed line and Michaelis-Menten model black solid line) reveal the subtle differences between the two models, particularly at higher substrate concentrations. The highest substrate point indicates a decrease in rate, suggesting potential substrate inhibition. However, the current data set is insufficient to confirm this model conclusively, as indicated by the marginal improvement in the R^2 value (0.9693 to 0.9681) and the limited number of data points demonstrating inhibition. This observation aligns with findings in related studies (Oldham *et al*., 2022), where higher acetyl-CoA concentrations were also

linked to substrate inhibition, but more extensive data would be required to validate this effect definitively. Future experiments at higher substrate concentrations could provide further insights into the inhibitory role of acetyl-CoA on CysE activity.

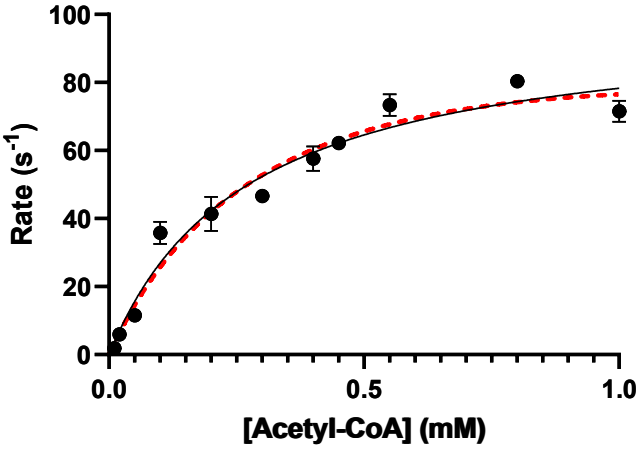

Figure 3.9: Kinetic analysis of substrate acetyl-CoA.

Michaelis-Menten (black solid line) and substrate inhibition equation (red dashed line) modelled. L-serine was maintained at saturating concentrations (10 mM). Each point represented the mean of duplicate measurements, with error bars showing the SD. Data was collected at 22°C.

The catalytic constant (k_{cat}) was calculated using the catalytic constant equation (Equation 2.4). The k_{cat} for AbaCysE2_long substrates L-serine and acetyl-CoA 1.24 x 10^2 ± 9.20 s^{-1} and 9.95 x 10^1 ± 1.22 x 10^1 s^{-1}, respectively, with CysE treated as a monomer (Table 3.3). The enzyme's rate falls below the theoretical diffusion limit of approximately 10^8 $M^{-1}.s^{-1}$, indicating that its activity is not constrained by diffusion limitations (Olsen *et al*., 2007).The kinetic parameters of AbaCysE2_long were compared with those of homologs from *N. gonorrhoeae, E. coli, S. typhimurium,* and *Haemophilus influenzae* to understand its catalytic efficiency and substrate affinity. The K_M values for L-serine and acetyl-CoA in *A. baumannii* (5.77 mM and 0.27 mM, respectively) suggests a lower affinity for L-serine compared to *N. gonorrhoeae* (1.21 mM and 0.149 mM), *E. coli* (1.3 mM and 0.3 mM), and *S. typhimurium* (3.2 mM and 0.4 mM), but a comparable affinity for acetyl-CoA. The k_{cat} values for *A. baumannii* (1.24 × 10^2 s^{-1} for L-serine and 9.95 × 10^1 s^{-1} for acetyl-CoA) indicate a lower catalytic efficiency than those reported for *N. gonorrhoeae* (240 s^{-1} and 196 s^{-1}) and *E. coli* (323 s^{-1} and 306 s^{-1}), suggesting a lower turnover rate. However, the k_{cat}/K_M values for *A. baumannii* (2.15 x 10^4 $M^{-1}.s^{-1}$ for L-

serine and 3.69 x 10^5 $M^{-1}.s^{-1}$ for acetyl-CoA) are consistent with the enzymatic efficiency seen in other homologs. These comparisons indicate that while *A. baumannii* may exhibit a lower substrate affinity, it demonstrates a competent turnover rate and effective enzymatic activity.

Table 3.3: Summary of Michaelis-Menten kinetic parameters for L-serine and acetyl-CoA substrates.

Values represent means from duplicate measurements and include SEM.

Parameter	**L-Serine**	**Acetyl-CoA**
K_M (mM)	5.77 ± 1.56	0.27 ± 8.78 x 10^{-2}
V_{max} (s^{-1})	1.24 x 10^2 ± 9.20	9.95 x 10^1 ± 1.22
k_{cat} (s^{-1})	1.24 x 10^2	9.95 x 10^1
k_{cat}/K_M ($M^{-1}.s^{-1}$)	2.15 x 10^4	3.69 x 10^5

Table 3.4: Comparison of CysE Enzyme Kinetics.

DTNB = DTNB coupled assay, A232 = monitors depletion of acetyl-CoA at 232nm, na = not available. kcat values reported for the CysE hexamer.

Organism	**K_M(mM) (ser/AcCoA)**	**k_{cat}(ser/AcCoA) (s^{-1})**	**k_{cat}/K_M ($M^{-1}.s^{-1}$)**	**pH, Temp., assay method**	**Reference**
A. baumannii	5.77/0.27	1.24*10^2/ 9.95*10^1	2.15*10^4/ 3.69*10^5	8.0, 22°C, A_{232}	This thesis
N. gonorrhoeae	1.21/0.149	240/ 196	1.19*10^6/ 7.89*10^6	8.0, 22°C, A_{232}	(Oldham *et al*., 2022)
E. coli	1.3/0.3	323/306	1.34*10^5/ 2.12*10^5	7.0, 22°C, A_{232}	(Benoni, De Bei, *et al*., 2017)
S. typhimurium	3.2/0.4	135/na	3.4*10^5/na	7.0, 25°C, DTNB	(Leu & Cook, 1994)
H. influenzae	4.7/0.7	2200/na	4.70x10^5/na	7.5, 25°C, DTNB	(Johnson *et al*., 2004)

3.1.2.3 Characterizing L-Cysteine inhibition of AbaCysE2_long

The feedback inhibition by L-cysteine for CysE proteins is well-established in both bacterial and plant species. To characterize this inhibition for AbaCysE2_long, IC_{50} analysis was conducted. The IC_{50} value provides a measure of the concentration of L-cysteine required to inhibit 50% of the enzyme activity. This is essential to determine the sensitivity of AbaCysE2_long to L-cysteine which can provide insights into the regulatory mechanisms governing cysteine biosynthesis.

3.1.2.4 L-cysteine IC_{50} assays

The inhibition of CysE by L-cysteine was quantified using IC_{50} assays, where the concentrations of serine and acetyl-CoA were kept constant. Acetyl-CoA was maintained at twice its K_M (0.5mM), and L-serine was at a non-saturating concentration (0.5x K_M, 3 mM). L-cysteine is a competitive inhibitor of serine, meaning they both compete for the same binding pocket on the enzyme. To effectively observe the competitive inhibition, L-serine was kept at 0.5x K_M. This sub-saturating concentration ensures that the binding sites on the enzyme are not fully occupied by serine, allowing for the competitive interactions between serine and L-cysteine to be accurately measured. An enzyme concentration of 0.044 µM was used consistently throughout all assays (Figure 3.10). For the IC_{50} calculation, the normalized enzyme activity rate was plotted against the logarithm of L-cysteine concentrations, and this data was fitted to the substrate inhibition model Equation 2.6 using GraphPad Prism (version 9.4.1, Windows, GraphPad Software, La Jolla, California, USA). The IC_{50}, which is the concentration of L-cysteine required to reduce enzyme activity by 50%, was determined to be 1.81 ± 1.03 µM. The goodness of fit for the model was represented by an R^2 value of 0.9213, indicating a high correlation. Assays were conducted across a range of L-cysteine concentrations from 0.01 µM to 50 µM in triplicate.

However, the data points at lower concentrations of L-cysteine exhibited significant variability, which may affect the accuracy of the IC_{50} calculation. The enzyme activity did not decrease to zero at the highest L-cysteine concentrations tested, indicating that complete inhibition was not achieved under the assay conditions. To improve the reliability of the findings, future experiments should aim to extend the range of L-cysteine concentrations tested, ensuring that enzyme activity can be driven to zero. More data points are also needed at critical concentrations, particularly between 0.1 µM and 10 µM,

where the dose-response curve exhibits the most curvature. This will help capture the transition more accurately and provide a more precise characterization of the inhibition dynamics. These results provide valuable insights into the inhibitory effect of L-cysteine on CysE, including the specific concentration range where inhibition occurs, the degree of sensitivity of CysE to L-cysteine, and potential mechanisms of inhibition.

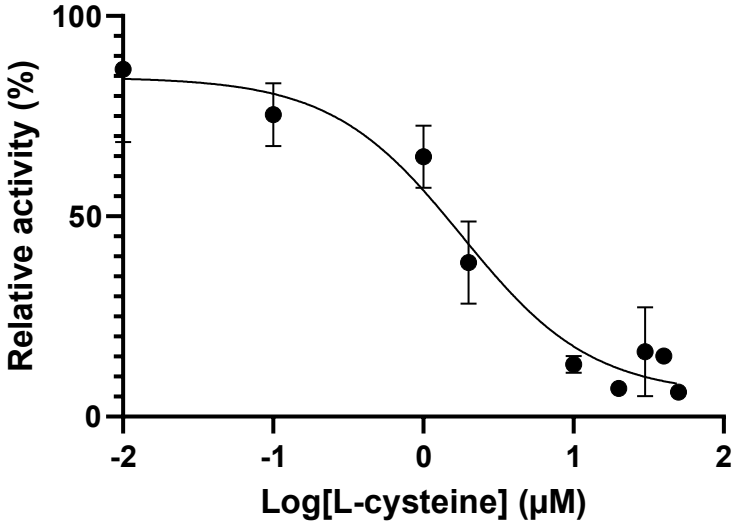

Figure 3.10: L-cysteine IC_{50} plot

Normalized rate plotted against $\log_{10}$ of L-cysteine concentrations. The line represents the fit of Equation 2.6. Acetyl-CoA and serine substrate concentrations were kept constant, at 0.5 mM and 3 mM, respectively. The IC_{50} for L-cysteine is 1.81 μM. CysE activity (s^{-1}) was normalized by dividing the rate by rate of the no-inhibitor control. Data points are mean and error bars are SD from triplicate data.

The IC_{50} value for L-cysteine inhibition of CysE from *A. baumannii* was determined to be 1.81 ± 1.03 μM under assay conditions of pH 8.0 and 22 °C using A_{232} nm. This value is comparable to IC_{50} values of homologs from *E. coli* (0.18 ± 0.02 μM), and *S. typhimurium* (1.1 μM), suggesting that *A. baumannii* CysE along with these species, is quite sensitive to L-cysteine. Conversely, the IC_{50} value for *N. gonorrhoeae* (5.01 ± 0.403 μM) (Table 3.5) is significantly higher, showing a reduced sensitivity to L-cysteine inhibition. The IC_{50} value for *C. glutamicum* is 2.0 μM, which is also higher than *A. baumannii* but lower than *N. gonorrhoeae*, suggesting a moderate sensitivity to L-cysteine inhibition.

Table 3.5: Comparison of CysE homologs IC_{50} measurements for L-cysteine

Na = not available, all values are mean ± SEM.

Organism	IC_{50}(μM)	Condition: pH, Temp, Assay Method	Reference
A. baumannii	1.81±1.03	8.0, 22 ºC, A_{232} nm	This thesis
N. gonorrhoeae	5.01±0.403	8.0, 22 ºC, A_{232} nm	(Oldham, 2020)
E. coli	0.18±0.02	7.5, 22 ºC, DTNB	(Benoni, *et al.*, 2017)
S. typhimurium	1.1	7.6, 25 ºC, DTNB	(Kredich & Tomkins, 1966)
C. glutamicum	2.0	8.0, 30 ºC, A_{232} nm	(Haitani *et al*., 2006)

3.2 Structural Characterization of CysE

3.2.1 Small angle X-ray Scattering Analysis

The SEC-SAXS analysis (Kirby *et al.*, 2016) of recombinant AbaCysE2_long was, performed at a concentration of 5.5 $mg.ml^{-1}$. This provided several key insights into the structural properties of the protein. Initially, the sample underwent gel filtration chromatography (as per section **Error! Reference source not found.**), and the corresponding UV absorbance at 280 nm confirmed the purity and homogeneity of the protein, as indicated by the distinct peak in the chromatogram (Figure 3.11: SEC-SAXS analysis of AbaCysE2_long.. The SAXS scattering profile (Figure 3.11B) revealed characteristics consistent with a globular protein, and the Guinier analysis (inset of Figure 3.11B) allowed for the calculation of the radius of gyration (Rg), confirming the data's quality and the protein's compact nature. The Kratky plot (Figure 3.11C) further supported these findings, displaying a bell-shaped curve typical of fully folded proteins, indicating that AbaCysE2_long does not possess significant disordered regions. Additionally, the pair wise distribution (P(r)) analysis (Figure 3.11D) provides further

validation of the SAXS data, with the calculated maximum particle dimension (D_{max}) and Rg aligning well with the Guinier analysis results. These combined analyses confirm that AbaCysE2_long is a well-folded, globular protein, with the SAXS data providing accurate structural insights. Additionally, the molecular weight of AbacysE2_long was calculated to be between 190-205 kDa using the SAXS data analyzed through primusqt method, within the ATSAS suit (Franke *et al.*, 2017). This molecular weight is consistent with the predicted molecular weight of the CysE hexamer and aligns with the size exclusion chromatography (209.9 kDa), confirming that AbaCysE2_long exits as a hexamer.

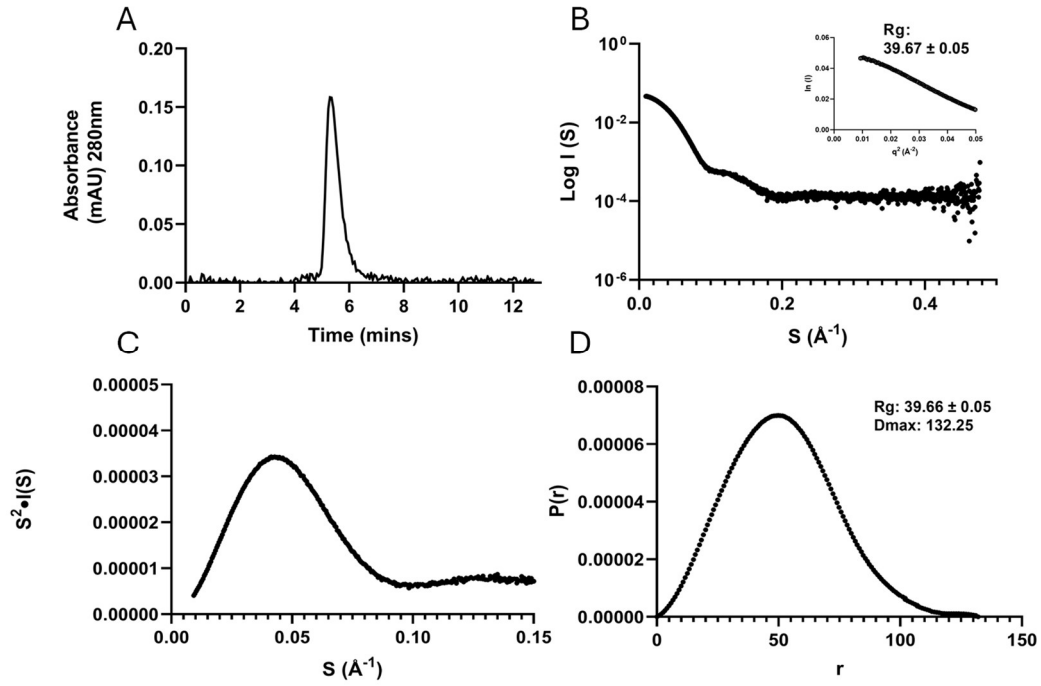

Figure 3.11: SEC-SAXS analysis of AbaCysE2_long.

A) Recombinant AbaCysE2_long at 5.5mg. ml^{-1} underwent gel filtration chromatography prior to scattering analysis UV absorbance at 280nm for the corresponding chromatogram. B) Scattering profile demonstrates globular protein and Guinier analysis (insert B) and calculated Rg value for the Guinier analysis are shown. C) The Kratky plot indicates the protein is fully folded. D) The P(r) distribution analysis highlights the data quality, calculated D_{max} and Rg values from the P(r) distribution analysis are shown on the plot.

3.2.2 Crystallization of CysE

High-throughput crystallization screening was conducted (as per section 2.9.2.2) resulting in the identification of several promising conditions that led to the formation of micro-

crystals. These initial conditions were further optimized by scaling up to fine screens (as per section 2.9.2.3), where we systematically varied parameters such as pH and reagent concentration. The most well-formed crystals developed under the conditions, 2.0M sodium formate, 0.1M sodium acetate trihydrate pH 4.6 (Figure 3.12A) and 2.4 M sodium formate, 0.1 M sodium acetate trihydrate pH 4.4 (Figure 3.12B) which resulted in well-formed crystals.

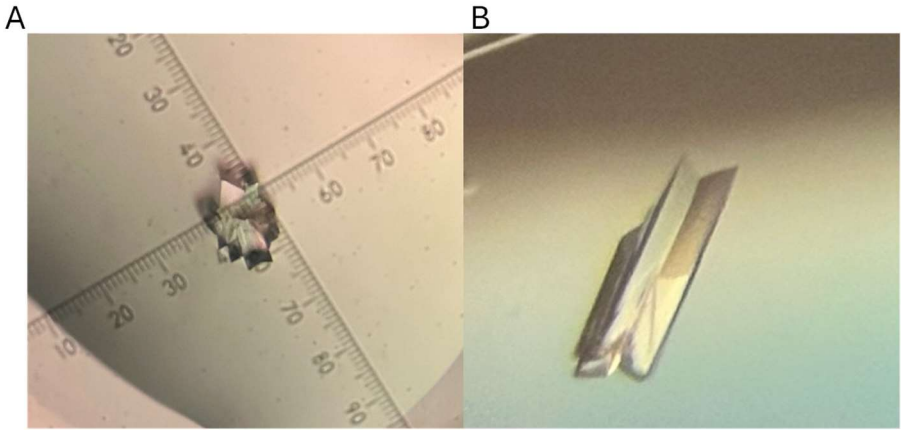

Figure 3.12: CysE apoenzyme crystals grown in sodium formate

A) Micro-crystal grown in 2.0 M sodium formate, 0.1 M sodium acetate trihydrate pH 4.6. B) Hanging drop crystal grown in 2.4 M sodium formate, 0.1 M sodium acetate trihydrate pH 4.4.

To prepare crystals for X-ray diffraction, they were immersed in a cryoprotectant solution composed of the crystallization solution supplemented with 15% (v/v) glycerol before being flash-frozen in liquid nitrogen. Diffraction data were gathered at the Australian Synchrotron on the MX2 beamline, which is equipped with an EIGER detector, as described in section 2.9.3. Data collection involved a 360° rotation of the crystal, capturing data every 0.5° with a wavelength of 0.95374 Å, at 100 K. The data were obtained from a single crystal grown in 2.4 M sodium formate, 0.1 M sodium acetate trihydrate, at pH 4.4, with a protein concentration of 4.7 mg. ml^{-1}.

3.2.3 CysE Data Processing

The data was indexed in the space group C121 using the CCP4 suite (Winn *et al.*, 2011). Integration and scaling were performed with XDS (Kabsch, 2010), and the data was subsequently merged with AIMLESS, also from the CCP4 suite (Winn *et al.*, 2011). AIMLESS was further utilized to generate a FreeR flag dataset for refinement and to calculate dataset quality statistics, as shown in Table 3.6. The CysE dataset achieved a

resolution of 2.14 Å. The data quality statistics indicate that the dataset is of good quality, meeting the following thresholds: $CC_{1/2} \geqslant 0.3$ (0.826), $I/\sigma I \geqslant 2.0$ (2.1), and overall completeness > 95% (100%) (values in the highest resolution shell reported). Despite an R_{merge} of 0.870, which exceeds the ideal threshold of $\leqslant 0.8$ (P. Evans, 2006), the data was retained for downstream processing as all other parameters were satisfactory, and resolution was not reduced.

Table 3.6: Data collection statistics for AbaCysE2_long

Statistics for the highest resolution shell are shown in brackets. The data statistics were generated using AIMLESS.

Data Statistics	**Apostructure**	
Space group	C121	
Wavelength (Å)	0.95374	
Cell dimensions		
a/b/c (Å)	331.69/108.79/73.01	
α/β/γ (̊)	90.00/95.09/90.00	
Mosaicity	0.09	
Monomers in asymmetric unit	9	
Resolution range (Å)	46.34-2.02	(2.02-2.14)
Number of observed reflections	1000246	(50083)
Number of unique reflections	142186	(6990)
R_{merge}	0.065	(0.870)
R_{pim}	0.040	(0.538)
$CC_{(1/2)}$	0.826	(0.999)
Mean I/ σI	16.0	(2.1)
Completeness	100	(100)
Multiplicity	7.1	(6.9)
Wilson B factor (Å)	40.7	

3.2.4 Structure Solving of AbaCysE2_long

The initial step in determining the structure of AbaCysE2_long involved a BLAST search of the AbaCysE2_long peptide sequence to identify suitable molecular replacement candidates with strong sequence identity ($\geqslant$ 30%) and conserved secondary structural features . The best match was serine acetyltransferase from *Planctomyces limnophilus*,

which shared 44.41% sequence identity. However, despite the reasonable sequence identity, molecular replacement using *P. limnophilus* model in Phenix Phaser did not result in a successful solution, as we were unable to generate an interpretable mtz map for model building. To overcome this, the AbaCysE2_long sequence was submitted to AlphaFold 3 (Abramson *et al.*, 2024), which generated a monomer (Figure 3.13). The model was largely reliable, except for the C-terminal tail, which exhibited low to very low predicted local distance difference test (pLDDT) confidence scores. Overall, the predicted alignment error across the sequence is low, indicating confidence in the accuracy of the predicted structure (Figure 3.13, right panel).

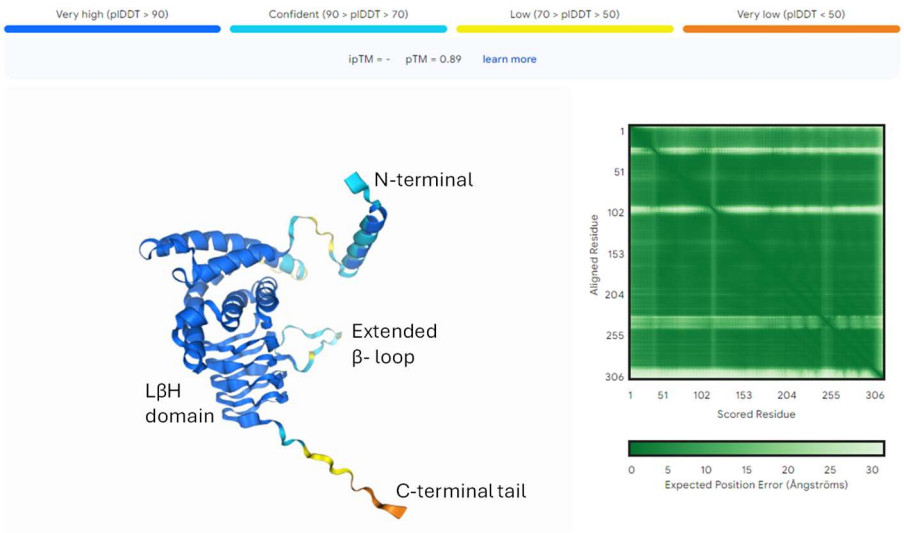

Figure 3.13: Predicted structure of AbaCysE2_long generated using AlphaFold 3.

The model highlights the N-terminal, LβH domain, extended β-loop, and the C-terminal tail. The pLDDT confidence score are color-coded, indicating low confidence in the C-terminal tail (yellow to orange). The right panel displays the predicted alignment error across the sequence (Abramson *et al.*, 2024).

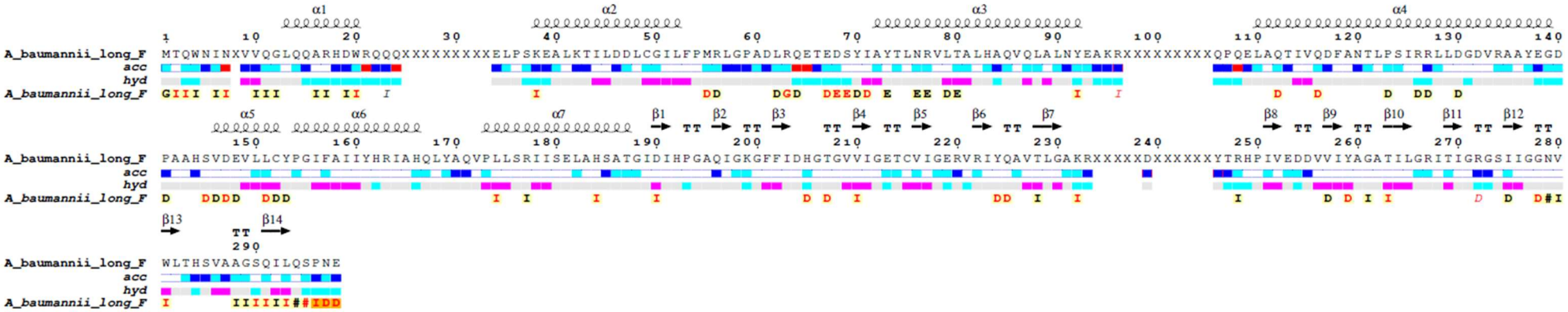

Figure 3.14: ENDscript analysis of the secondary structure of the long form CysE from *A. baumannii*

For each residue, solvent accessibility and hydrophobicity are indicated below the sequence. Solvent accessibility, marked as "acc," is color-coded: "Blue" denotes accessible residues, "cyan" indicates less accessible residues, "white" signifies residues that are completely buried from the solvent, and “red” indicates not calculated. Hydrophobicity is indicated as "hyd," with cyan representing hydrophilic residues, purple for hydrophobic residues, and white for neutral residues. Secondary structure elements are annotated in grey above the sequence, with helices, β-strands, and β-turns depicted as linked loops, arrows, and TT, respectively. Letters denote non-crystallographic interactions, with the chain identified by the corresponding letter. For chain labelling of the monomers in the ASU, refer to Appendix C.2. The analysis was performed using Chain F. The figure was generated with ENDscript 2.0 (Robert & Gouet, 2014).

Mathew's coefficient was employed to estimate the number of monomers in the asymmetric unit (ASU) (Matthews, 1968). The calculation suggested that nine monomer copies were most likely present, with a solvent percentage of 42.88%, based on a predicted molecular weight of 33.92 kDa for the monomer (excluding the Hexahis-tag). For molecular replacement, the CysE monomer (AlphaFold model, see Figure 3.13) served as the search model, assuming nine monomers in the ASU. *Phenix.phaser* program identified a single solution with strong TFZ and LLG scores of 24.6 and 2975.643, respectively (McCoy et al., 2007).

The CysE model was constructed using the *phenix.autobuild* program (as per section 2.9.5.3). The input for the program included the output model and map from *phenix.phaser*, the reflection file (with the FreeR flag dataset), and the CysE amino acid sequence. Default settings were applied (Appendix C.1.), except for the exclusion of water placement during refinement and setting the "rebuild in place" option to false. This adjustment allowed the program to modify the structure file sequence based on the provided sequence file and to build regions outside of the existing model if unmodeled density was present. The structure underwent six iterative rounds of building and three cycles of refinement. The resulting model achieved a satisfactory Rwork/Rfree score for an initial model, with values of 0.2441/0.2900. Interestingly, the program built nine monomers: six formed a homohexamer, while the remaining three assembled into an additional homotrimer (Appendix C.2.). The homohexamer and homotrimer structures were distinct, and the extra trimer did not integrate into the main hexameric assembly. Approximately 81% of each monomer was constructed through automated building using *phenix.autobuild*, although significant unmodeled density remained at both the N-terminal and C-terminal ends of each chain. The unbuilt regions of the peptide sequence were subsequently manually built in COOT.

3.2.5 Analysis of AbaCysE2_long structure

The final structure of AbaCysE2_long achieved an R_{work}/R_{free} score of 0.2214/0.2762 (Table 3.7). The associated structure and map files for this protein are provided in Appendix C.4. No electron density was observed for the N-terminal Hexahis-tag across any of the chains in the ASU. Additionally, three out of the nine chains in the ASU are missing the first 1-2 residues at the N-terminus. Overall, the structure is well-constructed,

with each monomer containing an average of 301 residues (of a total of 307 residues, or 98% completion). The CysE monomer is composed of an N-terminal α-helical domain (spanning residues Met1 - Thr187) followed by a left-handed parallel β-helix (LβH) domain (residues Gly188 – Leu293) (Figure 3.14 and Figure 3.15). The N-terminal loop adopts a winding path, positioning itself near the cleft of the trimer below (Figure 3.16). The N-terminal alpha-helical domain consists of seven α-helices. The first α-helix (α1) spans residues Asp7-Arg21 and appears to 'hug' the adjacent monomer (Figure 3.17). From α1 to the second alpha helix (α2) there is ~90^{o} turn that buries α2 at the base of the monomer. The α2 spans from Lys38-Ile51, followed by a meandering loop (Leu52-Ile71) that leads to an antiparallel third alpha helix (α3) which spans from Ala72-Glu93. There is then a ~180^{o} turn that leads to alpha helix four (α4) that spans from Leu110- Gly139 and sits on the outer edge of the monomer. The remaining three helices are arranged in a more compact manner than the proceeding helices. After α4, there is another 90^{o} turn that leads to the short fifth alpha helix (α5) spanning residues Val146-Cys152. This is immediately followed by alpha helix six (α6, Pro154-Gln171). The final seventh helix (α7) spanning from Pro173-Thr187, aligns α6 forming an antiparallel hairpin. Additionally, limited electron density was observed in the loop between α1 and α2, with chain B in the ASU being the only chain where no residues were missing, with on average this region is missing five residues. Moreover, limited electron density was also observed between residues His97-Glu109 in all chains of the ASU, specifically in the region connecting α3 and α4. The lack of electron density observed for these residues suggesting a high degree of flexibility for these loops and is commonly observed in apoenzyme structures due to the absence of stabilizing interactions with ligands (Bennett *et al*., 1984). Recently, a dataset for AbaCysE2_long (2.58 Å) was collected with the structure ligand serine bound. However, this structure remains unsolved due to time constraints. Binding of the serine ligand could help stabilize flexible regions, improving resolution in areas currently lacking density, such as the loop regions between α1 and α2, and α3 and α4, in the apo form.

Table 3.7: AbaCysE2_long final model quality statistics

Data statistics generated by *phenix.tableone* and AIMLESS

Data Statistics	AbaCysE2_long
R_{work}	0.2214
R_{Free}	0.2763
No. protein residues	2462
Total number of non-hydrogen atoms	19864
Macromolecules	19030
Ligands	0
Solvent	834
RMS	
Bonds (Å)	0.008
Angles (°)	0.88
Average B value (Å)	31.90
Macromolecules	32.06
Ligands	0
Solvent	28.23
Ramachandran analysis	
No. of residues in favored region (%)	94.82
No. of residues in allowed regions (%)	3.58
No. of residues in outlier regions (%)	1.60
Rotamer outliers (%)	2.49

The C-terminal domain is composed of a LβH domain with 15 turns and five distinct coils. Each monomer within the trimer exhibits variation in the number of β-sheets. Specifically, one monomer contains four β-sheets, another contains five, and the third monomer contains six, resulting in structural diversity within the trimer. The β-sheets span the following regions: β1 (Phe202-Asp204), β2 (Val221-Tyr224), β3 (Thr228-Gly230), β4 (Thr263-Leu265), β5 (Val280-Leu282), and β6 (Glu298-Tyr300) (Figure 3.15). The turn-sheet-turn arrangement is produced by the repeated occurrence of a tandem hexapeptide motif [LIV]-[GAED]-X_2-[STAV]-X (Figure 1.6 and Figure 3.14). There is one deviation from this repeat between β3 and β4 which forms the extended β-loop from Gly230-Pro250 (Figure 1.6 and Figure 3.15). Although the active site residues Arg248 and His249 are visible in this region, there is limited electron density in the extended β-loop region spanning residues 234-245. Immediately after the LβH domain, the C-termini consists of a C-terminal tail, previously shown to be flexible, which extends away from the monomer.

Similar to the N-terminus, minimal density for the final six C-terminal residues is observed resulting in them being absent from the model.

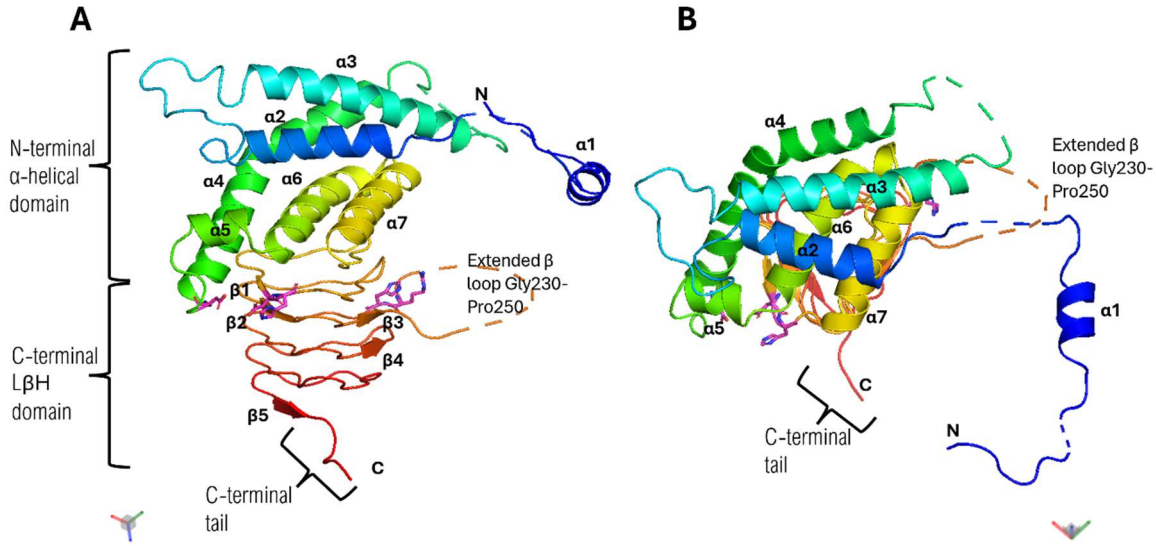

Figure 3.15: AbaCysE2_long monomer from *A. baumannii*

A) The monomer is colored using the chainbow scheme where the N-terminus is colored blue, and the C-terminus is depicted in red. All domains are labeled, along with the flexible C-terminal tail. Active site residues are displayed as sticks and colored in magenta. It's important to note that the active sites are shared between two monomers in the trimer, which accounts for the positioning of active site residues on opposite sides of each monomer. B) 90° forward rotation of the monomer compared to A. The figure was created using PyMOL.

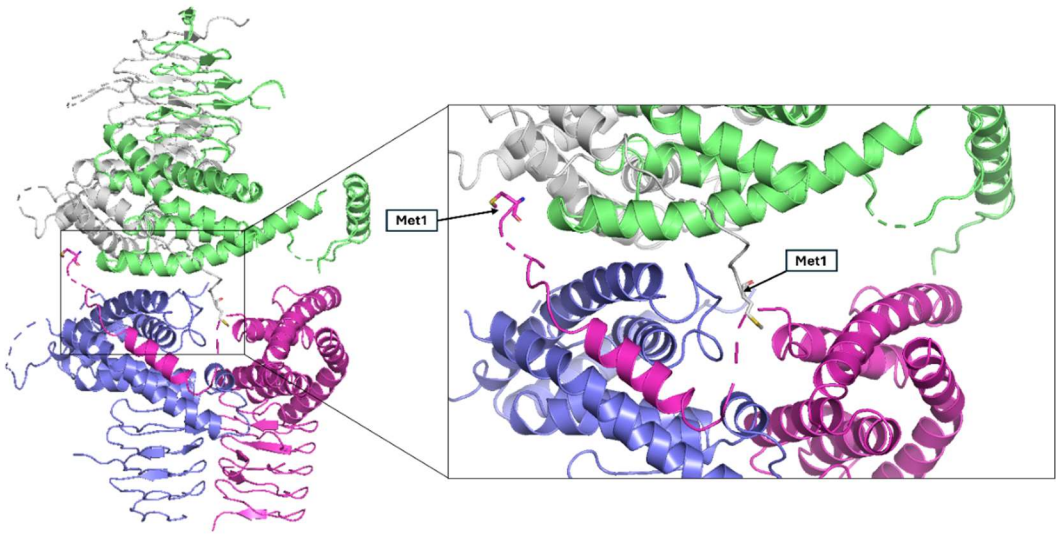

Figure 3.16: AbaCysE2_long N-terminal region conformation

Left panel: Two monomers from the trimer, highlighting the overall structure and orientation of the N-terminal region positioned within the cleft of the trimer below. Right panel: A close-up view of the N-terminal methionine buried within the cleft of the trimer below, stabilized by hydrophobic interactions. The non-interacting monomers have been removed for clarity. The figure was created using PyMOL.

3.2.5.1 Analysis of "hugging" conformation in AbaCysE2_long

The first α-helix of the N-terminal region seen in crystal structure adopts this "hugging" conformation of the adjacent monomer. This is seen in all chains of the ASU. A key salt bridge is formed between the residues Arg17 and Arg21 of α1 from one monomer with Glu67 and Asp68 of α3 of the adjacent monomer. The interaction occurs between the positively charged side chains of Arg17 and Arg21 and the negatively charged carboxyl side chains of Glu67 and Asp68, stabilizing the interaction between the two monomers (Figure 3.17). Interestingly, there are only two other structurally similar proteins in the Protein Data Bank (PDB) that share a similar "hugging" conformation with AbaCysE2_long: those from *Phocaeicola vulgatus* (PDB: 3f1x) and *Planctomyces limnophilus* (PDB: 6lcn) (Figure 3.18). Both 3f1x and 6lcn exhibit a high degree of structural similarity to AbaCysE2_long, with RMSD values of 0.715 Å and 0.707 Å, respectively (Figure 3.18). At the time of writing, the papers for these structures have not been published, limiting the analysis of these "hugging" CysE structures and their role. By comparing these "hugging" CysE structures to others that lack this conformation, it appears that the ability to "hug" is facilitated by an extension in the α1-α2 loop region (Figure 1.6 residues 5 to 6). Additionally, the α1 helix in the "hugging" CysE structures

is longer than in non-hugging ones, suggesting a structural basis for this interaction. However, it is unclear whether the “hugging” interaction is an artifact of crystallization or whether it would occur in solution. It could be speculated that this interaction stabilizes the trimer by forming additional salt bridges between the monomers. Ultimately, further studies are required to determine the molecular role and biological significance of this “hugging” interaction.

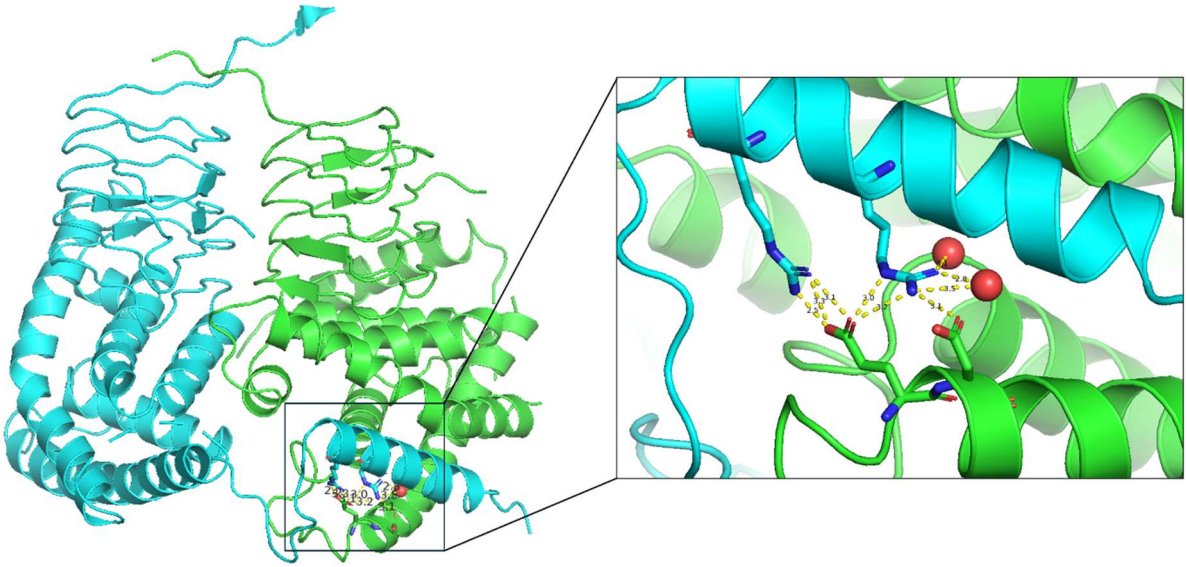

Figure 3.17: AbaCysE2_long "hugging" conformation

Left panel: The overall structure of two adjacent monomers from the AbaCysE2_long trimer (Chain A in green and Chain B in cyan). This highlights the interaction where α1 from Chain B appears to “hug” the adjacent monomer (Chain A). Right panel: close-up view of the interaction between Arg21 on Chain B α1 helix and Glu67 on Chain A α3 helix with a bond length of 2.5 Å; Arg17 on Chain B and Asp68 on Chain A with a bond length of 3.1 Å. The bond length of Asp17 to two water molecules is 3.1 Å and 2.8 Å, respectively. Interactions denoted as dashed lines, side chains are denoted as sticks, colored based on which chain they are from and water molecules as red spheres. The figured was created in PyMOL with non-interacting monomers removed for clarity.

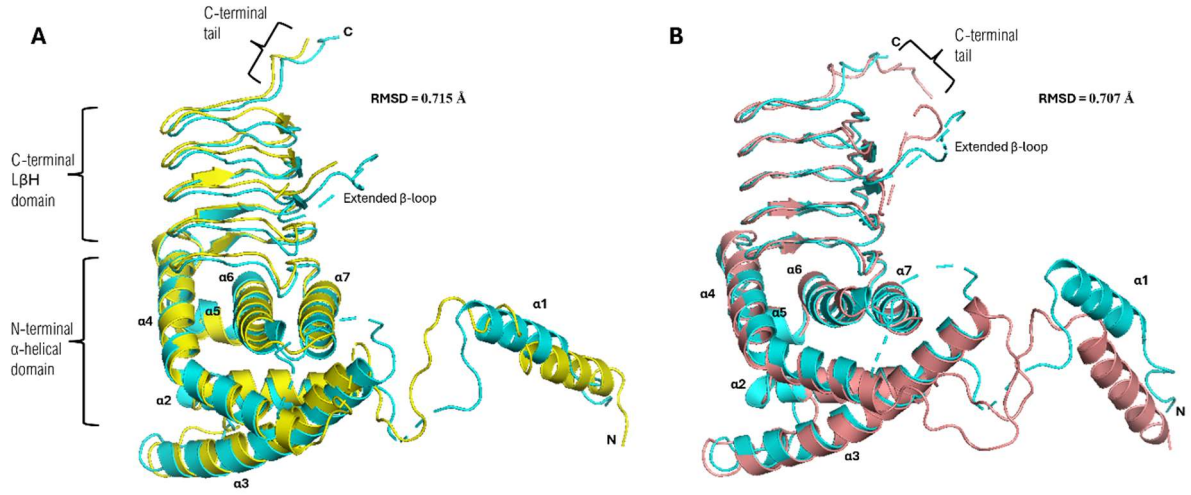

Figure 3.18: Structural comparison of AbaCysE2_long to CysE homologs

A) Superimposition of AbaCysE2_long (cyan) with CysE from *P. vulgatus* (3f1x) (yellow); and B) CysE from *P. limnophilus* (PDB: 6lcn). The figure was created in PyMOL.

3.2.6 Analysis of the AbaCysE2_long Hexamer

Each monomer (Figure 3.15) assembles into a trimer, displaying three-fold symmetry, which in turn interacts with another trimer to form a dimeric hexamer , exhibiting three-fold and 2-fold symmetry (Figure 3.19A and B). The primary interactions within the trimer are mediated by the N-terminal helices α5 and α7 between adjacent monomers. The hexamer measures 108.9 Å in length, with a width of 65.6 Å at the N-terminal region and 49.3 Å at the C-terminal region. The hexamer is stabilized via interactions between the N-terminal domains of two trimers, which contribute to dimer formation. The hexamer has a total surface area of 60,400 Å, with over half of this surface area 34,230 Å (calculated as per section 2.9.5) being buried, suggesting strong inter-subunit interactions within the trimer and also between trimers to form the hexamer. The calculated free Gibbs energy of dissociation (ΔG^{diss}) for the hexamer is 11.5 kcal/mol, indicating a thermodynamically stable hexameric arrangement. This is further supported by our analytical size exclusion data that AbaCysE2_long exists as a hexamer in solution.

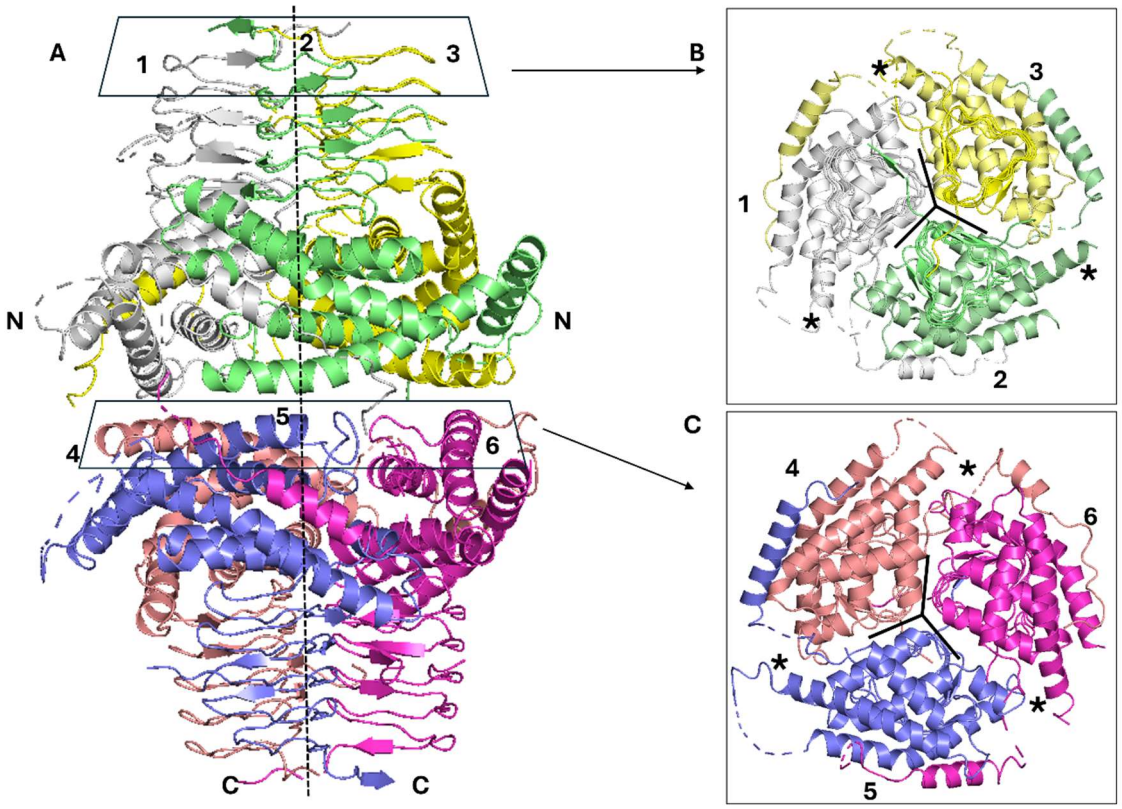

Figure 3.19: Quaternary arrangement of CysE *A. baumannii* (AbaCysE2_long)

A) Structural overview of AbaCysE2_long hexamer with vertical dashed line represents the axis of rotation for the three-fold symmetry of each trimer, dividing the hexamer into two trimers (B) and (C). B) top-down view of C-terminal region with individual trimers, monomers (1-3) labeled; and C) bottom-down view of N-terminal region with monomers 4-6 labeled. Asterisks indicate the location of CysE active sites. The figure was created in PyMOL.

3.2.7 AbaCysE2_long Active Site

Each hexamer contains six active sites, with each active site formed at the interface between two adjacent monomers within the trimeric arrangement (Figure 3.19). Sequence alignment analysis (Figure 1.6) identified the key residues involved in catalysis. Importantly, Arg 248 and His249, located on the β-extended loop of one monomer and Asp190, positioned immediately following helix α7, contribute to the active site. On the adjacent monomer Asp140, Asp204 and His205, contribute to the formation of the active site (Figure 3.20). This arrangement is consistent with observations from other homologs of CysE (Gorman & Shapiro, 2004; Kumar *et al*., 2014, p. 4; Oldham *et al*., 2022; Olsen *et al*., 2004; Pye *et al.*, 2004).

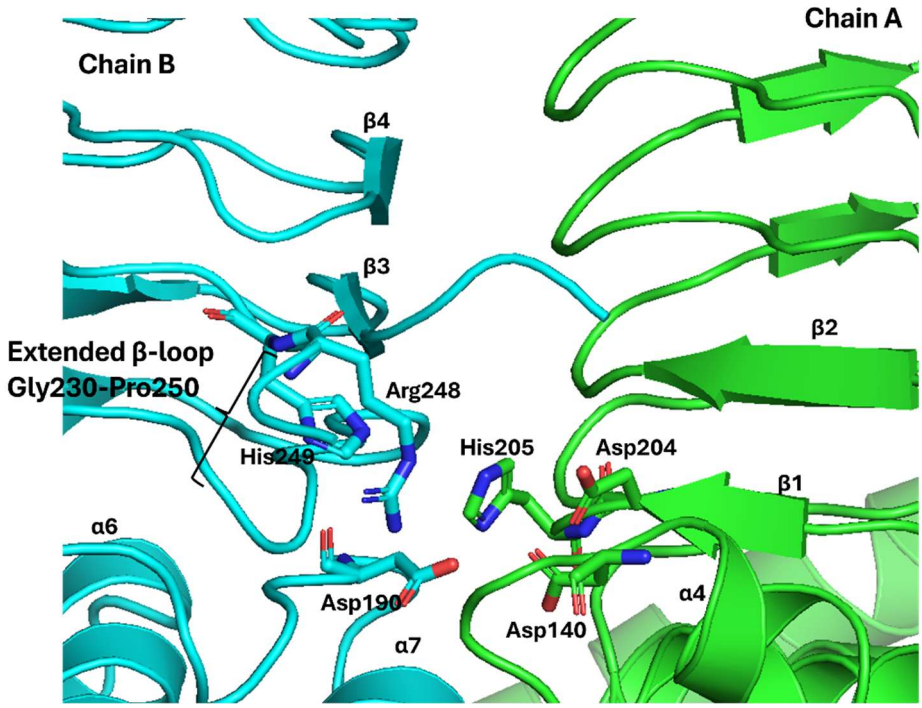

Figure 3.20: Active site residues of AbaCysE2_long

Active site residues are displayed as sticks, labeled; Chain A in green and Chain B in cyan from monomers of adjacent chains. The figure was created in PyMOL.

The active site in AbaCysE2_long reveals key catalytic residues, including Asp140, Asp190, Asp204, His205, Arg248 and His249. Notably, His205 serves as the catalytic base, while Asp140 acts as the catalytic acid, together forming the catalytic dyad that facilitates the enzyme's reaction mechanism. These residues are crucial for catalysis and are positioned similarly to those in the L-cysteine-bound *E. coli* structure (PDB: 1t3d) (Figure 3.21A and B). The overlay of the two active sites (Figure 3.21C), demonstrates a high level of structural similarity, with an RMSD of 0.330 Å, indicating a conserved active site geometry between these two species. One notable difference between the two structures is the orientation of Asp190 in AbaCysE2_long. In AbaCysE2_long, the carboxylic group of Asp190 is bent away from His205, whereas, in *E. coli* (PDB: 1t3d), Asp92A remains closer to His158A, forming a more direct interaction. The overall conservation of the catalytic triad residues, despite minor conformational differences, suggests that AbaCysE2_long retains the necessary structural features for catalysis.

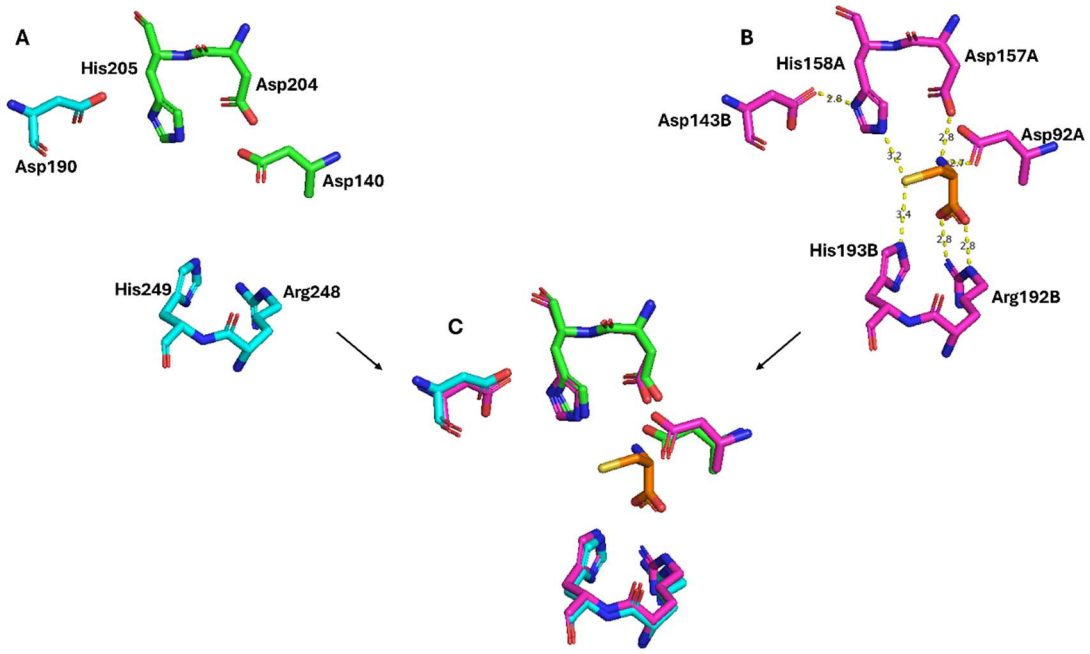

Figure 3.21: Comparison of AbaCysE2_long and *E. coli* (PDB: 1td3d) active sites with L-cysteine bound.

A) AbaCysE2_long active site labeled, and color-coded cyan and green representing chain A and B. B) CysE active site from *E. coli* (PDB: 1t3d) with L-cysteine (orange) bound, labeled with chain they belong to, and dashed lines represent hydrophilic interactions in angstroms. C) Overlay of AbaCysE2_long with 1td3d. The figure was created in PyMOL.

Attempts have been made to co-crystallize the inhibitor L-cysteine with AbaCysE2_long. As described previously we obtained diffraction data with L-serine bound recently, but due to time restrictions have not solved this structure as part of this Masters thesis. Further optimization of the crystallization conditions with L-cysteine will be necessary to obtain high-quality crystals suitable for structural analysis.

Chapter Four

Conclusions and Future Research

4.1 Conclusions and Future Directions

The research conducted has significantly advanced our understanding of the cysteine biosynthesis pathway, presenting the first biochemical and structural characterization of the long form of CysE from *A. baumannii*. Although all attempts at expressing and purifying the short form of *A. baumannii* were unsuccessful, there are methods available to optimize this process, which are detailed below. This research focused on the long form of the CysE enzyme, resulting in successful expression, purification, kinetic analysis, and structural analysis, providing insights into its role in cysteine biosynthesis. By applying the Fa'afaletui framework, this chapter synthesizes the results from different perspectives, aligning with the holistic approach of integrating scientific inquiry with Indigenous Samoan knowledge.

4.1.1 Canoe View

The long form of CysE from *A. baumannii* has been successfully characterized as a functional serine acetyltransferase. The enzyme has kinetic parameters comparable to homologous enzymes from other bacteria (Benoni, De Bei, *et al.*, 2017; Leu & Cook, 1994; Oldham *et al.*, 2022). The Michaelis constants (K_M) for L-serine and acetyl-CoA were 5.77 mM and 0.27 mM, respectively, with corresponding catalytic constants (k_{cat}) of 1.24 x 10^2 s^{-1} and 9.95 x 10^1 s^{-1}. The specificity constants (k_{cat}/K_M) were 2.15 x 10^4 $M^{-1}.s^{-1}$ for L-serine and 3.69 x 10^5 $M^{-1}.s^{-1}$for acetyl-CoA. This demonstrates that AbaCysE2_long has an effective turnover rate and enzymatic activity to allow cysteine biosynthesis in *A. baumannii*. Other CysE enzymes typically exhibit inhibition by L-serine (Kredich & Tomkins, 1966; Olsen *et al*., 2004), *A. baumannii* CysE does not display this substrate inhibition. Instead, it may be subject to inhibition by acetyl-CoA, as seen in the CysE enzyme from *N. gonorrhoeae* (Oldham *et al.*, 2022). However, due to limitations in the dataset, specifically the limited number of data points at higher acetyl-CoA concentrations, further experiments are needed to confirm and fully characterize the extent of this inhibition. Additionally, feedback inhibition by L-cysteine was observed, with an IC_{50} value of 1.81 μM consistent with the inhibition observed in other CysE homologs. This finding is crucial, as it confirms that *A. baumannii* CysE is subject to the

same regulatory mechanism of feedback inhibition as its homologs, suggesting that the enzyme plays a conserved role in cysteine biosynthesis.

The crystal structure of the long form of CysE from *A. baumannii* was solved to a resolution of 2.14 Å. The AbaCysE2_long structure demonstrated that CysE had crystallized as a homohexamer. SAXS data validated that the enzyme maintains its hexameric structure in solution, providing complementary insights into the enzyme's oligomerization in a more native environment. The SAXS analysis also revealed a radius of gyration (Rg) of 39.67 ± 0.05 Å, further supporting the well-folded, globular nature of the enzyme. Key active site residues, including Asp140, Asp190, Asp204, His205, His249 and Arg248 were found to be conserved, aligning with homologous enzymes and reinforcing the catalytic mechanism of CysE (Pye *et al.*, 2004). These conserved residues are consistent with the enzyme's activity measured in kinetic assays, which demonstrated feedback inhibition by L-cysteine. This alignment between structural data and functional assays underscores the importance of these residues in maintaining CysE's catalytic efficiency, further reinforcing its role in cysteine biosynthesis. The findings highlight the potential for targeting CysE in the design of novel antimicrobials. The structural insights gained from crystallography and SAXS, alongside the functional evidence from enzyme kinetics, point to CysE as a crucial enzyme in *A. baumannii* metabolism, making it an important focus for further drug development efforts.

4.1.2 Treetop View

Operationally, in this research, the application of the Fa'afaletui framework provided a more circular and iterative approach to scientific inquiry, which contrasts with the linear progression typical of conventional methodologies. This Pacific methodology fostered a holistic perspective that allowed flexibility and adaptability in steering the research, particularly in the face of experimental limitations. The framework enabled resilience, encouraging a broader view of the research goals and guiding adjustments, such as the decision to focus on the long form of *A. baumannii* CysE when the short form proved difficult to express and purify. While the Fa'afaletui framework is traditionally used in qualitative research settings, applying it here to molecular and cellular science has demonstrated that it can fit and work within this domain. The method facilitated a deeper engagement with the research process, especially in incorporating diverse perspectives

from other researchers and gaining their expertise. This collaborative approach, central to Fa'afaletui, ensured that the research design was robust and informed by both cultural values and scientific rigor.

Conversely, the framework's limitations in addressing the more quantitative aspects of the research were acknowledged. Rather than forcing the framework onto every aspect of the study, it was applied strategically to guide the research process where it naturally aligned. This selective application has proven effective, especially in maintaining a focus on the broader objectives while navigating experimental challenges. As future research continues to explore community perspectives and their relation to scientific inquiry, this work aligns well with those insights, demonstrating how Indigenous methodologies can complement and enhance traditional scientific methods.

4.1.3 Mountain Top View

Future research will focus on exploring the inhibition mechanisms of *A. baumannii* CysE, particularly with respect to its substrates. While this research demonstrated feedback inhibition by L-cysteine, it is important to fully characterize the mode of inhibition, using both Dixon and Michaelis-Menten inhibition plots. Previous studies on CysE homologs, demonstrated that cysteine exhibits competitive inhibition against both substrates (Johnson *et al*., 2004; Pye *et al*., 2004). For *A. baumannii*, understanding these inhibition dynamics will provide key insights into the regulation of CysE and its critical role in cysteine biosynthesis. Given the importance of this pathway to bacterial survival, these findings could open new pathways for the development of antimicrobial therapies targeting cysteine biosynthesis in *A. baumannii*.

The roles of two isoforms of CysE in *A. baumannii* remain largely unexplored, making this research a significant step toward understanding why the bacterium maintains two distinct isoforms. The long form has been successfully characterized here, but limited research exists on the short form, and little is known about its role or regulation. The poorer expression and solubility of short form CysE's, as observed in this study, may partly explain the dearth of available data. While kinetic data exists for substrates like L-serine and acetyl-CoA, to date there are no reports of cysteine inhibition data for the short form CysE isoforms. This gap in knowledge raises the possibility that the short form

might be less sensitive to feedback inhibition by L-cysteine, which could explain why *A. baumannii* maintains both isoforms—to allow for greater flexibility in regulating cysteine biosynthesis under varying environmental conditions. Further research will also focus on optimizing the expression of the short form of *A. baumannii* CysE. Exploring approaches such as recloning with a C-terminal Histidine-tag may prove effective, as it has been for other species, including *S. aureus* and *M. tuberculosis* (C. Chen *et al.*, 2019; Qiu *et al.*, 2013). Additionally, alternative construct designs, such as removing the flexible C-terminal region, could improve expression yields. The successful expression and characterization of this short form of CysE would provide valuable insights into whether the presence of two isoforms serves a redundant function or if one isoform exhibits greater activity or sensitivity to L-cysteine. In addition, characterizing the enzyme's feedback mechanism will allow for the identification of potential inhibitors through computational screening. These lead compounds can then be validated through activity assays using methods that have been established as part of this thesis. Together, this provides a pathway toward novel antimicrobial agents that target CysE, a critical enzyme in the cysteine biosynthesis pathway of *A. baumannii*.

The formation of the cysteine synthase complex (CSC), driven by the binding of the C-terminal tail of CysE into one active site of CysK, is crucial for regulating cysteine biosynthesis and meeting the cysteine requirements of the organism. We have demonstrated that CysE is a functional serine acetyltransferase and is regulated by L-cysteine. The C-terminus isoleucine residue has been shown to act as an anchor in CSC formation, supporting its role in stabilizing the interaction (Campanini et al., 2005; Huang et al., 2005; C. Zhao et al., 2006). While *A. baumannii* lacks an isoleucine at the C-terminus, it does have Ile305 followed by two hydrophobic residues, Ala306 and Gly307, which may facilitate the formation of the CSC. Future research will involve expressing *A. baumannii* CysK and using analytical size exclusion chromatography and SAXS to investigate the potential formation of the CSC *in vitro*.

Interestingly, the discovery of the "hugging" conformation between monomers in the long form of CysE from *A. baumannii* has only been reported in two other enzymes, *P. vulgatus* (PDB: 3f1x) and *P. limnophilus* (PDB: 6lcn). However, at the time of writing this thesis, there are no associated published papers for these structures, meaning the functional significance of this interaction remains entirely unexplored for any organism.

This research represents the first step toward understanding the potential role of this conformation. Further experiments will be conducted to investigate whether this interaction enhances the stability of the hexamer. Generating deletion mutants targeting the α1 helix and performing stability assays, such as thermal shift assays, could help determine whether this “hugging” interaction contributes to the overall stability and function of the enzyme. Understanding this novel structural feature could provide new insights into CysE’s function, regulation, and its potential as a drug target.

As a Samoan researcher, this work holds deep significance for addressing AMR within Pacific communities. By understanding both the biochemical mechanisms behind bacterial resistance and the broader cultural perspectives, this research bridges scientific discovery with culturally informed solutions. Bringing this knowledge back to my community is seen as a crucial first step in addressing the specific health challenges faced by Pacific peoples. Weaving the Fa'afaletui framework into this research emphasizes the importance of involving Pacific voices early in the research process, ensuring that solutions developed are not only scientifically rigorous but also culturally relevant. This research exemplifies how Indigenous methodologies, like the Fa'afaletui framework, can enrich molecular and cellular biology, bringing together cultural and scientific knowledge to tackle global health challenges, such as AMR. By addressing the issues of AMR in a culturally sensitive manner, this work contributes to the empowerment of Pacific communities, ensuring that they are part of the solution to one of the most pressing global health problems.

References

Abramson, J., Adler, J., Dunger, J., Evans, R., Green, T., Pritzel, A., Ronneberger, O., Willmore, L., Ballard, A. J., Bambrick, J., Bodenstein, S. W., Evans, D. A., Hung, C.-C., O'Neill, M., Reiman, D., Tunyasuvunakool, K., Wu, Z., Žemgulytė, A., Arvaniti, E., … Jumper, J. M. (2024). Accurate structure prediction of biomolecular interactions with AlphaFold 3. *Nature*, *630*(8016), 493–500. https://doi.org/10.1038/s41586-024-07487-w

Adams, P. D., Afonine, P. V., Bunkóczi, G., Chen, V. B., Davis, I. W., Echols, N., Headd, J. J., Hung, L.-W., Kapral, G. J., Grosse-Kunstleve, R. W., McCoy, A. J., Moriarty, N. W., Oeffner, R., Read, R. J., Richardson, D. C., Richardson, J. S., Terwilliger, T. C., & Zwart, P. H. (2010). PHENIX: A comprehensive Python-based system for macromolecular structure solution. *Acta Crystallographica. Section D, Biological Crystallography*, *66*(Pt 2), 213–221. https://doi.org/10.1107/S0907444909052925

Afonine, P. V., Grosse-Kunstleve, R. W., Echols, N., Headd, J. J., Moriarty, N. W., Mustyakimov, M., Terwilliger, T. C., Urzhumtsev, A., Zwart, P. H., & Adams, P. D. (2012). Towards automated crystallographic structure refinement with phenix.refine. *Acta Crystallographica. Section D, Biological Crystallography*, *68*(Pt 4), 352–367. https://doi.org/10.1107/S0907444912001308

Agarwal, S. M., Jain, R., Bhattacharya, A., & Azam, A. (2008). Inhibitors of *Escherichia coli* serine acetyltransferase block proliferation of *Entamoeba histolytica* trophozoites. *International Journal for Parasitology*, *38*(2), 137–141. https://doi.org/10.1016/j.ijpara.2007.09.009

Aguilar-Barajas, E., Díaz-Pérez, C., Ramírez-Díaz, M. I., Riveros-Rosas, H., & Cervantes, C. (2011). Bacterial transport of sulfate, molybdate, and related oxyanions. *Biometals: An International Journal on the Role of Metal Ions in Biology, Biochemistry, and Medicine*, *24*(4), 687–707. https://doi.org/10.1007/s10534-011-9421-x

Akerley, B. J., Rubin, E. J., Novick, V. L., Amaya, K., Judson, N., & Mekalanos, J. J. (2002). A genome-scale analysis for identification of genes required for growth or survival of Haemophilus influenzae. *Proceedings of the National Academy of Sciences*, *99*(2), 966–971. https://doi.org/10.1073/pnas.012602299

Baker, M. G., Barnard, L. T., Kvalsvig, A., Verrall, A., Zhang, J., Keall, M., Wilson, N., Wall, T., & Howden-Chapman, P. (2012). Increasing incidence of serious infectious diseases and

inequalities in New Zealand: A national epidemiological study. *Lancet*, *379*(9821), 1112–1119. https://doi.org/10.1016/s0140-6736(11)61780-7

Baleivanualala, S. C., Isaia, L., Devi, S. V., Howden, B., Gorrie, C. L., Matanitobua, S., Sharma, S., Wilson, D., Kumar, S., Maharaj, K., Beatson, S., Boseiwaqa, L. V., Dyet, K., Crump, J. A., Hill, P. C., & Ussher, J. E. (2023). Molecular and clinical epidemiology of carbapenem resistant Acinetobacter baumannii ST2 in Oceania: A multicountry cohort study. *The Lancet Regional Health – Western Pacific*, *40*. https://doi.org/10.1016/j.lanwpc.2023.100896

Bennett, W. S., Huber, R., & Engel, Jür. (1984). Structural and Functional Aspects of Domain Motions in Proteins. *Critical Reviews in Biochemistry*, *15*(4), 291–384. https://doi.org/10.3109/10409238409117796

Benoni, R., Beck, C. M., Garza-Sánchez, F., Bettati, S., Mozzarelli, A., Hayes, C. S., & Campanini, B. (2017). Activation of an anti-bacterial toxin by the biosynthetic enzyme CysK: mechanism of binding, interaction specificity and competition with cysteine synthase. *Sci Rep*, *7*(1), 8817. https://doi.org/10.1038/s41598-017-09022-6

Benoni, R., De Bei, O., Paredi, G., Hayes, C. S., Franko, N., Mozzarelli, A., Bettati, S., & Campanini, B. (2017). Modulation of Escherichia coli serine acetyltransferase catalytic activity in the cysteine synthase complex. *FEBS Lett*, *591*(9), 1212–1224. https://doi.org/10.1002/1873-3468.12630

Bergogne-Bérézin, E., & Joly-Guillou, M. L. (1991). Hospital infection with Acinetobacter spp.: An increasing problem. *The Journal of Hospital Infection*, *18 Suppl A*, 250–255. https://doi.org/10.1016/0195-6701(91)90030-c

Bergogne-Bérézin, E., & Towner, K. J. (1996). Acinetobacter spp. as nosocomial pathogens: Microbiological, clinical, and epidemiological features. *Clinical Microbiology Reviews*, *9*(2), 148–165. https://doi.org/10.1128/CMR.9.2.148

Bick, J. A., Dennis, J. J., Zylstra, G. J., Nowack, J., & Leustek, T. (2000). Identification of a new class of 5'-adenylylsulfate (APS) reductases from sulfate-assimilating bacteria. *Journal of Bacteriology*, *182*(1), 135–142. https://doi.org/10.1128/JB.182.1.135-142.2000

Blakiston, M. R., Schultz, M. B., Basu, I., Ballard, S. A., Williamson, D., & Roberts, S. (2022). Epidemiology of carbapenem resistant Acinetobacter baumannii in New Zealand. *The New Zealand Medical Journal*, *135*(1561), 76–82.

Bonomo, R. A., & Szabo, D. (2006). Mechanisms of multidrug resistance in Acinetobacter species and Pseudomonas aeruginosa. *Clinical Infectious Diseases: An Official Publication of the Infectious Diseases Society of America*, *43 Suppl 2*, S49-56. https://doi.org/10.1086/504477

Bornhorst, J. A., & Falke, J. J. (2000). Purification of proteins using polyhistidine affinity tags. *Methods in Enzymology*, *326*. https://doi.org/10.1016/s0076-6879(00)26058-8

Brisou, J., & Prévot, A. (1954). Études de systématique bactérienne. 10. Révision des espèces réunies dans le genre Achromobacter. *Annales De L Institut Pasteur*, *86*(6), 722–728.

Burns-Huang, K., & Mundhra, S. (2019). Mycobacterium tuberculosis cysteine biosynthesis genes mec+-cysO-cysM confer resistance to clofazimine. *Tuberculosis*, *115*, 63–66. https://doi.org/10.1016/j.tube.2019.02.002

Campanini, B., Pieroni, M., Raboni, S., Bettati, S., Benoni, R., Pecchini, C., Costantino, G., & Mozzarelli, A. (2015). Inhibitors of the sulfur assimilation pathway in bacterial pathogens as enhancers of antibiotic therapy. *Curr Med Chem*, *22*(2), 187–213. https://doi.org/10.2174/0929867321666141112122553

Campanini, B., Speroni, F., Salsi, E., Cook, P. F., Roderick, S. L., Huang, B., Bettati, S., & Mozzarelli, A. (2005). Interaction of serine acetyltransferase with O-acetylserine sulfhydrylase active site: Evidence from fluorescence spectroscopy. *Protein Science*, *14*(8), 2115–2124. https://doi.org/10.1110/ps.051492805

Carmel-Harel, O., & Storz, G. (2000). Roles of the glutathione- and thioredoxin-dependent reduction systems in the Escherichia coli and saccharomyces cerevisiae responses to oxidative stress. *Annual Review of Microbiology*, *54*, 439–461. https://doi.org/10.1146/annurev.micro.54.1.439

Chen, C., Yan, Q., Tao, M., Shi, H., Han, X., Jia, L., Huang, Y., Zhao, L., Wang, C., Ma, X., & Ma, Y. (2019). Characterization of serine acetyltransferase (CysE) from methicillin-resistant *Staphylococcus aureus* and inhibitory effect of two natural products on CysE. *Microbial Pathogenesis*, *131*, 218–226. https://doi.org/10.1016/j.micpath.2019.04.002

Chen, V. B., Arendall, W. B., Headd, J. J., Keedy, D. A., Immormino, R. M., Kapral, G. J., Murray, L. W., Richardson, J. S., & Richardson, D. C. (2010). MolProbity: All-atom structure validation for macromolecular crystallography. *Acta Crystallographica. Section D, Biological Crystallography*, *66*(Pt 1), 12–21. https://doi.org/10.1107/S0907444909042073

Cho, H., Uehara, T., & Bernhardt, T. G. (2014). Beta-Lactam Antibiotics Induce a Lethal Malfunctioning of the Bacterial Cell Wall Synthesis Machinery. *Cell*, *159*(6), 1300–1311. https://doi.org/10.1016/j.cell.2014.11.017

Chronis, D., & Krishnan, H. B. (2004). Sulfur assimilation in soybean (Glycine max [L.] Merr.): Molecular cloning and characterization of a cytosolic isoform of serine acetyltransferase. *Planta*, *218*(3), 417–426. https://www.jstor.org/stable/23388269

Coyne, S., Courvalin, P., & Périchon, B. (2011). Efflux-Mediated Antibiotic Resistance in Acinetobacter spp. *Antimicrobial Agents and Chemotherapy*, *55*(3), 947–953. https://doi.org/10.1128/AAC.01388-10

Djahanschiri, B., Venanzio, G. D., Distel, J. S., Breisch, J., Dieckmann, M. A., Goesmann, A., Averhoff, B., Göttig, S., Wilharm, G., Feldman, M. F., & Ebersberger, I. (2022). Evolutionarily stable gene clusters shed light on the common grounds of pathogenicity in the Acinetobacter calcoaceticus-baumannii complex. *PLOS Genetics*, *18*(6), e1010020. https://doi.org/10.1371/journal.pgen.1010020

Eijkelkamp, B., Hassan, K., Paulsen, I., & Brown, M. (2011). Investigation of the human pathogen Acinetobacter baumannii under iron limiting conditions. *BMC Genomics*, *12*. https://doi.org/10.1186/1471-2164-12-126

Emsley, P., & Cowtan, K. (2004). Coot: Model-building tools for molecular graphics. *Acta Crystallographica. Section D, Biological Crystallography*, *60*(Pt 12 Pt 1), 2126–2132. https://doi.org/10.1107/S0907444904019158

Evans, & Murshudov, G. N. (2013). How good are my data and what is the resolution? *Acta Crystallographica. Section D, Biological Crystallography*, *69*(Pt 7), 1204–1214. https://doi.org/10.1107/S0907444913000061

Evans, P. (2006). Scaling and assessment of data quality. *Acta Crystallographica Section D: Biological Crystallography*, *62*(1), 72–82. https://doi.org/10.1107/S0907444905036693

Ezelarab, H. A. A., Abbas, S. H., Hassan, H. A., & Abuo-Rahma, G. E.-D. A. (2018). Recent updates of fluoroquinolones as antibacterial agents. *Archiv Der Pharmazie*, *351*(9), 1800141. https://doi.org/10.1002/ardp.201800141

Falagas, M. E., Siempos, I. I., Rafailidis, P. I., Korbila, I. P., Ioannidou, E., & Michalopoulos, A. (2009). Inhaled colistin as monotherapy for multidrug-resistant gram (−) nosocomial pneumonia: A case series. *Respiratory Medicine*, *103*(5), 707–713. https://doi.org/10.1016/j.rmed.2008.11.018

Fersht, A. (2017). *Structure and Mechanism in Protein Science | Series in Structural Biology*. https://worldscientific.com/worldscibooks/10.1142/10574

Fischbach, M. A., & Walsh, C. T. (2009). Antibiotics for emerging pathogens. *Science*, *325*(5944), 1089–1093.

Franke, D., Petoukhov, M. V., Konarev, P. V., Panjkovich, A., Tuukkanen, A., Mertens, H. D. T., Kikhney, A. G., Hajizadeh, N. R., Franklin, J. M., Jeffries, C. M., & Svergun, D. I. (2017). ATSAS 2.8: A comprehensive data analysis suite for small-angle scattering from macromolecular solutions. *Journal of Applied Crystallography*, *50*(4), 1212–1225. https://doi.org/10.1107/S1600576717007786

Frávega, J., Álvarez, R., Díaz, F., Inostroza, O., Tejías, C., Rodas, P. I., Paredes-Sabja, D., Fuentes, J. A., Calderón, I. L., & Gil, F. (2016). *Salmonella Typhimurium exhibits fluoroquinolone resistance mediated by the accumulation of the antioxidant molecule H2S in a CysK-dependent manner*. https://academic.oup.com/jac/article/71/12/3409/2631268

Gandra, S., Barter, D., & Laxminarayan, R. (2014). Economic burden of antibiotic resistance: How much do we really know? *Clinical Microbiology and Infection*, *20*(10), 973–980.

Gasteiger, E., Hoogland, C., Gattiker, A., Duvaud, S., Wilkins, M. R., Appel, R. D., & Bairoch, A. (2005). Protein Identification and Analysis Tools on the ExPASy Server. In J. M. Walker (Ed.), *The Proteomics Protocols Handbook* (pp. 571–607). Humana Press. https://doi.org/10.1385/1-59259-890-0:571

Gebhardt, M. J., Czyz, D. M., Singh, S., Zurawski, D. V., Becker, L., & Shuman, H. A. (2020). GigC, a LysR Family Transcription Regulator, Is Required for Cysteine Metabolism and Virulence in Acinetobacter baumannii. *Infection and Immunity*, *89*(1), 10.1128/iai.00180-20. https://doi.org/10.1128/iai.00180-20

Goodyear-Smith, F., & ‘Ofanoa, M. (2022). *Fa’afaletui: A Pacific Research Framework*. https://doi.org/10.1177/1558689820985948

Gorman, J., & Shapiro, L. (2004). Structure of serine acetyltransferase from Haemophilus influenzae Rd. *Acta Crystallographica. Section D, Biological Crystallography*, *60*(Pt 9), 1600–1605. https://doi.org/10.1107/S0907444904015240

Griffith, O. W. (1987). Mammalian sulfur amino acid metabolism: An overview. In *Methods in Enzymology* (Vol. 143, pp. 366–376). Academic Press. https://doi.org/10.1016/0076-6879(87)43065-6

Guan, R., Roderick, S. L., Huang, B., & Cook, P. F. (2008). Roles of histidines 154 and 189 and aspartate 139 in the active site of serine acetyltransferase from Haemophilus influenzae. *Biochemistry*, *47*(24), 6322–6328. https://doi.org/10.1021/bi800075c

Guédon, E., & Martin-Verstraete, I. (2006). Cysteine Metabolism and Its Regulation in Bacteria. In *Amino Acid Biosynthesis ~ Pathways, Regulation and Metabolic Engineering* (pp. 195–218). Springer Berlin Heidelberg. https://doi.org/10.1007/7171_2006_060

Haitani, Y., Awano, N., Yamazaki, M., Wada, M., Nakamori, S., & Takagi, H. (2006). Functional analysis of l-serine O-acetyltransferase from Corynebacterium glutamicum. *FEMS Microbiology Letters*, *255*(1), 156–163. https://doi.org/10.1111/j.1574-6968.2005.00068.x

Hamidian, M., & Nigro, S. J. (2019). Emergence, molecular mechanisms and global spread of carbapenem-resistant Acinetobacter baumannii. *Microbial Genomics*, *5*(10), e000306. https://doi.org/10.1099/mgen.0.000306

Henikoff, S., Haughn, G. W., Calvo, J. M., & Wallace, J. C. (1988). A large family of bacterial activator proteins. *Proceedings of the National Academy of Sciences of the United States of America*, *85*(18), 6602–6606. https://doi.org/10.1073/pnas.85.18.6602

Hicks, J. L., & Mullholland, C. V. (2018). Cysteine biosynthesis in Neisseria species. *Microbiology (Reading)*, *164*(12), 1471–1480. https://doi.org/10.1099/mic.0.000728

Hicks, J. L., Oldham, K. E. A., McGarvie, J., & Walker, E. J. (2022). Combatting antimicrobial resistance via the cysteine biosynthesis pathway in bacterial pathogens. *Bioscience Reports*, *42*(10). https://doi.org/10.1042/bsr20220368

Higgins, P. G., Dammhayn, C., Hackel, M., & Seifert, H. (2010). Global spread of carbapenem-resistant Acinetobacter baumannii. *The Journal of Antimicrobial Chemotherapy*, *65*(2), 233–238. https://doi.org/10.1093/jac/dkp428

Hindson, V. J., & Shaw, W. V. (2003). Random-Order Ternary Complex Reaction Mechanism of Serine Acetyltransferase from Escherichia coli. *Biochemistry*, *42*(10), 3113–3119. https://doi.org/10.1021/bi0267893

Huang, B., Vetting, M. W., & Roderick, S. L. (2005). The active site of O-acetylserine sulfhydrylase is the anchor point for bienzyme complex formation with serine acetyltransferase. *J Bacteriol*, *187*(9), 3201–3205. https://doi.org/10.1128/jb.187.9.3201-3205.2005

Institute for Health Metrics and Evaluation. (2024). *The Burden of Antimicrobial Resistance (AMR) in New Zealand*. Institute for Health Metrics and Evaluation. chrome-

extension://efaidnbmnnnibpcajpcglclefindmkaj/https://www.healthdata.org/sites/default/files/files/Projects/GRAM/New_Zealand_0.pdf

Jeelani, G., Sato, D., Soga, T., & Nozaki, T. (2017). Genetic, metabolomic and transcriptomic analyses of the de novo L-cysteine biosynthetic pathway in the enteric protozoan parasite Entamoeba histolytica. *Scientific Reports*, *7*(1), 15649. https://doi.org/10.1038/s41598-017-15923-3

Jeffrey, G., A. (1997). *An Introduction to Hydrogen Bonding By George A. Jeffrey (University of Pittsburgh). Oxford University Press: New York and Oxford. 1997. Ix + 303 pp. $60.00. ISBN 0-19-509549-9. | Journal of the American Chemical Society*. https://pubs.acs.org/doi/10.1021/ja9756331

Jia, Y., & Zhao, L. (2021). The antibacterial activity of fluoroquinolone derivatives: An update (2018–2021). *European Journal of Medicinal Chemistry*, *224*, 113741. https://doi.org/10.1016/j.ejmech.2021.113741

Jiménez-Guerra, G., Heras-Cañas, V., Gutiérrez-Soto, M., del Pilar Aznarte-Padial, M., Expósito-Ruiz, M., Navarro-Marí, J. M., & Gutiérrez-Fernández, J. (2018). Urinary tract infection by Acinetobacter baumannii and Pseudomonas aeruginosa: Evolution of antimicrobial resistance and therapeutic alternatives. *Journal of Medical Microbiology*, *67*(6), 790–797. https://doi.org/10.1099/jmm.0.000742

Johnson, C. M., Huang, B., Roderick, S. L., & Cook, P. F. (2004). Kinetic mechanism of the serine acetyltransferase from Haemophilus influenzae. *Archives of Biochemistry and Biophysics*, *429*(2), 115–122. PubMed. https://doi.org/10.1016/j.abb.2004.06.006

Johnson, C. M., Roderick, S. L., & Cook, P. F. (2005). The serine acetyltransferase reaction: Acetyl transfer from an acylpantothenyl donor to an alcohol. *Archives of Biochemistry and Biophysics*, *433*(1), 85–95. https://doi.org/10.1016/j.abb.2004.08.014

Juttukonda, L. J., Green, E. R., Lonergan, Z. R., Heffern, M. C., Chang, C. J., & Skaar, E. P. (2018). Acinetobacter baumannii OxyR Regulates the Transcriptional Response to Hydrogen Peroxide. *Infection and Immunity*, *87*(1), 10.1128/iai.00413-18. https://doi.org/10.1128/iai.00413-18

Kabsch, W. (2010). XDS. *Acta Crystallographica. Section D, Biological Crystallography*, *66*(Pt 2), 125–132. https://doi.org/10.1107/S0907444909047337

Kaplan, N., Rosenberg, E., Jann, B., & Jann, K. (1985). Structural studies of the capsular polysaccharide of Acinetobacter calcoaceticus BD4. *European Journal of Biochemistry*, *152*(2), 453–458. https://doi.org/10.1111/j.1432-1033.1985.tb09218.x

Kessler, D. (2006). Enzymatic activation of sulfur for incorporation into biomolecules in prokaryotes. *FEMS Microbiology Reviews*, *30*(6), 825–840. https://doi.org/10.1111/j.1574-6976.2006.00036.x

Kirby, N., Cowieson, N., Hawley, A. M., Mudie, S. T., McGillivray, D. J., Kusel, M., Samardzic-Boban, V., & Ryan, T. M. (2016). *Improved radiation dose efficiency in solution SAXS using a sheath flow sample environment*. https://journals.iucr.org/d/issues/2016/12/00/jc5006/index.html

Kredich, N. M. (2008). Biosynthesis of Cysteine. *EcoSal Plus*, *3*(1). https://doi.org/10.1128/ecosalplus.3.6.1.11

Kredich, N. M., Becker, M. A., & Tomkins, G. M. (1969). Purification and Characterization of Cysteine Synthetase, a Bifunctional Protein Complex, from Salmonella typhimurium. *Journal of Biological Chemistry*, *244*(9), 2428–2439. https://doi.org/10.1016/S0021-9258(19)78241-6

Kredich, N. M., & Tomkins, G. M. (1966). The Enzymic Synthesis of l-Cysteine in Escherichia coli and Salmonella typhimurium. *Journal of Biological Chemistry*, *241*(21), 4955–4965. https://doi.org/10.1016/S0021-9258(18)99657-2

Krissinel, E., & Henrick, K. (2007). Inference of macromolecular assemblies from crystalline state. *Journal of Molecular Biology*, *372*(3), 774–797. https://doi.org/10.1016/j.jmb.2007.05.022

Kumar, S., Kumar, N., Alam, N., & Gourinath, S. (2014). Crystal structure of serine acetyl transferase from Brucella abortus and its complex with coenzyme A. *Biochimica Et Biophysica Acta*, *1844*(10), 1741–1748. https://doi.org/10.1016/j.bbapap.2014.07.009

Kumaran, S., Yi, H., Krishnan, H. B., & Jez, J. M. (2009). Assembly of the cysteine synthase complex and the regulatory role of protein-protein interactions. *J Biol Chem*, *284*(15), 10268–10275. https://doi.org/10.1074/jbc.M900154200

Kyriakidis, I., Vasileiou, E., Pana, Z. D., & Tragiannidis, A. (2021). Acinetobacter baumannii Antibiotic Resistance Mechanisms. *Pathogens*, *10*(3), Article 3. https://doi.org/10.3390/pathogens10030373

Leu, L. S., & Cook, P. F. (1994). Kinetic mechanism of serine transacetylase from Salmonella typhimurium. *Biochemistry*, *33*(9), 2667–2671. https://doi.org/10.1021/bi00175a040

Lin, M.-F., & Lan, C.-Y. (2014). Antimicrobial resistance in Acinetobacter baumannii: From bench to bedside. *World Journal of Clinical Cases : WJCC*, *2*(12), 787–814. https://doi.org/10.12998/wjcc.v2.i12.787

Luna, C. M., & Aruj, P. K. (2007). Nosocomial Acinetobacter pneumonia. *Respirology*, *12*(6), 787–791. https://doi.org/10.1111/j.1440-1843.2007.01147.x

Madeira, F., Madhusoodanan, N., Lee, J., Eusebi, A., Niewielska, A., Tivey, A. R. N., Lopez, R., & Butcher, S. (2024). The EMBL-EBI Job Dispatcher sequence analysis tools framework in 2024. *Nucleic Acids Research*, *52*(W1), W521–W525. https://doi.org/10.1093/nar/gkae241

Magalhães, J., Franko, N., Raboni, S., Annunziato, G., Tammela, P., Bruno, A., Bettati, S., Mozzarelli, A., Pieroni, M., Campanini, B., & Costantino, G. (2020). Inhibition of Nonessential Bacterial Targets: Discovery of a Novel Serine O-Acetyltransferase Inhibitor. *ACS Medicinal Chemistry Letters*, *11*(5), 790–797. https://doi.org/10.1021/acsmedchemlett.9b00627

Marchand, I., Damier-Piolle, L., Courvalin, P., & Lambert, T. (2004). Expression of the RND-type efflux pump AdeABC in Acinetobacter baumannii is regulated by the AdeRS two-component system. *Antimicrobial Agents and Chemotherapy*, *48*(9), 3298–3304. https://doi.org/10.1128/AAC.48.9.3298-3304.2004

Martho, K. F., Brustolini, O. J. B., Vasconcelos, A. T., Vallim, M. A., & Pascon, R. C. (2019). The Glycerol Phosphatase Gpp2: A Link to Osmotic Stress, Sulfur Assimilation and Virulence in Cryptococcus neoformans. *Frontiers in Microbiology*, *10*. https://doi.org/10.3389/fmicb.2019.02728

Matthews, B. W. (1968). Solvent content of protein crystals. *Journal of Molecular Biology*, *33*(2), 491–497. https://doi.org/10.1016/0022-2836(68)90205-2

McCoy, A. J., Grosse-Kunstleve, R. W., Adams, P. D., Winn, M. D., Storoni, L. C., & Read, R. J. (2007). Phaser crystallographic software. *Journal of Applied Crystallography*, *40*(Pt 4), 658–674. https://doi.org/10.1107/S0021889807021206

McPhillips, T. M., McPhillips, S. E., Chiu, H.-J., Cohen, A. E., Deacon, A. M., Ellis, P. J., Garman, E., Gonzalez, A., Sauter, N. K., Phizackerley, R. P., Soltis, S. M., & Kuhn, P. (2002). Blu-Ice and the Distributed Control System: Software for data acquisition and instrument control at macromolecular crystallography beamlines. *Journal of Synchrotron Radiation*, *9*(6), 401–406. https://doi.org/10.1107/S0909049502015170

Meister, A., & Anderson, M. E. (1983). GLUTATHIONE. *Annual Review of Biochemistry*, *52*(Volume 52, 1983), 711–760. https://doi.org/10.1146/annurev.bi.52.070183.003431

Metcalfe, S., Bhawan, S. S., Vallabh, M., Murray, P., Proffitt, C., & Williams, G. (2019). Over and under? Ethnic inequities in community antibacterial prescribing. *N Z Med J*, *132*(1488), 65–68.

Mino, K., Imamura, K., Sakiyama, T., Eisaki, N., Matsuyama, A., & Nakanishi, K. (2001). Increase in the stability of serine acetyltransferase from Escherichia coli against cold inactivation and proteolysis by forming a bienzyme complex. *Biosci Biotechnol Biochem*, *65*(4), 865–874. https://doi.org/10.1271/bbb.65.865

Mino, K., Yamanoue, T., Sakiyama, T., Eisaki, N., Matsuyama, A., & Nakanishi, K. (1999). Purification and characterization of serine acetyltransferase from Escherichia coli partially truncated at the C-terminal region. *Biosci Biotechnol Biochem*, *63*(1), 168–179. https://doi.org/10.1271/bbb.63.168

Mino, K., Yamanoue, T., Sakiyama, T., Eisaki, N., Matsuyama, A., & Nakanishi, K. (2000). Effects of bienzyme complex formation of cysteine synthetase from escherichia coli on some properties and kinetics. *Biosci Biotechnol Biochem*, *64*(8), 1628–1640. https://doi.org/10.1271/bbb.64.1628

Mugnier, P., Poirel, L., Pitout, M., & Nordmann, P. (2008). Carbapenem-resistant and OXA-23-producing Acinetobacter baumannii isolates in the United Arab Emirates. *Clinical Microbiology and Infection: The Official Publication of the European Society of Clinical Microbiology and Infectious Diseases*, *14*(9), 879–882. https://doi.org/10.1111/j.1469-0691.2008.02056.x

Murray, C. J. L., Ikuta, K. S., Sharara, F., Swetschinski, L., Aguilar, G. R., Gray, A., Han, C., Bisignano, C., Rao, P., Wool, E., Johnson, S. C., Browne, A. J., Chipeta, M. G., Fell, F., Hackett, S., Haines-Woodhouse, G., Hamadani, B. H. K., Kumaran, E. A. P., McManigal, B., … Naghavi, M. (2022). Global burden of bacterial antimicrobial resistance in 2019: A systematic analysis. *The Lancet*, *399*(10325), 629–655. https://doi.org/10.1016/S0140-6736(21)02724-0

Niu, C., Clemmer, K. M., Bonomo, R. A., & Rather, P. N. (2008). Isolation and characterization of an autoinducer synthase from Acinetobacter baumannii. *Journal of Bacteriology*, *190*(9), 3386–3392. https://doi.org/10.1128/JB.01929-07

Oldham, K. (2020). *Cysteine biosynthesis and the role of CysE in Neisseria gonorrhoeae: Vol. Master of Science (Research) (MSc(Research))* [Masters, The University of Waikato]. https://hdl.handle.net/10289/13461

Oldham, K., Prentice, E. J., Summers, E. L., & Hicks, J. L. (2022). Serine acetyltransferase from Neisseria gonorrhoeae; structural and biochemical basis of inhibition. *Biochem J*, *479*(1), 57–74. https://doi.org/10.1042/bcj20210564

Olsen, L. R., Huang, B., Vetting, M. W., & Roderick, S. L. (2004). Structure of Serine Acetyltransferase in Complexes with CoA and Its Cysteine Feedback Inhibitor,. *Biochemistry*, *43*(20), 6013–6019. https://doi.org/10.1021/bi0358521

Olsen, L. R., Vetting, M. W., & Roderick, S. L. (2007). Structure of the E. coli bifunctional GlmU acetyltransferase active site with substrates and products. *Protein Science*, *16*(6), 1230–1235. https://doi.org/10.1110/ps.072779707

O'neill, J. (2014). Antimicrobial resistance: Tackling a crisis for the health and wealth of nations. *Rev. Antimicrob. Resist.*

Papp-Wallace, K. M., McLeod, S. M., & Miller, A. A. (2023). Durlobactam, a Broad-Spectrum Serine β-lactamase Inhibitor, Restores Sulbactam Activity Against Acinetobacter Species. *Clinical Infectious Diseases*, *76*(Supplement_2), S194–S201. https://doi.org/10.1093/cid/ciad095

Peleg, A. Y., Seifert, H., & Paterson, D. L. (2008). Acinetobacter baumannii: Emergence of a Successful Pathogen. *Clinical Microbiology Reviews*, *21*(3), 538–582. https://doi.org/10.1128/CMR.00058-07

Perez, F., Hujer, A. M., Hujer, K. M., Decker, B. K., Rather, P. N., & Bonomo, R. A. (2007). Global Challenge of Multidrug-Resistant Acinetobacter baumannii. *Antimicrobial Agents and Chemotherapy*, *51*(10), 3471–3484. https://doi.org/10.1128/AAC.01464-06

Pokhrel, A., Dinh, H., Li, L., Hassan, K. A., Cain, A. K., & Paulsen, I. T. (2023). Identification of a Novel LysR Family Transcriptional Regulator Controlling Acquisition of Sulfur Sources in Acinetobacter baumannii. *Microbial Physiology*, *33*(1), 27–35. https://doi.org/10.1159/000529038

Pye, V. E., Tingey, A. P., Robson, R. L., & Moody, P. C. E. (2004). The Structure and Mechanism of Serine Acetyltransferase from *Escherichia coli**. *Journal of Biological Chemistry*, *279*(39), 40729–40736. https://doi.org/10.1074/jbc.M403751200

Qiu, J., Wang, D., Ma, Y., Jiang, T., & Xin, Y. (2013). Identification and characterization of serine acetyltransferase encoded by the Mycobacterium tuberculosis Rv2335 gene. *International Journal of Molecular Medicine*, *31*(5), 1229–1233. https://doi.org/10.3892/ijmm.2013.1298

Quinn, D., & Sutton, L. (2011). *Enzyme mechanism from isotope effects*. https://openlibrary.org/books/OL1851061M/Enzyme_mechanism_from_isotope_effects

Raetz, C. R. H., & Roderick, S. L. (1995). *A Left-Handed Parallel β Helix in the Structure of UDP-N-Acetylglucosamine Acyltransferase | Science*. https://www.science.org/doi/10.1126/science.270.5238.997

Rahisuddin, R., Payal, T., Kumar, N., Saini, N., Banerjee, S., Singh, R. P., Patel, M., & Kumaran, S. (2024). Multi-oligomeric and catalytically compromised serine acetyltransferase and cysteine

regulatory complex of *Mycobacterium tuberculosis*. *Biochimie*, *221*, 110–124. https://doi.org/10.1016/j.biochi.2024.01.009

Rhomberg, P. R., & Jones, R. N. (2009). Summary trends for the Meropenem Yearly Susceptibility Test Information Collection Program: A 10-year experience in the United States (1999-2008). *Diagnostic Microbiology and Infectious Disease*, *65*(4), 414–426. https://doi.org/10.1016/j.diagmicrobio.2009.08.020

Richards, A. M., Kwaik, Y. A., & Lamont, R. J. (2015). Code blue: Acinetobacter baumannii, a nosocomial pathogen with a role in the oral cavity. *Molecular Oral Microbiology*, *30*(1), 2–15. https://doi.org/10.1111/omi.12072

Robert, X., & Gouet, P. (2014). Deciphering key features in protein structures with the new ENDscript server. *Nucleic Acids Research*, *42*(W1), W320–W324. https://doi.org/10.1093/nar/gku316

Rosa, B., Marchetti, M., Paredi, G., Amenitsch, H., Franko, N., Benoni, R., Giabbai, B., De Marino, M. G., Mozzarelli, A., Ronda, L., Storici, P., Campanini, B., & Bettati, S. (2019). Combination of SAXS and Protein Painting Discloses the Three-Dimensional Organization of the Bacterial Cysteine Synthase Complex, a Potential Target for Enhancers of Antibiotic Action. *Int J Mol Sci*, *20*(20). https://doi.org/10.3390/ijms20205219

Russo, A., Bassetti, M., Ceccarelli, G., Carannante, N., Losito, A. R., Bartoletti, M., Corcione, S., Granata, G., Santoro, A., Giacobbe, D. R., Peghin, M., Vena, A., Amadori, F., Segala, F. V., Giannella, M., Di Caprio, G., Menichetti, F., Del Bono, V., Mussini, C., … Venditti, M. (2019). Bloodstream infections caused by carbapenem-resistant *Acinetobacter baumannii*: Clinical features, therapy and outcome from a multicenter study. *Journal of Infection*, *79*(2), 130–138. https://doi.org/10.1016/j.jinf.2019.05.017

Ryder, C., Mackean, T., Coombs, J., Williams, H., Hunter, K., Holland, A. J. A., & Ivers, R. Q. (2020). Indigenous research methodology – weaving a research interface. *International Journal of Social Research Methodology*, *23*(3), 255–267. https://doi.org/10.1080/13645579.2019.1669923

Salsi, E., Bayden, A. S., Spyrakis, F., Amadasi, A., Campanini, B., Bettati, S., Dodatko, T., Cozzini, P., Kellogg, G. E., Cook, P. F., Roderick, S. L., & Mozzarelli, A. (2010). Design of O-Acetylserine Sulfhydrylase Inhibitors by Mimicking Nature. *Journal of Medicinal Chemistry*, *53*(1), 345–356. https://doi.org/10.1021/jm901325e

Samuelson, J. C. (2011). Recent Developments in Difficult Protein Expression: A Guide to E. coli Strains, Promoters, and Relevant Host Mutations. In Jr. Evans Thomas C. & M.-Q. Xu (Eds.),

Heterologous Gene Expression in E.coli: Methods and Protocols (pp. 195–209). Humana Press. https://doi.org/10.1007/978-1-61737-967-3_11

Seifert, H., Baginski, R., Schulze, A., & Pulverer, G. (1993). The Distribution of Acinetobacter Species in Clinical Culture Materials. *Zentralblatt Für Bakteriologie*, *279*(4), 544–552. https://doi.org/10.1016/S0934-8840(11)80427-5

Seifert, H., Blondeau, J., Lucaßen, K., & Utt, E. A. (2022). Global update on the in vitro activity of tigecycline and comparators against isolates of *Acinetobacter baumannii* and rates of resistant phenotypes (2016–2018). *Journal of Global Antimicrobial Resistance*, *31*, 82–89. https://doi.org/10.1016/j.jgar.2022.08.002

Seo, S.-K., & Kwon, B. (2023). Immune regulation through tryptophan metabolism. *Experimental & Molecular Medicine*, *55*(7), 1371–1379. https://doi.org/10.1038/s12276-023-01028-7

Siegman-Igra, Y., Bar-Yosef, S., Gorea, A., & Avram, J. (1993). Nosocomial Acinetobacter Meningitis Secondary to Invasive Procedures: Report of 25 Cases and Review. *Clinical Infectious Diseases*, *17*(5), 843–849. https://doi.org/10.1093/clinids/17.5.843

Silver, S., & Walderhaug, M. (1992). Gene regulation of plasmid- and chromosome-determined inorganic ion transport in bacteria. *Microbiological Reviews*, *56*(1), 195–228. https://doi.org/10.1128/mr.56.1.195-228.1992

Sproston, E. L., Wimalarathna, H. M. L., & Sheppard, S. K. (2018). *Trends in fluoroquinolone resistance in Campylobacter*. https://www.microbiologyresearch.org/content/journal/mgen/10.1099/mgen.0.000198

Tamasese, K., Peteru, C., Waldegrave, C., & Bush, A. (2005). Ole Taeao Afua, the New Morning: A Qualitative Investigation Into Samoan Perspectives on Mental Health and Culturally Appropriate Services. *Australian & New Zealand Journal of Psychiatry*, *39*(4), 300–309. https://doi.org/10.1080/j.1440-1614.2005.01572.x

Terwilliger, T. C., Grosse-Kunstleve, R. W., Afonine, P. V., Moriarty, N. W., Zwart, P. H., Hung, L. W., Read, R. J., & Adams, P. D. (2008). Iterative model building, structure refinement and density modification with the PHENIX AutoBuild wizard. *Acta Crystallographica. Section D, Biological Crystallography*, *64*(Pt 1), 61–69. https://doi.org/10.1107/S090744490705024X

Tiseo, K., Huber, L., Gilbert, M., Robinson, T. P., & Van Boeckel, T. P. (2020). Global Trends in Antimicrobial Use in Food Animals from 2017 to 2030. *Antibiotics*, *9*(12), 918. https://doi.org/10.3390/antibiotics9120918

Toh-e, A., Ohkusu, M., Shimizu, K., Ishiwada, N., Watanabe, A., & Kamei, K. (2018). Novel biosynthetic pathway for sulfur amino acids in Cryptococcus neoformans. *Current Genetics*, *64*(3), 681–696. https://doi.org/10.1007/s00294-017-0783-7

Turnbull, A. L., & Surette, M. G. (2010). Cysteine biosynthesis, oxidative stress and antibiotic resistance in Salmonella typhimurium. *Research in Microbiology*, *161*(8), 643–650. https://doi.org/10.1016/j.resmic.2010.06.004

Usu, J. E. (2023). *Cysteine biosynthesis and the role of the cysteine synthase complex* [Summer research project].

Vázquez-López, R., Solano-Gálvez, S. G., Juárez Vignon-Whaley, J. J., Abello Vaamonde, J. A., Padró Alonzo, L. A., Rivera Reséndiz, A., Muleiro Álvarez, M., Vega López, E. N., Franyuti-Kelly, G., Álvarez-Hernández, D. A., Moncaleano Guzmán, V., Juárez Bañuelos, J. E., Marcos Felix, J., González Barrios, J. A., & Barrientos Fortes, T. (2020). Acinetobacter baumannii Resistance: A Real Challenge for Clinicians. *Antibiotics*, *9*(4), Article 4. https://doi.org/10.3390/antibiotics9040205

Verma, D., & Gupta, V. (2021). New insights into the structure and function of an emerging drug target CysE. *3 Biotech*, *11*(8), 373. https://doi.org/10.1007/s13205-021-02891-9

Vila, J., Ruiz, J., Goñi, P., & Jimenez de Anta, T. (1997). Quinolone-resistance mutations in the topoisomerase IV parC gene of Acinetobacter baumannii. *The Journal of Antimicrobial Chemotherapy*, *39*(6), 757–762. https://doi.org/10.1093/jac/39.6.757

Walsh, B. J. C., Wang, J., Edmonds, K. A., Palmer, L. D., Zhang, Y., Trinidad, J. C., Skaar, E. P., & Giedroc, D. P. (2020). The Response of Acinetobacter baumannii to Hydrogen Sulfide Reveals Two Independent Persulfide-Sensing Systems and a Connection to Biofilm Regulation. *mBio*, *11*(3), 10.1128/mbio.01254-20. https://doi.org/10.1128/mbio.01254-20

Wang, T., & Leyh, T. S. (2012). Three-stage Assembly of the Cysteine Synthase Complex from Escherichia coli*. *Journal of Biological Chemistry*, *287*(6), 4360–4367. https://doi.org/10.1074/jbc.M111.288423

Warr, A. R., Hubbard, T. P., Munera, D., Blondel, C. J., Wiesch, P. A. zur, Abel, S., Wang, X., Davis, B. M., & Waldor, M. K. (2019). Transposon-insertion sequencing screens unveil requirements for EHEC growth and intestinal colonization. *PLOS Pathogens*, *15*(8), e1007652. https://doi.org/10.1371/journal.ppat.1007652

Wellcome Trust & UK Government. (2016). *Tackling drug-resistant infections globally: Final report and recommendations*.

Wendt, C., Dietze, B., Dietz, E., & Rüden, H. (1997). Survival of Acinetobacter baumannii on dry surfaces. *Journal of Clinical Microbiology*, *35*(6), 1394–1397. https://doi.org/10.1128/jcm.35.6.1394-1397.1997

Wilson, S. (2008). *Research Is Ceremony: Indigenous Research Methods*. https://fernwoodpublishing.ca/book/research-is-ceremony-shawn-wilson

Winn, M. D., Ballard, C. C., Cowtan, K. D., Dodson, E. J., Emsley, P., Evans, P. R., Keegan, R. M., Krissinel, E. B., Leslie, A. G. W., McCoy, A., McNicholas, S. J., Murshudov, G. N., Pannu, N. S., Potterton, E. A., Powell, H. R., Read, R. J., Vagin, A., & Wilson, K. S. (2011). Overview of the CCP4 suite and current developments. *Acta Crystallographica. Section D, Biological Crystallography*, *67*(Pt 4), 235–242. https://doi.org/10.1107/S0907444910045749

Wirtz, M., & Hell, R. (2006). Production of cysteine for bacterial and plant biotechnology: Application of cysteine feedback-insensitive isoforms of serine acetyltransferase. *Amino Acids*, *24*(1), 195–203. https://doi.org/10.1007/s00726-002-0313-9

Wong, D., Nielsen, T. B., Bonomo, R. A., Pantapalangkoor, P., Luna, B., & Spellberg, B. (2017). *Clinical and Pathophysiological Overview of Acinetobacter Infections: A Century of Challenges*. https://www.ncbi.nlm.nih.gov/pmc/articles/PMC5217799/

World Health Organization. (2017). *Antimicrobial resistance*. https://www.who.int/westernpacific/health-topics/antimicrobial-resistance

World Health Organization. (2023). *Antimicrobial resistance*. https://www.who.int/news-room/fact-sheets/detail/antimicrobial-resistance

Yam, E. L. Y., Hsu, L. Y., Yap, E. P.-H., Yeo, T. W., Lee, V., Schlundt, J., Lwin, M. O., Limmathurotsakul, D., Jit, M., Dedon, P., Turner, P., & Wilder-Smith, A. (2019). Antimicrobial Resistance in the Asia Pacific region: A meeting report. *Antimicrobial Resistance & Infection Control*, *8*(1), 202. https://doi.org/10.1186/s13756-019-0654-8

Yi, H., Dey, S., Kumaran, S., Lee, S. G., Krishnan, H. B., & Jez, J. M. (2013). Structure of Soybean Serine Acetyltransferase and Formation of the Cysteine Regulatory Complex as a Molecular Chaperone*. *Journal of Biological Chemistry*, *288*(51), 36463–36472. https://doi.org/10.1074/jbc.M113.527143

Yoneyama, H., & Katsumata, R. (2006). Antibiotic resistance in bacteria and its future for novel antibiotic development. *Bioscience, Biotechnology, and Biochemistry*, *70*(5), 1060–1075.

Zhang, X., & Studier, F. W. (1997). Mechanism of inhibition of bacteriophage T7 RNA polymerase by T7 lysozyme 1. *Journal of Molecular Biology*, *269*(1), 10–27. https://doi.org/10.1006/jmbi.1997.1016

Zhao, C., Moriga, Y., Feng, B., Kumada, Y., Imanaka, H., Imamura, K., & Nakanishi, K. (2006). On the interaction site of serine acetyltransferase in the cysteine synthase complex from *Escherichia coli*. *Biochemical and Biophysical Research Communications*, *341*(4), 911–916. https://doi.org/10.1016/j.bbrc.2006.01.054

Zhao, Y., Wei, H.-M., Yuan, J.-L., Xu, L., & Sun, J.-Q. (2023). A comprehensive genomic analysis provides insights on the high environmental adaptability of Acinetobacter strains. *Frontiers in Microbiology*, *14*. https://doi.org/10.3389/fmicb.2023.1177951

Appendices

Appendix A: Cloning information of AbaCysE2_long

A.1. Sequences of AbaCysE2_long (AE30_00942)

AbaCysE2_long (AE30_00942) | *Acinetobacter Baumannii (strain BIDMC 56)*

location

CysE KDF08297.1 nucleotide sequence | JMUH01000007| JMUH01000000|

(19481..20404)

TTAACCGGCAATATGATTTTTTTGATAAGACTCATTCGGTGACTGTAAAATC
TGGCTACCTGCAGCAACACTATGGGTTAGCCAGACATTTCCCCCAATGATTG
ATCCTCGGCCAATGGTAATACGACCTAAAATAGTCGCACCTGCATAGATCA
CAACGTCATCTTCAACAATTGGATGGCGTGTATAGTCTTTTTTCAAAGCGCC
ATCATCATTGGTTTCAAAGCGTTTCGCTCCAAGAGTCACTGCTTGATAAATA
CGAACGCGTTCTCCAATCACGCAAGTCTCACCAATCACCACACCCGTACCAT
GATCAATGAAAAATCCTTTACCGATTTGCGCACCCGGATGAATATCAATACC
TGTTGCAGAGTGAGCCAACTCCGAAATAATGCGTGACAATAAAGGCACTTG
AGCATAGAGCTGATGGGCAATTCGGTGATAGATAATCGCAAATATGCCCGG
ATAGCAGAGTAATACTTCATCTACACTATGTGCTGCTGGATCACCTTCATAA
GCCGCCCGCACATCGCCGTCTAAAAGGCGCCGTATAGAGGGCAAAGTGTTG
GCAAAATCCTGCACAATAGTTTGAGCAAGTTCTTGTGGCTGCTGCACTGGGC
TTGAATGACTCAAATGACGTTTTGCTTCATAATTTAAAGCCAGTTGTACTTG
AGCATGTAAAGCTGTTAGTACCCGATTTAAAGTATAGGCAATATAAGAATC
TTCAGTTTCCTGACGTAAGTCGGCAGGGCCTAAACGCATTGGAAATAAAAT
GCCGCACAGGTCATCTAAAATAGTTTTTAAAGCTTCTTTAGATGGAAGTTCA
CGGCCCCCAAATTCTTTTGTCCTGTGCTGTTGCTGACGCCAGTCATGCCTTGC
TTGTTGTAAACCTTGTACAACCGCATTAATGTTCCATTGAGTCAC

CysE peptide sequence|33.92kDa| EC 2.3.1.30

MTQWNINAVVQGLQQARHDWRQQQHRTKEFGGRELPSKEALKTILDDLCGIL
FPMRLGPADLRQETEDSYIAYTLNRVLTALHAQVQLALNYEAKRHLSHSSPVQ
QPQELAQTIVQDFANTLPSIRRLLDGDVRAAYEGDPAAHSVDEVLLCYPGIFAII
YHRIAHQLYAQVPLLSRIISELAHSATGIDIHPGAQIGKGFFIDHGTGVVIGETCVI

GERVRIYQAVTLGAKRFETNDDGALKKDYTRHPIVEDDVVIYAGATILGRITIG
RGSIIGGNVWLTHSVAAGSQILQSPNESYQKNHIAG

CysE peptide sequence |N-terminal HexaHis-tag and leader sequence (underlined) 328 residues|36.216/217.296 kDa (monomer/hexamer) | theoretical pI 6.72

MGSSHHHHHHSSGLVPRGSHMMTQWNINAVVQGLQQARHDWRQQQHRTKE
FGGRELPSKEALKTILDDLCGILFPMRLGPADLRQETEDSYIAYTLNRVLTALHA
QVQLALNYEAKRHLSHSSPVQQPQELAQTIVQDFANTLPSIRRLLDGDVRAAYE
GDPAAHSVDEVLLCYPGIFAIIYHRIAHQLYAQVPLLSRIISELAHSATGIDIHPGA
QIGKGFFIDHGTGVVIGETCVIGERVRIYQAVTLGAKRFETNDDGALKKDYTRH
PIVEDDVVIYAGATILGRITIGRGSIIGGNVWLTHSVAAGSQILQSPNESYQKNHI
AG

pET-28a description

Vector	Description
pET-28a+	*E. coli* expression vector, 6,216 bps, Kanamycin resistance, N- terminal His-tags, T7-promoter.

GMO approval number:

E. coli GMD101146

A.2 Luria Bertani (LB) Agar (1L)

Components mixed:

5g Peptone

10g NaCl

5g Yeast extract

5g Agar

1L distilled water

Autoclaved at 121°C before use

LB Broth

Same as LB agar, but exclude the addition of agar.

Appendix B: Protein Purification and kinetic information

B.1. Purification buffers for kinetics and crystallography

Component	Composition
Lysis Buffer	50mM Tris (pH8.0)
	200mM NaCl
	20mM Imidazole
Elution Buffer	50mM Tris (pH8.0)
	200mM NaCl
	1M Imidazole
Gel Filtration Buffer	50mM Tris (pH8.0)
	100mM NaCl

B.2. SDS-PAGE and Native-PAGE gel buffers compositions

4 x SDS loading dye

250mM Tris (pH6.8)

20% glycerol (w/v)

4% SDS (w/v)

10% beta-2-mercaptoethanol (w/v)

0.025% bromophenol blue (w/v)

Tris-glycine SDS buffer

25mM Tris (pH 8.5)

250mM glycine

0.1% SDS (w/v)

Fairbanks Staining Solution

0.05% coomasie blue

25% isopropanol

10% acetic acid

Destaining solution

10% acetic acid

B.3. Gel Filtration Calibration Curve for Enrich 650

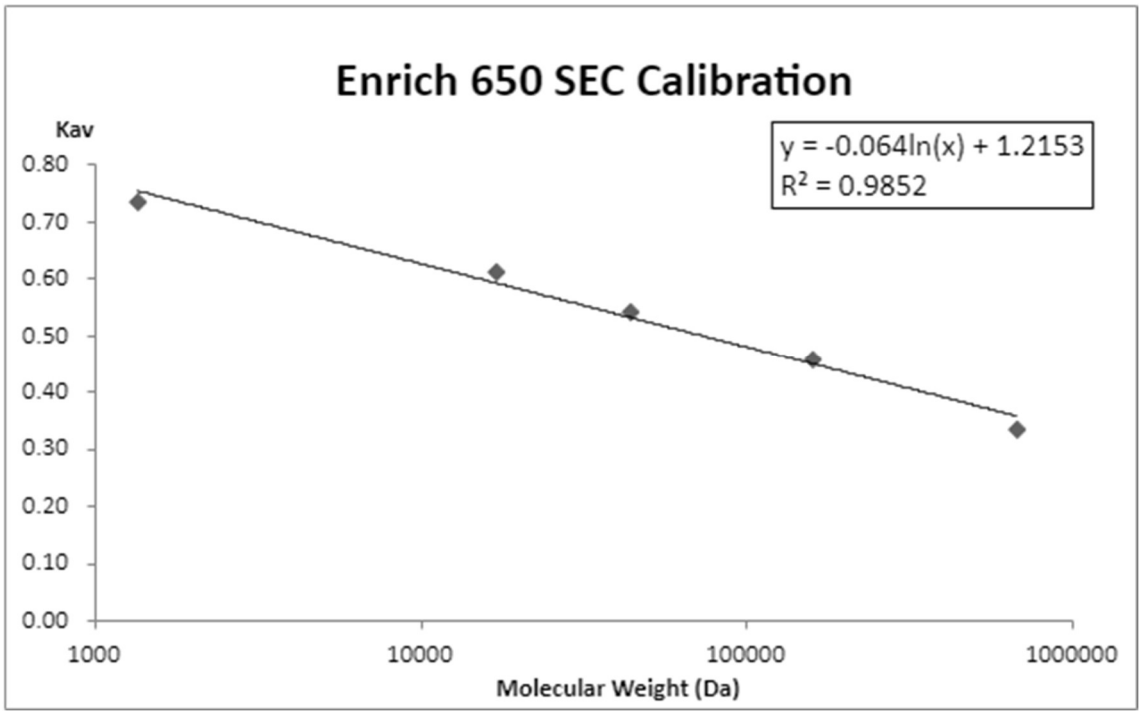

B.4. Raw data used in method optimization, Michaelis Menten and inhibition assays

https://drive.google.com/drive/folders/1xnqfSJ4Xp97egcr4QEFbRiikP1T5PE7k?usp=sharing

Appendix C: Crystallization and Structure solving

C.1. Input settings for *phenix.autobuild*

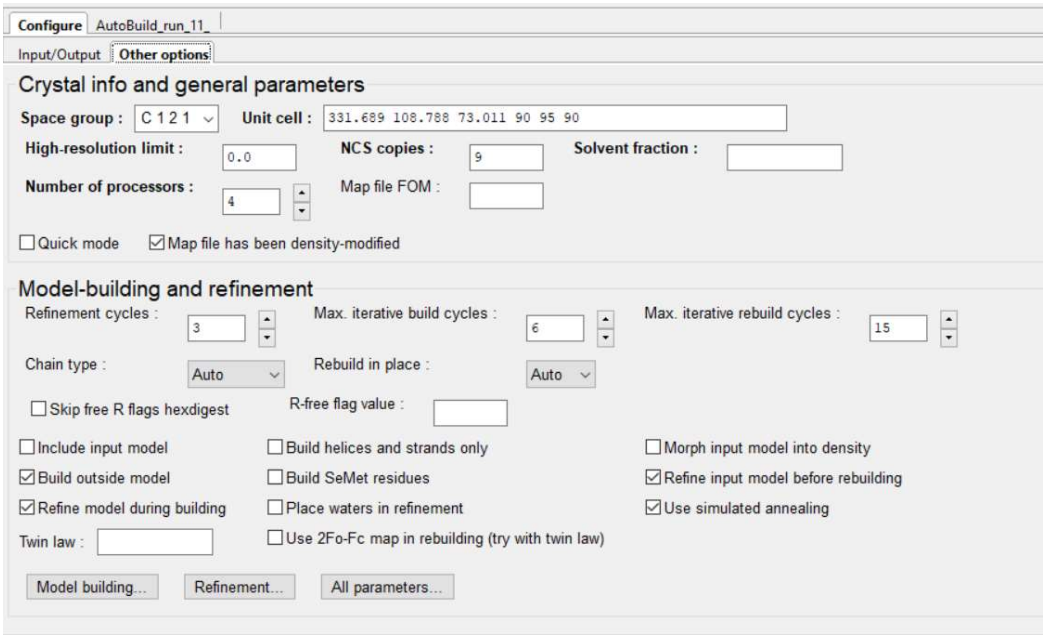

Screenshot of input settings for *phenix.autobuild* used for building the model of AbaCysE2_long.

C.2. Asymmetric unit for CysE

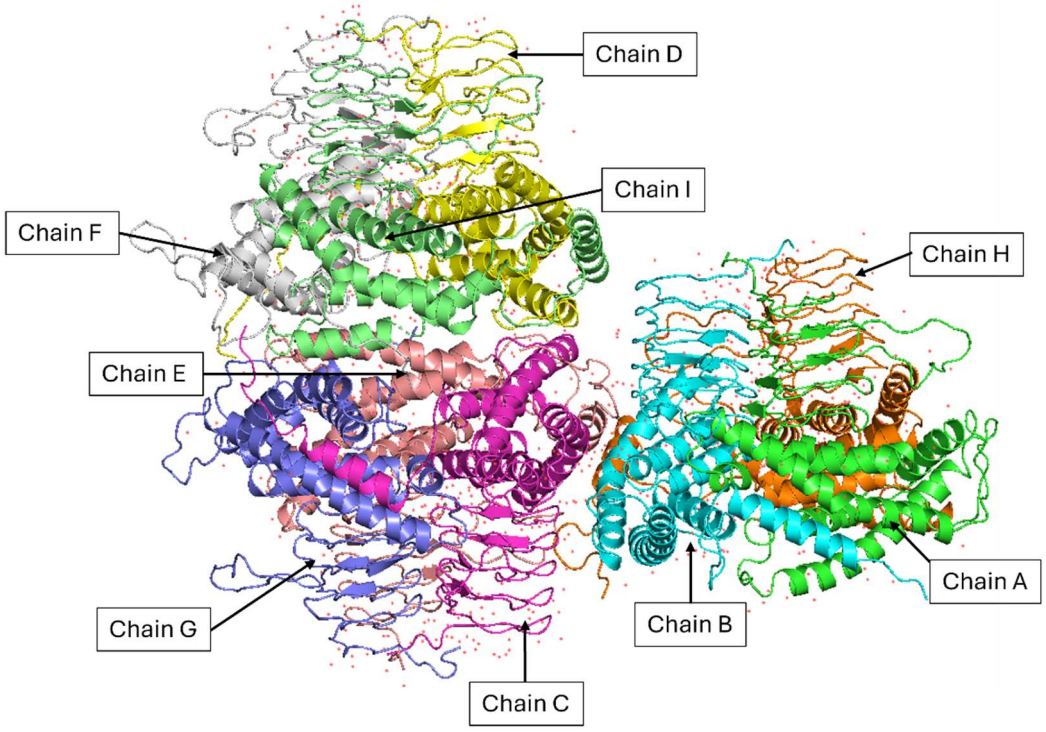

Asymmetric unit contents of CysE model in space group C121. Waters are represented as red crosses. Figure generated in PyMOL.

C.3. Statistics by resolution shell

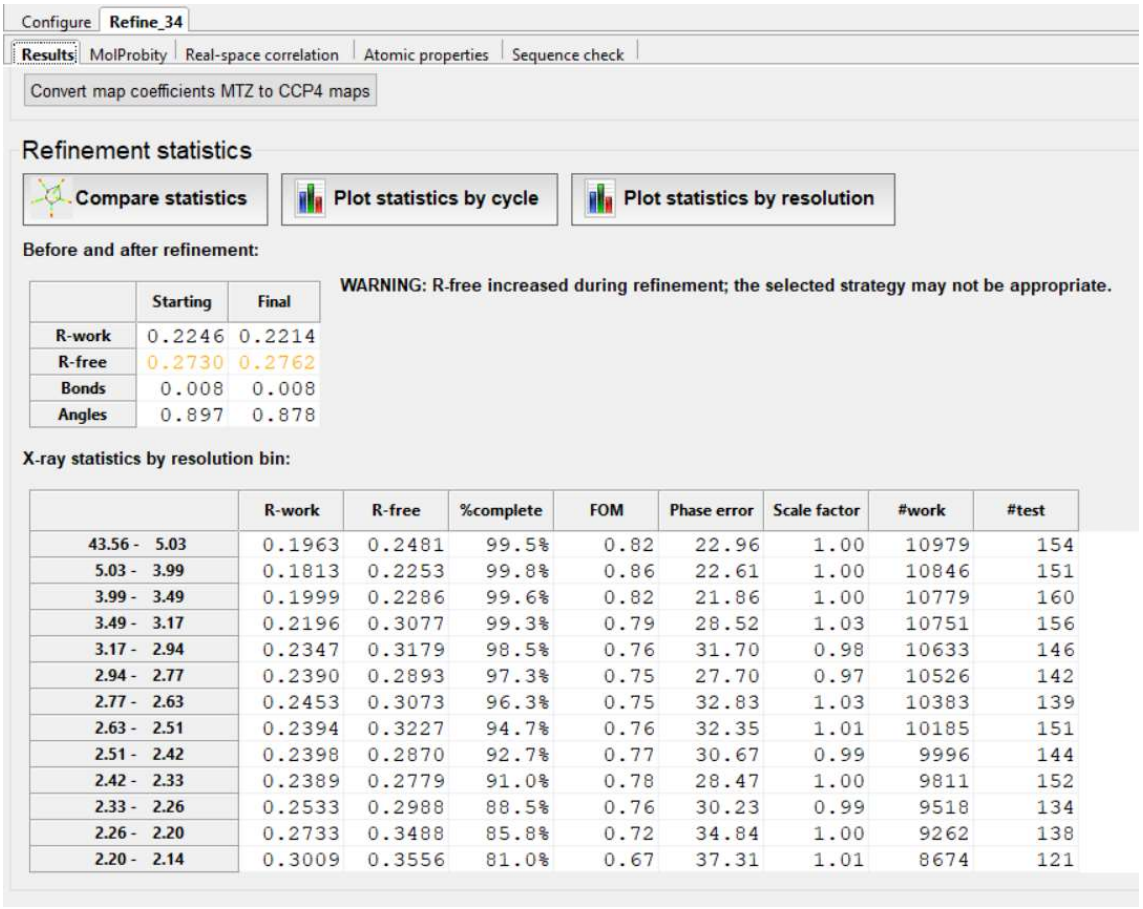

Configure | Refine_34

Results | MolProbity | Real-space correlation | Atomic properties | Sequence check

Convert map coefficients MTZ to CCP4 maps

Refinement statistics

Compare statistics | Plot statistics by cycle | Plot statistics by resolution

Before and after refinement:

	Starting	Final
R-work	0.2246	0.2214
R-free	0.2730	0.2762
Bonds	0.008	0.008
Angles	0.897	0.878

WARNING: R-free increased during refinement; the selected strategy may not be appropriate.

X-ray statistics by resolution bin:

	R-work	R-free	%complete	FOM	Phase error	Scale factor	#work	#test
43.56 - 5.03	0.1963	0.2481	99.5%	0.82	22.96	1.00	10979	154
5.03 - 3.99	0.1813	0.2253	99.8%	0.86	22.61	1.00	10846	151
3.99 - 3.49	0.1999	0.2286	99.6%	0.82	21.86	1.00	10779	160
3.49 - 3.17	0.2196	0.3077	99.3%	0.79	28.52	1.03	10751	156
3.17 - 2.94	0.2347	0.3179	98.5%	0.76	31.70	0.98	10633	146
2.94 - 2.77	0.2390	0.2893	97.3%	0.75	27.70	0.97	10526	142
2.77 - 2.63	0.2453	0.3073	96.3%	0.75	32.83	1.03	10383	139
2.63 - 2.51	0.2394	0.3227	94.7%	0.76	32.35	1.01	10185	151
2.51 - 2.42	0.2398	0.2870	92.7%	0.77	30.67	0.99	9996	144
2.42 - 2.33	0.2389	0.2779	91.0%	0.78	28.47	1.00	9811	152
2.33 - 2.26	0.2533	0.2988	88.5%	0.76	30.23	0.99	9518	134
2.26 - 2.20	0.2733	0.3488	85.8%	0.72	34.84	1.00	9262	138
2.20 - 2.14	0.3009	0.3556	81.0%	0.67	37.31	1.01	8674	121

Dataset completeness for each resolution shell. Values generated by *phenix.refine*

C.4. AbaCysE2_long structural files

Link to google drive folder:
https://drive.google.com/drive/folders/1xnqfSJ4Xp97egcr4QEFbRiikP1T5PE7k?usp=sharing